Spring 5-7-2021

Environment-Friendly Flame Retardants for Bio-Based Polyurethanes

Felipe Martins de Souza
Pittsburg State University, fdesouza@gus.pittstate.edu

ENVIRONMENT-FRIENDLY FLAME RETARDANTS FOR BIO-BASED POLYURETHANES

A Thesis Submitted to the Graduate School
in Partial Fulfillment of the Requirements
For the Degree of
Master of Science

Felipe Martins de Souza

Pittsburg State University

Pittsburg, Kansas

May 2021

ENVIRONMENT-FRIENDLY FLAME RETARDANTS FOR BIO-BASED POLYURETHANES

Felipe Martins de Souza

APPROVED:

Thesis Advisor _____
Dr. Ram Gupta, Department of Chemistry

Committee Member _____
Dr. Khamis Siam, Department of Chemistry

Committee Member _____
Dr. Timothy Dawsey, Kansas Polymer Research Center

Committee Member _____
Dr. Anuradha Ghosh, Department of Biology

Acknowledgments

First of all, I would like to thank Dr. Ram Gupta for being this benevolent mentor that allowed me to develop technical skills, acquire knowledge, and was able to reignite my passion for science by showing how interesting it can be. His brightness, charisma, and inspirational behavior are some of his features that I really admire and would like to have one day. Hence, I appreciate his mentorship as it helped me to see my life from a better and more optimistic perspective. I would like to thank Marina Leite, the love of my life, for being much more than I could have ever wished for. Thank you for being the life partner that went through this arduous process with me. Despite the physical distance, you have always made yourself present. Even though missing you was a crushing feeling it only showed me how much I love you and how much I want you to be part of my life more and more. I can easily rephrase what you told me "Time will show how much I love you" and it totally did since my love for you only increased regardless of the time and distance. I would like to thank my family, my father Lázaro Luis, my mother Sílvia Helena, and my brother Vitor Martins for the genuine support and for always keeping me motivated no matter how hard any situation may look. I would like to thank my best friend and host father, Robert "Bob" Walter, for the super interesting conversations on various topics, your company, good food, and refreshing moments. By far one of the best things that happened in my life was to have you in it. I would like to thank Dr. Khamis Siam, Dr. Tim Dawsey, and Dr. Anuradha Ghosh for being on my thesis committee. Last but definitely not least, I would like to thank the Chemistry Department for providing me with the coursework and the scholarship to proudly study at Pittsburg State University, which

was a life-changing opportunity. I deeply appreciate it. To all other parts involved in this journey, I leave here my deepest thanks!

ENVIRONMENT-FRIENDLY FLAME RETARDANTS FOR BIO-BASED POLYURETHANES

An Abstract of the Thesis by
Felipe Martins de Souza

Finding alternative ways to decrease the large consumption of non-renewable resources has been one of the greatest challenges faced by the industry and academia. The trend of using bio-renewable based materials is an interesting alternative to tackle environmental issues as well as provide economically viable materials. In this work, carvone, an essential oil, was used to synthesize a bio-based polyol through a thiol-ene reaction. The chemical functions were analyzed through Fourier transformed infrared spectrum (FTIR), gel permeation chromatography (GPC), viscosity, and hydroxyl number, which confirmed the synthesis of carvone-based polyol. The latter was then physically blended with three different flame-retardants separately: expandable graphite (EG), aluminum trihydroxide (ATH), and aluminum hypophosphite (AHP). This facile method was demonstrated to be efficient as the inherently poor resistance to fire of polyurethane foams (PUF) was decreased due to the self-quenching fire properties. During the testing for the foams, it was observed that all three sets had a closed-cell content of around 95%, density in the range of 28-50 kg/m^3, and average compressive strength of 210 kPa. Also, the flame retardancy presented a drastic decrease in the burning time and weight loss as the neat sample burned from 98 s and 40.7% and dropped to 11 s and 3.55 % (EG), 58 s, and 12.23 % (ATH), and 5.2 s and 3.6 % (AHP), respectively. Hence, an effective, and facile route to develop bio-based flame-retardant polyurethane is presented in this thesis, showing promising large-scale applications.

TABLE OF CONTENTS

CHAPTER		PAGE
I.	INTRODUCTION	1
	1.1. Polyurethanes: Values and applications	1
	1.2. Chemistry of bio-based polyurethanes	10
	1.3. Flame-retardant polyurethane foams	21
	1.4. The objective of the thesis	23
II.	EXPERIMENTAL DETAILS	25
	2.1. Starting materials	25
	2.1.1. Isocyanate	25
	2.1.2. Polyol	26
	2.1.3. Photoinitiator	27
	2.1.4. Catalyst	27
	2.1.5. Blowing agent	27
	2.1.6. Surfactant	27
	2.1.7. Flame-retardants	28
	2.2. Synthesis of carvone-based polyol	30
	2.3. Characterization of polyol	31
	2.3.1. Gel permeation chromatography (GPC)	31
	2.3.2. Viscosity measurement	32
	2.3.3. Fourier transform infrared spectroscopy (FT-IR)	32
	2.3.4. Iodine value	32
	2.3.5. Hydroxyl number determination	32
	2.4. Preparation of flame-retardant rigid polyurethane foams	33
	2.5. Characterization of the rigid polyurethane foams	35
	2.5.1. Apparent density	35
	2.5.2. Compression test	35
	2.5.3. Closed-cell content	36
	2.5.4. Thermogravimetric analysis (TGA)	36
	2.5.5. Scanning electron microscope (SEM)	36
	2.5.6. Horizontal burning test	36
III.	RESULTS AND DISCUSSIONS	38
	3.1. Polyol data and discussions	38
	3.1.1. Gel permeation chromatography	38
	3.1.2. Viscosity measurement	38
	3.1.3. Fourier transform infrared spectroscopy	39
	3.1.4. Hydroxyl number determination	42

3.2. Properties of carvone-based polyurethane foams…… 43
3.2.1. Digital photos of rigid polyurethane foams…… 43
3.2.2. Fourier transformed infrared for polyurethane foams…… 46
3.2.3. Apparent density…… 49
3.2.4. Closed-cell Content…… 52
3.2.5. Microstructure and morphology of the polyurethane foams…… 54
3.2.6. Compression test…… 59
3.2.7. Thermogravimetric analysis…… 62
3.2.8. Horizontal burning test…… 76

IV. CONCLUSION…… 86

CONSIDERATIONS FOR THE FUTURE…… 87

REFERENCES…… 88

LIST OF TABLES

TABLE		PAGE
Table 2.1.	Formulation for polyurethane foams containing EG……..	34
Table 2.2.	Formulation for polyurethane foams containing ATH……	34
Table 2.3.	Formulation for polyurethane foams containing AHP……..	35
Table 3.1.	Thermal properties of polyurethane foams containing EG……..	68
Table 3.2.	Thermal properties of polyurethane foams containing ATH……	70
Table 3.3.	Thermal properties of polyurethane foams containing AHP……..	73

LIST OF FIGURES

FIGURE		PAGE
Figure 1.1.	Global usage of polyurethanes……	3
Figure 1.2.	A general reaction between polyol and diisocyanate to form a polyurethane……	3
Figure 1.3.	Main raw materials for polyether polyol synthesis……	4
Figure 1.4.	General ring-opening polymerization for polyether polyols……	5
Figure 1.5.	A general polyesterification reaction for the synthesis of polyester polyols……	5
Figure 1.6.	A general structure of polycarbonate, polyacrylic, and polybutadiene-based polyols……	6
Figure 1.7.	Name and structure of most common diisocyanates used for preparation polyurethanes……	7
Figure 1.8.	Name and structure of common amine-based catalysts……	9
Figure 1.9.	The chemical structure of castor oil……	13
Figure 1.10.	Chemical structure of some terpenes……	15
Figure 1.11.	The polymerization reaction of poly(limonene carbonate)……	17
Figure 1.12.	Synthesis of a limonene oxide-based polyurethane through isocyanate-free polymerization……	19
Figure 1.13.	Synthesis of polyols based on limonene by using thiol-ene ‘‘click’’ chemistry……	19
Figure 1.14.	Possible structures of phenol alkylated with limonene……	20
Figure 1.15.	Synthesis of polyols based on α-phellandrene by thiol-ene ‘‘click’’ chemistry……	20
Figure 2.1.	Chemical structure of MDI……	26
Figure 2.2.	Chemical structure of expandable graphite……	29
Figure 2.3.	Chemical structure of aluminum trihydroxide……	29
Figure 2.4.	Chemical structure of aluminum hypophosphite……	30
Figure 2.5.	The chemical reaction for the synthesis of carvone-based polyol…	31
Figure 2.6.	(A) Gel permeation chromatography instrument by Waters system software. (B) Rheometer model AR 2000 dynamic stress. (C) Fourier transformed Infra-red equipment by PerkinElmer Spectrum……	33
Figure 2.7.	Some of the instruments used for foam’s characterization. (A) Ultra Pycnometer Ultra-foam 1000. (B) Instron instrument operated by Blue Hill software**.** (C) Horizontal burner coupled with timer. (D) SEM from Thermo Scientific. (E) TGA from Q500 Discovery from Trios……	37
Figure 3.1.	Gel permeation chromatography for carvone, 2-mercaptoethanol (2-ME), and carvone-based polyol……	39
Figure 3.2.	FTIR spectra for AHP and its starting reagents……	40

Figure 3.3.	FTIR spectra for carvone, 2-mercaptoethanol, and carvone based polyol	41
Figure 3.4.	The chemical reaction for the synthesis of carvone-based polyol (A) along with expected byproduct (B)	42
Figure 3.5.	Rigid polyurethane foams containing EG	44
Figure 3.6.	Rigid polyurethane foams containing ATH	45
Figure 3.7.	Rigid polyurethane foams containing AHP	46
Figure 3.8.	FTIR for the rigid polyurethane foams containing EG	47
Figure 3.9.	FTIR for the rigid polyurethane foams containing ATH	48
Figure 3.10.	FTIR for the rigid polyurethane foams containing increasing concentrations of AHP	48
Figure 3.11.	Density for polyurethane foam containing EG	50
Figure 3.12.	Density for polyurethane foam containing ATH	51
Figure 3.13.	Density for polyurethane foam containing AHP	51
Figure 3.14.	Closed-cell content for rigid polyurethane foams containing EG	53
Figure 3.15.	Closed-cell content for rigid polyurethane foams containing ATH	53
Figure 3.16.	Closed-cell content for rigid polyurethane foams containing AHP	54
Figure 3.17.	Micrographs for the rigid polyurethane foams containing EG	56
Figure 3.18.	Micrographs for the rigid polyurethane foams containing ATH	57
Figure 3.19.	Micrographs for the rigid polyurethane foams containing AHP	58
Figure 3.20.	Compressive strength for EG containing polyurethane foams	60
Figure 3.21.	Compressive strength for ATH containing polyurethane foams	61
Figure 3.22.	Compressive strength for AHP containing polyurethane foams	61
Figure 3.23.	TGA for the foam containing EG in nitrogen atmosphere	66
Figure 3.24.	DTGA for the foam containing EG in nitrogen atmosphere	66
Figure 3.25.	TGA for the foam containing EG in air atmosphere	67
Figure 3.26.	DTGA for the foam containing EG in the air atmosphere	67
Figure 3.27.	TGA for the polyurethanes containing ATH under nitrogen	68
Figure 3.28.	DTGA for the polyurethanes containing ATH under nitrogen	69
Figure 3.29.	TGA for the polyurethanes containing ATH under air	69
Figure 3.30.	DTGA for the polyurethanes containing ATH under air	70
Figure 3.31.	TGA for the polyurethanes containing AHP under nitrogen	71
Figure 3.32.	DTGA for the polyurethanes containing AHP under nitrogen	71
Figure 3.33.	TGA for the polyurethanes containing AHP under air	72
Figure 3.34.	DTGA for the polyurethanes containing AHP under air	72
Figure 3.35.	TGA for pure ATH under nitrogen and air	73
Figure 3.36.	TGA for pure AHP under nitrogen and air	74
Figure 3.37.	FTIR for the foam containing ATH and pure ATH before and after burning	74
Figure 3.38.	FTIR for the foam containing AHP and pure AHP before and after burning	75
Figure 3.39.	Burning time for the polyurethane foams containing EG	78
Figure 3.40.	Weight loss % for polyurethane foams containing EG	79

Figure 3.41. Digital images for the flame retardant rigid polyurethane foams containing EG before and after the burning test..... 80
Figure 3.42. Burning time for the polyurethane foams containing ATH..... 81
Figure 3.43. Weight loss % for polyurethane foams containing ATH..... 81
Figure 3.44. Digital images for the flame retardant rigid polyurethane foams containing ATH before and after the burning test..... 82
Figure 3.45. Burning time for the polyurethane foams containing AHP..... 83
Figure 3.46. Weight loss % for polyurethane foams containing AHP..... 83
Figure 3.47. Digital images for the flame retardant rigid polyurethane foams containing AHP before and after the burning test..... 84
Figure 3.48. Visual aspect of the burnt samples..... 85

LIST OF SCHEMES

SCHEME		PAGE
Scheme 3.1.	Thermal decomposition reaction sequence for AHP……..	75

CHAPTER I

INTRODUCTION

1.1. Polyurethanes: Concepts and development

Polyurethanes are a vital class of polymers due to their vast range of properties and applications. These polymers can be rigid, flexible, elastomeric, thermoplastic, thermoset, and waterborne. The field of application for polyurethanes is related to adhesives, coatings, sealants, binders, and more which transformed the modern industry by introducing low-cost starting materials with high effectiveness. Polyurethanes improved human quality of life in so many aspects that it would be nearly impossible to detach it from daily routine nowadays. The polyurethane industry established its share in the market back in 1937, thanks to the research of Professor Dr. Otto Bayer and colleagues [1]. Since then it thrived reaching currently a $69.2 billion net worth market in 2019, which projects a promising future with an expected growth of around 5.0 to 5.6% per year until 2025 [2]. This increase comes from the many applications of polyurethanes, for example, furniture where a large number of polyurethanes are used for making chairs, mattresses, and sofas. The flexible structure of some foams allows them to be soft yet

resistant to creep maintaining their shape for long period. A common example is the memory foam that adapts according to the body to provide a proper rest, encouraging its use in health centers to relieve pressure sores [3]. The automotive industry also takes advantage of polyurethanes to manufacture seats, armrests, headrests, and interior components due to both lightweight and strong mechanical properties, which make them fit precisely for this use, providing comfort as well as fuel efficiency [4]. The footwear industry uses it for similar reasons, to add comfort, durability, and resistance to abrasion. Due to their low heat transfer properties, polyurethanes are usable as thermal insulators in buildings, which besides providing a pleasant environment also contributes to energy saving due to reduced use of heaters and air conditioning. This supports decreasing emissions of CO_2 and greenhouse gases. For the same reasons, they are widely used in freezers, being responsible for up to 60% improvement of refrigeration efficiency [5]. Another field of their application is in coatings, bonding agents, and sealants due to their stability against corrosion, heat, and radiation, enabling them to connect, or cover, many surfaces like rubber, wood, and even glass [3]. The classification and application of polyurethanes worldwide are shown in **Figure 1.1**.

Polyurethanes are synthesized through a reaction between hydroxyl (-OH) and isocyanate (-N=C=O) groups that lead to the urethane linkage [-HN-C(O)-O-]. To form a polyurethane, both starting materials must be at least bifunctional as described in **Figure 1.2**. This reaction can be performed by using a vast number of starting materials, granting many possible combinations that provide a broad set of properties for the final products, which

is why polyurethanes are so versatile and continue to grow every year. The main reagents required to make polyurethanes are polyols, isocyanates, catalysts, and in some cases surfactants, and blowing agents are also required.

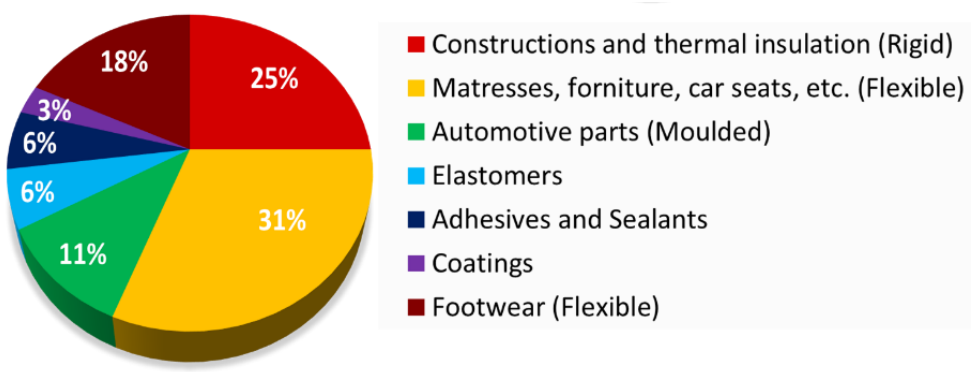

Figure 1.1. Global usage of polyurethanes. "Adapted with permission from [2]. Copyright (2018) Multidisciplinary Digital Publishing Institute."

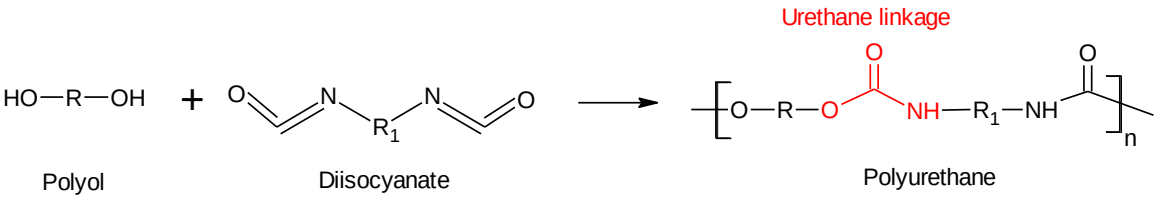

Figure 1.2. A general reaction between polyol and diisocyanate to form a polyurethane [1].

Polyols are compounds with two or more -OH groups. There are two groups of polyols, (polyether, and polyester) which together represent more than 80% of oligo-polyols manufacture [1]. The main starting materials for the synthesis of polyether-based polyols

are given in **Figure 1.3**. Ethylene, propylene, or butylene oxides are effective starting reagents because their structure has significant ring strain (Baeyer's tension). They can be polymerized through ring-opening polymerization, which can be initiated by a starter polyol, which is a compound that contains multiple hydroxyl groups in its structure, which increases the functionality of the final polyol as described in **Figure 1.4**.

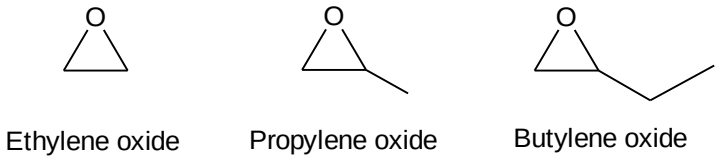

Figure 1.3. Main raw materials for polyether polyols synthesis.

Polyesters are another large group used as polyols that can be synthesized through an esterification reaction mostly between dicarboxylic acids and diols or polyols. A general reaction describing esterification is shown in **Figure 1.5**. Other groups of polyols used for the synthesis of polyurethanes are polycarbonates, polyacrylates, and polybutadiene diols. Their general structures are provided in **Figure 1.6**. The polyol's main chain length is an important factor that dictates the properties of the final polyurethane; high molecular weight polyols (2,000 to 10,000 Da) may yield more flexible polyurethanes while lower molecular weights or smaller polyol molecules, yield rigid ones [1].

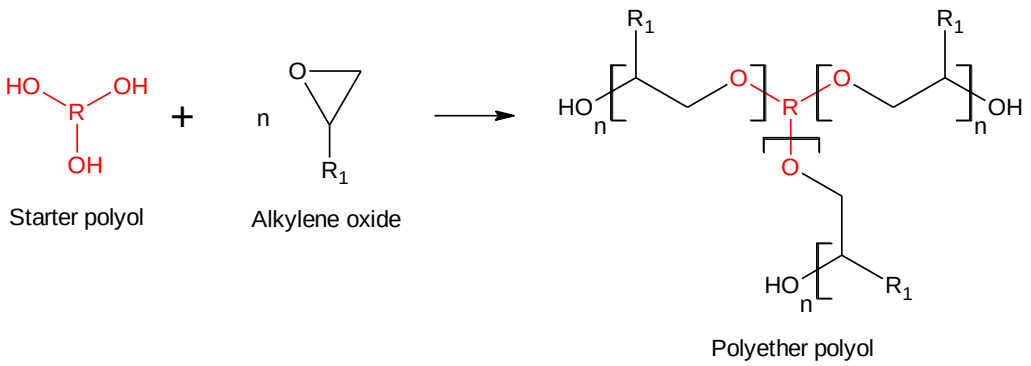

Figure 1.4. A general ring-opening polymerization for polyether polyols. "Adapted with permission from [6]. Copyright (2002) Elsevier."

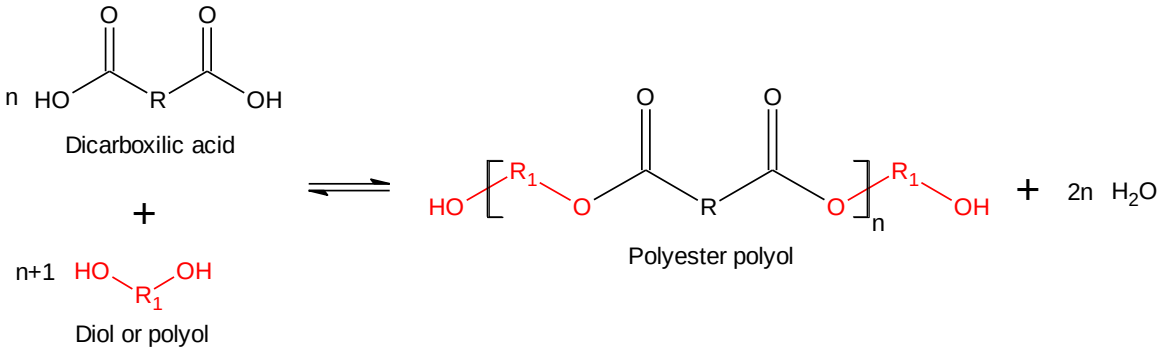

Figure 1.5. A general polyesterification reaction for the synthesis of polyester polyols. "Adapted with permission from [7]. Copyright (2014) American Chemical Society."

Isocyanates are the other main component for the synthesis of polyurethanes. Most of the isocyanates used for the synthesis of polyurethanes are bifunctional and thus referred to as diisocyanates. The molecular structure of isocyanates can vary from more rigid to

flexible, which can influence the properties of the final polyurethanes. For example, with a proper combination of polyols, toluene diisocyanate (TDI) provides polyurethanes with the most rigid structure while hexamethylene diisocyanate (HDMI) produces flexible polyurethanes.

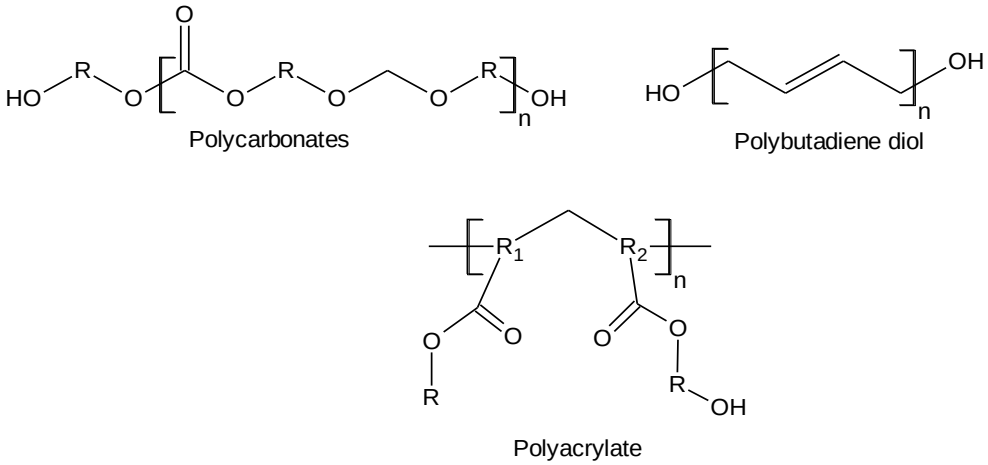

Figure 1.6. A general structure of polycarbonate, polyacrylate, and polybutadiene-based polyols.

Based on their properties, they are used for thermal insulators (rigid), production of mattresses (flexible), soles of shoes (elastomer), etc. **Figure 1.7** shows the name and structure of the most used diisocyanates. Despite the essential role of isocyanates in the synthesis of polyurethanes, these compounds raise concerns regarding their toxicity and environmental issues. There is a growing need to find alternative synthetic routes for polyurethanes that do not demand or at least diminish the use of isocyanates. Recently, non-isocyanate-based polyurethanes are being researched. For example, the reaction

between carbonated vegetable oil with aminosiloxanes yielded a non-isocyanate compound able to react with hydroxyl groups from natural-based materials such as lignin, which demonstrated a promising alternative route [8].

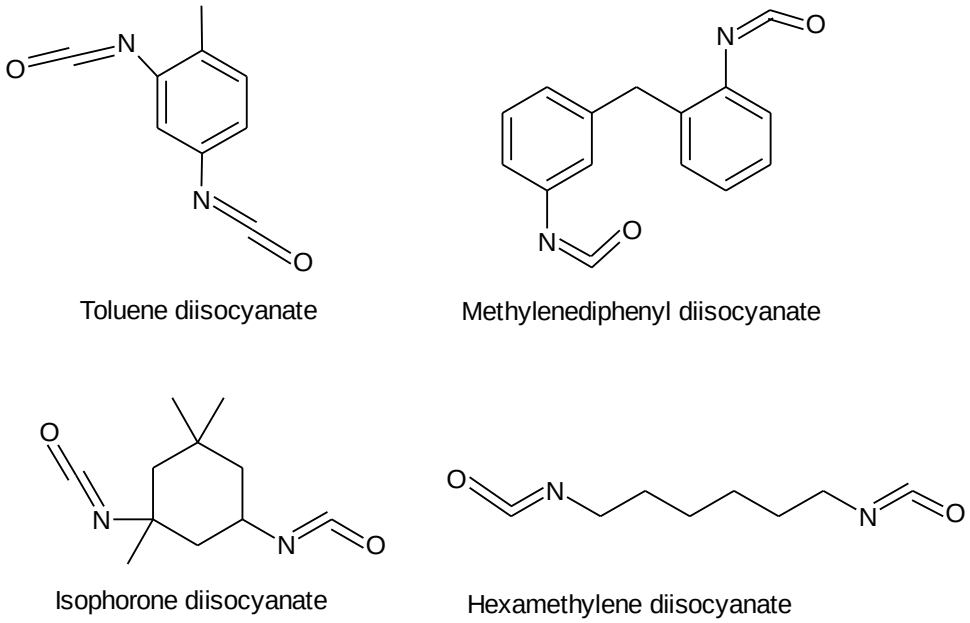

Figure 1.7. Name and structure of most common diisocyanates used for preparation polyurethanes.

The catalysts for polyurethanes are important to accelerate the foaming process, which is crucial for the industry. Mainly two types of catalysts are used, even simultaneously, during the formulation of a foam. They can be amines and/or metal complex-based compounds based on zinc, bismuth, tin, or lead. Some examples of tertiary amine-based catalysts are triethylenediamine (TEDA), dimethylethanolamine (DMEA), dimethyl cyclohexylamine (DMCHA) and, 1,4-diazabicylo[2.2.2]octane (DABCO) [1]. Some of the

most common amine-based catalysts are displayed in **Figure 1.8**. Similar to isocyanates, catalysts for polyurethanes are essential components, especially for large-scale applications, but also present both health and environmental concerns especially for the lead and tin-based, which again drive researchers to develop new approaches that are less harmful and eco-friendly.

Surfactants in polyurethanes play the role of forming an emulsion to allow proper mixing of the components, which is important during the foaming process to control and stabilize cell size as well as the structure of the foam to avoid flaws. When used in non-foaming procedures, surfactants are used to prevent inner bubbles to obtain a uniform surface. Generally, surfactants can be cationic or anionic, the former is used for better emulsification action while the latter provides stability against corrosion [3]. Similar to surfactants, the blowing agents also have the role of controlling the cellular size because of the formation of bubbles within the foam. Blowing agents also minimize the cost due to an increase in the volume of the foams, making them less dense, which requires less material to cover a larger area. However, there is an optimum amount of blowing agent that can be added to the formulation, otherwise, it can compromise the foam's mechanical properties and cellular structure, making it highly friable and brittle. There are two types of blowing agents, chemical and physical. Water is a chemical blowing agent as it reacts with isocyanate during the foaming process to produce CO_2 gas. Water is a preferred blowing agent for many industrial foaming processes due to its effectiveness, low cost, and environmentally friendly nature. Physical blowing agents are mainly gases

that are physically injected during the foaming process. The most commonly used physical blowing agents were chlorofluorocarbons (CFCs) based compounds, although effective they raised many environmental concerns as they can ascend to the stratosphere and deplete the ozone layer. The use of chlorofluorocarbons-based compounds was restricted by the Montreal Protocol back in 1989. Nowadays, aside from water as a chemical blowing agent, *n*-pentane, or methyl methanoate have been used as physical blowing agents.

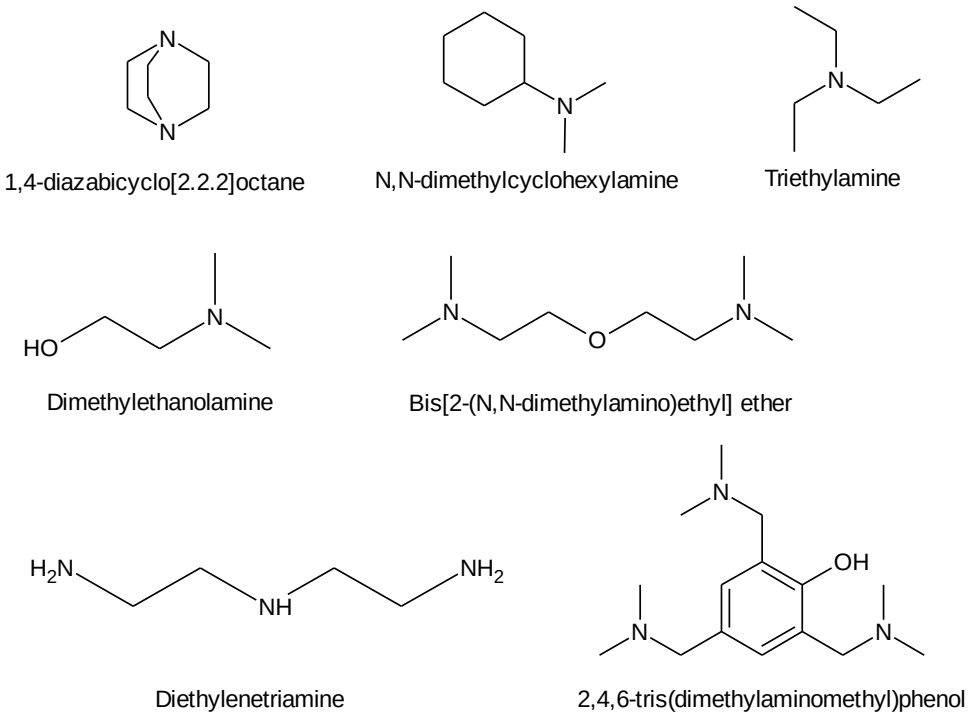

Figure 1.8. Name and structure of common amine-based catalysts.

1.2. Chemistry of bio-based polyurethanes

The worldwide concern about environmental issues came mostly after the escalation of global warming due to high emission levels of greenhouse gases, which led to

international protocols that pushed the development of new materials obtained from renewable sources. This situation led to more investment in recycling. For example, the United States recycled about 8.4% of the produced plastics while Europe recycled about 40% in 2017 [14]. Recycling is a convenient process to reintroduce materials into the production line as it eliminates some of the harvestings of raw materials. Thus, as recycling technology evolves, it can decrease the overall cost of manufacture as well as greenhouse gas emissions that comes from virgin plastics. These are compelling factors for the development of sustainable routes for the manufacture of commercial polymers [11].

Green synthesis involving new methods and chemicals derived from plant-based sources offers advantages for being environmentally friendly compared to oil-derived sources. Plant-based chemicals can be produced annually while oil-based chemicals take several years to regenerate. Another important feature of bio-based materials is the possibility of introducing biodegradability, which not only gives them a proper final destination but also implements a more effective recycling step to the process unlike some petrochemical-based materials [12]. This scenario provides a stable schedule for long-term production and pricing since the harvesting of these renewable sources no longer require petroleum reservoirs that are spread randomly around the globe, which leads to more stability for nations to harvest their resources and decreases the dependence on petro-based materials. Petrochemicals are widely used in many areas such as automotive, households, aircraft, and clothing, which create a large demand for the starting materials,

hence the use of alternative sources decreases the dependence on non-renewable raw materials by providing reasonable and possibly cheaper paths. Many biomass-derived compounds can be used as raw materials for the synthesis of polyols, mostly because of double bonds that can be converted into hydroxyls groups in a variety of ways. Typically, primary or secondary hydroxyl groups are desired in the bio-derived polyols as they are more reactive with isocyanates [13]. The biomaterials suitable for polyols cover a broad range of structures that grant distinct properties to their derived polyurethanes. Examples of suitable biomaterials are triglycerides of oleic, linoleic, and linolenic acids that present one, two, and three unsaturated bonds, respectively along with 18 carbons in its chains. These triglycerides can be found in corn, soybean, canola, rapeseed, olive oil, sunflower oils among others [14].

The depletion, and price instability, of petroleum-based resources along with growing environmental concerns, have created a need to find sustainable starting materials that provide similar properties with production costs comparable to petrochemical-derived products. To attend to this requirement, the scientific community has made efforts to create alternative routes for the synthesis of polyurethanes using renewable sources. From this line of work, bio-polyols were synthesized using various methods. For example, soybean oil that was epoxidized, followed by a ring-opening reaction using methanol provides a rigid polyurethane with mechanical, insulating, and thermal properties similar to petrochemical-based polyurethanes [15]. In another approach, transesterification with glycerol, catalyzed by triethanolamine, was used to synthesize a castor oil-based rigid

polyurethane [16]. Another interesting example was the conversion of rapeseed oil into a polyol through microwave synthesis that yielded a flexible polyurethane [17].

The starting point in considering the use of a bio-oil is the presence of double bonds, which are the versatile reactive sites that can be functionalized in many ways. Conversion of a double bond to -OH group is one of the highly studied and developed processes as it provides a reaction site for the isocyanate to form a urethane linkage [18–20]. Some common examples of bio-oils that have double bonds in their structures and can be converted into polyols are soybean, corn, canola, limonene, carvone, and palm oil [20–22]. Some natural oils can be directly used as polyols to make polyurethanes due to the inherent hydroxyl groups in their structure. Castor and Lesquerella oils are among the few natural oils which possess hydroxyl groups in their structure and therefore could be directly used for the preparation of polyurethanes. Such oils are currently leveraged in the industrial production of polyurethanes as well as in research and development [14].

Initially, the castor oil extracted from the castor plant, *Ricinus communis*, had no commercial use due to its unsuitability for diet and the presence of a deadly protein named ricin [23]. Also, the castor plant spread easily in other commercial crops making it often undesirable for farmers to grow. However, after seeing its commercial value for the production of polyurethanes and increasing demand for renewable resources for industrial applications, there has been increased interest in harvesting castor plants, mostly in India [24]. The increased demand for castor oil for industrial applications is due to the uniqueness of this oil. Castor oil contains almost 90% of a single triglyceride from

glycerin and ricinoleic acid, which contains a secondary hydroxyl group and double bonds as shown in **Figure 1.9** [25]. On the other hand, most of the other plants possess a mixture of several oils. As noted, castor oil contains three hydroxyl groups in its structure which allow its use as a polyol without any chemical modification. Also, the presence of unsaturation opens many possibilities for synthetic approaches, which can provide a wide range of properties. Currently, castor oil is widely used for flexible polyurethane foams, rigid foams, elastomers, and lubricants due to facile growth, extraction, low-cost and satisfactory properties [25].

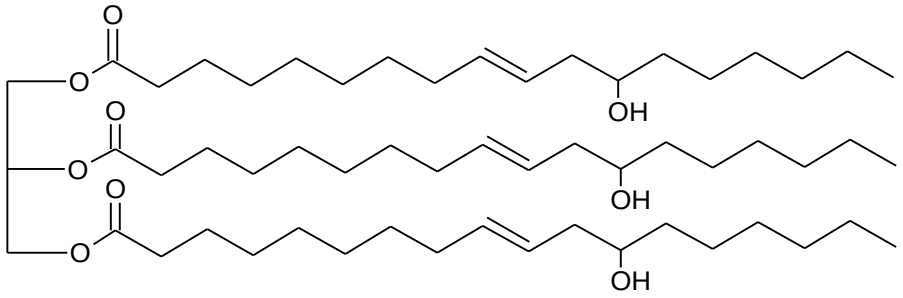

Figure 1.9. The chemical structure of castor oil.

Lesquerella oil, extracted from *Lesquerella fendleri*, also presents a chemical structure similar to castor oil. Lesquerella oil contains a double bond at C_{11} and -OH group at C_{14} in a backbone of 21 carbons. It can be found in slightly dry and alkaline environments, such as the southwestern regions in the United States. Although the chemical structure of Lesquerella oil is suitable for the polyurethane industry, the low quantity of extractable oil from the plant (a maximum of 25% by weight) restricts its industrial applications.

Despite the low industrial demand of *Lesquerella fendleri* for the polyurethane industry, it can be used for food purposes as its seed is non-toxic and contains a high protein concentration of around 35%. Yet, Lesquerella-based polyurethanes have been reported for coating applications, due to their satisfactory chemical stability against corrosive environments [25].

As demonstrated, many vegetable oils can be used in industry as an alternative for non-renewable sources. Among renewable sources for chemicals, the terpenes are a large group of bio-derived materials that mostly originate from plants as well as from insects, fungi, and aqueous microorganisms [26]. In plants, the terpenes are secondary metabolic products that can function as a defense mechanism to expel or attract some insects to induce pollination. These natural compounds were studied by Dr. Otto Wallach, which won the Nobel Prize in Chemistry in 1910 for his research on alicyclic compounds. He analyzed the structural pattern of terpenes and created the 'Isoprene rule' which stated that terpenes are substances with a 2-methyl-1,4-butadiene backbone that are derived from condensation reactions [27]. Later in 1950 Leopold Ruzicka, also a Nobel Prize winner in Chemistry in 1939, proposed the 'Biogenic isoprene rule' that stated that besides condensation, terpenes can also be obtained through cyclization and rearrangement from precursors such as geranyl pyrophosphate, which can form different structures of terpenes [28]. The chemical structure of a few terpenes is shown in **Figure 1.10**. As noted, terpenes present a diverse number of structures that derive from similar carbon skeletons, yielding different structures. They also present oxygenated derivatives

named terpenoids that bear functions as carboxylic acids, aldehydes, ketones, and alcohols. This broad range of materials find applications as insecticides, repellents, cosmetics, medicines, and many others [26, 29–33]

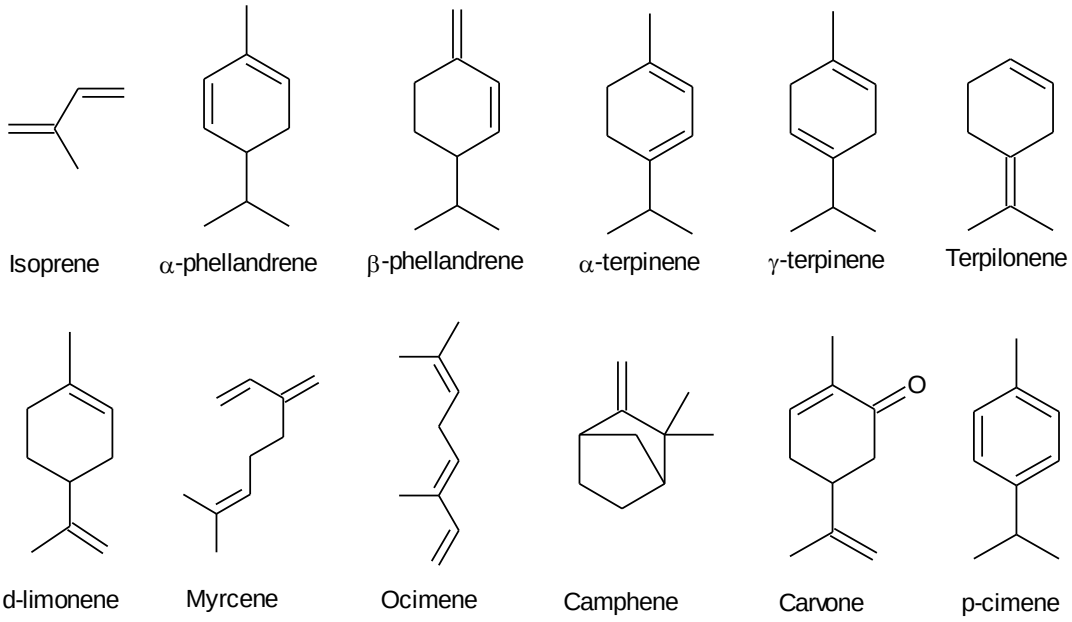

Figure 1.10. Chemical structure of some terpenes.

Recently, terpenes have gained more presence in polymer and materials science. However, these compounds were noticed mostly following the work of Hermann Staudinger, the 'father of polymer science', due to his work in the 'macromolecular hypothesis' that awarded him the Nobel Prize in 1953 [34]. The basis of his work consisted of reactions with isoprene which had a great impact in the industry to produce latex. Isoprene is the main component of gloves, balloons, swim caps, and others.

The 1,4-addition polyisoprene received special attention because the double bond in the middle of the main chain allows crosslink bonds. Because of that, Goodyear developed a process named “vulcanization”. It consisted of a mixture of a copolymer of polyisoprene and polystyrene with orthorhombic sulfur (S_6) that breaks the double bonds creating a chemical linkage between two polymeric chains. This process enhanced the mechanical properties, which made possible the application in tires for vehicles [35].

Among terpenes, limonene is a low-cost and versatile chemical that can be used in the preparation of polyurethanes. A group of researchers performed an interesting green approach by using limonene oxide and carbon dioxide as monomers to synthesize a bio-derived polymer named poly(limonene carbonate) shown in **Figure 1.11** [36]. This synthesis is one of the rare cases in which carbon dioxide, a greenhouse gas, is incorporated into a polymeric chain along with a bio-derived material. These starting materials make this process both profitable and environmentally friendly.

In theory, this process can be applied to most bio-derived materials that present at least one double bond that can be epoxidized. Also, the polymerization procedures do not require a large use of energy or expensive catalysts [36, 37]. Even 100% bio-derived and isocyanate-free routes for polyurethane were obtained from the work of Bahr et al. [38] as described in **Figure 1.12**.

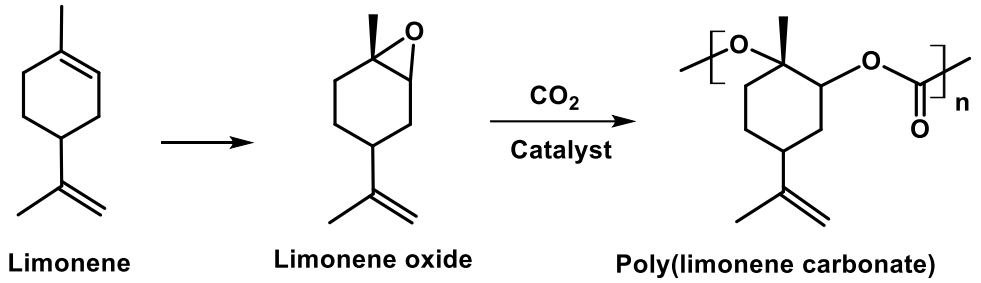

Figure 1.11. The polymerization reaction of poly(limonene carbonate).“Adapted with permission from [36]. Copyright (2015) The Royal Society of Chemistry.”

Terpenes can be converted into polyols through several chemical approaches. Among those, thiol-ene is a convenient method that uses UV-light, either from an electric source or sunlight, mild conditions such as room temperature, and solvent-free procedures. Hence, a facile and environmentally friendly method. Based on that, many authors reported terpene or terpenoid-based polyols used for polyurethanes that yielded satisfactory properties compared to petro-based polyurethanes [18, 19, 22]. For example, Gupta et al. used a thiol-ene reaction to synthesize limonene-based polyol for polyurethanes [19, 39, 40]. A derivative of limonene, limonene dimercaptan, was also used for the preparation of polyol as shown in **Figure 1.13**. The polyurethane foams prepared from these limonene-based polyols showed thermal stability up to 250 ^{o}C with regular shaped cells and uniform cell size distribution. Also, the highest compressive strength found among the synthesized foams in this study was 195 kPa. Terpenes were also chemically modified through other procedures. For example, Gupta and his team

used limonene as a starting material for the synthesis of a polyol through the Mannich reaction [39]. The Mannich polyol was synthesized in three steps. In the first step, Friedel–Crafts alkylation of phenol with limonene was carried out in the presence of HBF_4 as a catalyst (**Figure 1.14**). In the second step, the Mannich base was synthesized by the reaction of oxazolidine with phenol alkylated limonene. In the third step, the Mannich base was propoxylated to synthesize Mannich polyol. The polyurethane foams prepared using limonene base Mannich polyol showed thermal stability up to 250 °C with a high glass transition temperature of ~200 °C. The high reactivity of the limonene-based Mannich polyol makes it suitable to be as "spray" polyurethane foam. Another example of terpenes that can be converted into polyurethane is α-phellandrene. This compound is a monoterpene that contains two endocyclic carbon double bonds in its structure. Elbers and his colleagues have used thiol-ene chemistry to synthesize an α-phellandrene based polyol for the preparation of rigid polyurethane foams [19]. α-phellandrene reacted with 2-mercaptoethanol and α-thioglycerol to form two polyols with different hydroxyl functionalities as shown in **Figure 1.15**. The prepared polyurethanes showed high closed-cell content (over 90%) with apparent density in the range of 28-39 kg/m^3. It was observed that the polyol synthesized using α-phellandrene and α-thioglycerol provided higher compressive strength of 220 kPa which could be due to the higher hydroxyl functionalities of the polyol compared to polyol synthesized using α-phellandrene and 2-mercaptoethanol.

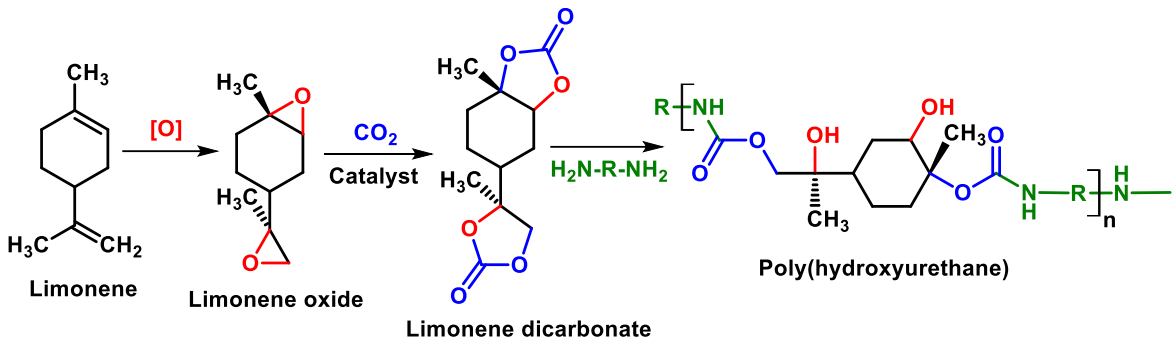

Figure 1.12. Synthesis of a limonene oxide-based polyurethane through isocyanate-free polymerization. "Adapted with permission from [38]. Copyright (2012) The Royal Society of Chemistry."

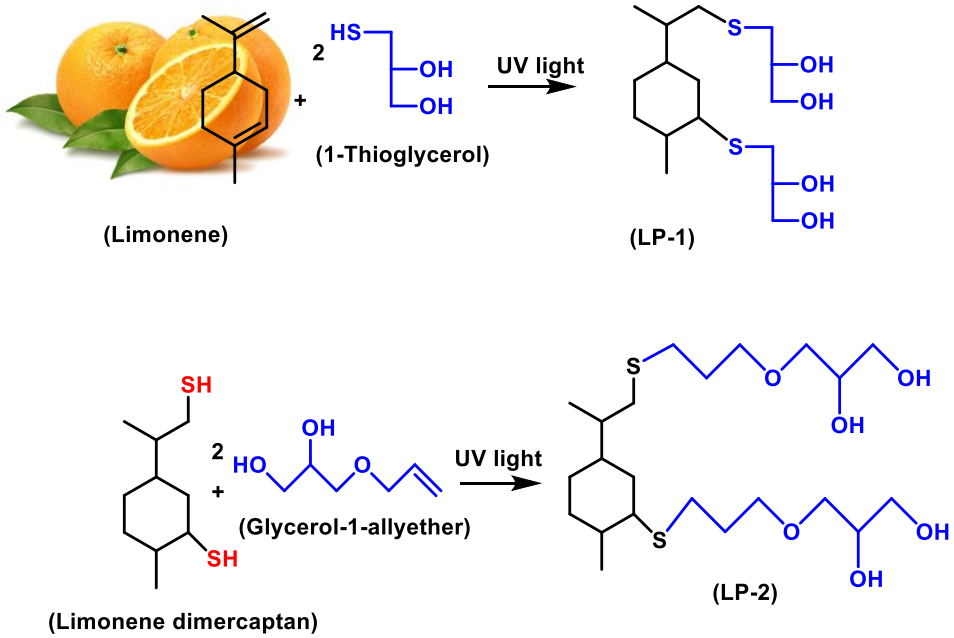

Figure 1.13. Synthesis of polyols based on limonene by using thiol-ene ''click'' chemistry. "Adapted with permission from [41]. Copyright (2014) Springer Nature."

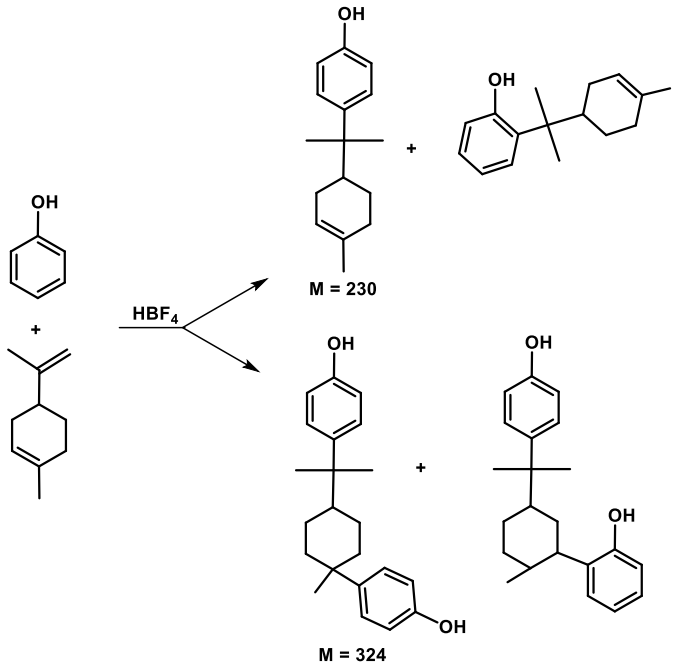

Figure 1.14. Possible structures of phenol alkylated with limonene. "Adapted with permission from [39]. Copyright (2015) Springer Nature."

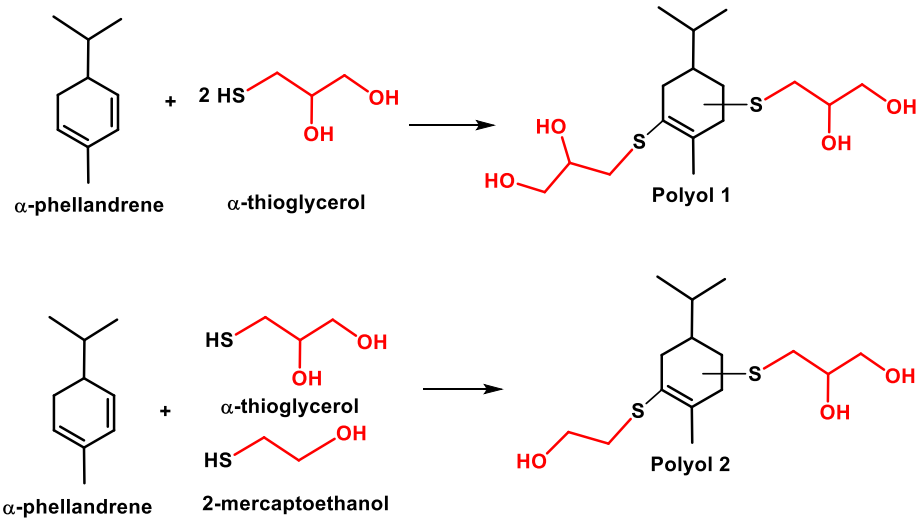

Figure 1.15. Synthesis of polyols based on α-phellandrene by thiol-ene ''click'' chemistry. "Adapted with permission from [19]. Copyright (2017) Journal of Renewable Materials."

1.3. Flame-retardant polyurethane foams

Despite all the effective properties of polyurethanes that make it versatile for many applications that include a wide range of mechanical properties, low density, and facile processing, it also carries an inherent issue, which is poor fire resistance. Based on that, the use of components able to improve its flame resistance is of extreme importance. Compounds known as flame retardants (FR) can be classified into two categories. The first is the additive FR, which are materials that are physically blended during prepolymer preparation. These are not incorporated into the chemical structure of polyurethane. Most of the procedures use additive FR due to the facile, lower-cost procedure, generally effective and lack of an active site on the FR molecule to enable chemical attachment with the polymeric matrix. Some drawbacks can occur such as slow migration of the FR over time, which may cause unstable behavior against fire, because of phase separation. Also, excessive amounts of additive FR may be required to achieve a satisfactory flame retardant. This factor may imply an increase of mixing due to increased viscosity and negatively affect some properties such as mechanical, along with an increase in density [42, 43].

The second category is known as reactive FR. In this case, the FR molecule is chemically introduced into the polymeric structure. It adds an extra synthetic step, which increases cost. However, lower amounts of reactive FR are usually required to achieve effective FR properties. Also, the FR active molecules are more evenly distributed throughout the polyurethane, which allows it to have consistency in the flame retardancy throughout the

foam. The FR molecule can be incorporated into the backbone of the polyurethane or as a grafting group. The latter, in some cases, may yield a dangling group on the chain that lowers the mechanical strength due to the plasticizer effect [42, 44].

The effect of diminishing flammability can occur through different forms, in which the main objective is to cease the fire and smoke generated during the combustion process. The effect can be directed to diminish the heat, smoke being released, thermal degradation (pyrolysis), and dilution of oxygen in the media. The mechanism in which it takes place can be divided into two main forms: one is physical activity and the other is chemical action. The physical action is occasioned when an FR can absorb the heat of the environment to undergo an endothermic reaction, usually referred to as a "heat sink". The FR is then converted into a thermostable char layer that can physically separate the combustible material and oxygen. Simultaneously, inert gases are also released such as CO_2, NH_3, and H_2O, that dilute the concentration of oxygen by creating a diffuse gas layer while cooling down the system. Aluminum trihydroxide (ATH) and magnesium dihydroxide (MDH) are classic examples of materials that present this type of mechanism, in which, during their endothermic decomposition, there is the formation of a metal oxide, layer and mostly water vapor that is released to cooldown the neighborhood below the polymer's combustion temperature.

The chemical action can be subdivided into physical phases where it happens: the gas phase and the condensed phase. The gas-phase mechanism occurs when an FR releases volatile radical fragments such as $Cl^{\bullet}$, $Br^{\bullet}$, $PO^{\bullet}$, $PH_2^{\bullet}$ among others. These radicals play

the important role of scavenging $H^{\bullet}$ and $OH^{\bullet}$ to form either stable volatile substances or less reactive ones. It is an effective mechanism to quench the fire because the species $H^{\bullet}$ and $OH^{\bullet}$ are highly reactive pyrolytic products. Hence, when they come in contact with the polymeric matrix a highly exothermic process occurs releasing more heat and propagating the fire. Thus, by preventing these radical species from reaching the unburnt polyurethane the flames can be more rapidly extinguished. The condensed phase mechanism takes place when the FR forms a compact char layer that acts as a shield, preventing the permeation of oxygen and radical species within the polyurethane. This char layer is usually composed of the thermal decomposition of the FR as well as the degraded polymer. The latter forming a carbonaceous or vitreous layer. The other possible way to prevent fire by a solid-phase mechanism is through dripping, which removes the fraction of the polymer that is on fire. However, this effect may not be desired in closed environments since the dripping material may just propagate the fire in another area.

1.4. The objective of this research

The objective of this work was to synthesize a bio-based polyol to make rigid polyurethane foams and blend them with flame retardants to improve their fire resistance. A facile thiol-ene method was used to convert an essential oil named carvone into a polyol. This essential oil is extracted from bay leaf (*Laurus nobilis*), spearmint (*Mentha spicata*), caraway (*Carum carvi*), and dill (*Anethum graveolans*) [29]. The carvone-based polyol was

used to make rigid polyurethane foams. Then flame retardancy properties were introduced to each of the foams by individually adding three flame retardants, those being expandable graphite, aluminum trihydroxide, and aluminum hypophosphite.

CHAPTER II

EXPERIMENTAL DETAILS

2.1. Starting materials

2.1.1. Isocyanate

Isocyanates are key components for the synthesis of polyurethanes and despite presenting a lesser number of commercially available materials compared to polyols, their chemical structure also influences the properties of the final polyurethane. Its reaction with hydroxyl groups yields the urethane linkage through an addition reaction. The isocyanate composes the phases known as the hard domains of the polyurethane since the urethane linkage can form hydrogen bonds with other polymeric chains, hence decreasing the mobility. On top of that, most of the isocyanates used in industry, especially for the development of more rigid polyurethanes, are aromatic which are inherently rigid chemical structures. The most common examples are methylene diisocyanate (MDI) and TDI. In this work, MDI was used as the diisocyanate. Its chemical structure is provided in **Figure 2.1**, named as Rubinate M isocyanate. Its -N=C=O content was around 31%, equivalent weight was 135, and viscosity was 0.21 Pa.s at room

temperature. It was kindly provided by Huntsman Industry, located in Woodlands, TX, USA.

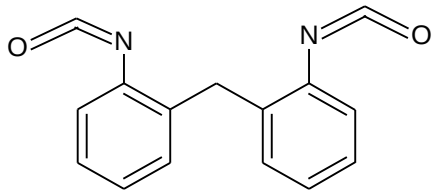

Figure 2.1. Chemical structure of MDI.

2.1.2. Polyols

Polyols are the most explored compounds for the synthesis of polyurethanes and are defined as reagents with multiple hydroxyl groups. The chemical structure of these components is inherently related to the final properties of PUF, hence its great importance. In this work, carvone was used as a starting material for the synthesis of the carvone-based polyol, it was purchased from Sigma-Aldrich, St. Louis, MO, USA. 2-mercaptoethanol is the other main component for the synthesis, which has a low viscosity of 0.0068 Pa.s, a molecular weight of 78.13 g/mol and it decomposes around 158 °C. It was purchased from Acros Organic, USA. To complement the formulation a commercially available polyol based on sucrose was also employed, named Jeffol 520. It was also donated by Huntsman Industry, located in Woodlands, TX, USA. Jeffol 520 has a hydroxyl number of 520 mg KOH/mg, the functionality of 5, a viscosity of around 27.0 Pa.s

molecular weight of 539 g/mol, the equivalent weight of 108, and specific gravity of around 1.17 at room temperature.

2.1.3. Photoinitiator

The thiol-ene reaction is a radical addition that requires UV-light along with a photocatalyst initiator to cause a monolithic scission and generate a radical that can form a thyil radical able to break the double bonds and start the desired reaction. For that purpose, 2-hydroxy-2-methyl propiophenone was used. It was purchased from Sigma-Aldrich, St. Louis, MO, USA.

2.1.4. Catalyst

Catalysts are important to increase the reaction rate and guarantee an effective curing process, being critically important for industries. Two main types of catalysts often used are tertiary amine and organometallic based. For that, NIAX-A1 and T-12 were used, respectively. Both were acquired from Air Products, Allentown, PA, USA.

2.1.5. Blowing agent

Distilled water was used as the blowing agent in this work as it is a viable, low-cost, and eco-friendly material. It plays the role of controlling the polyurethane's cellular structure, as it can also be used to control the density. The purpose of water is to react with the isocyanate which forms an unstable carbamic acid that quickly decomposes into a primary amine and CO_2, which is the gas responsible for making the foamed and porous structure. The distilled water was purchased from the local Walmart, Pittsburg, KS.

2.1.6. Surfactant

Isocyanates and hydroxyl groups present high reactivity towards each other. However, they form a heterogenous phase due to a lack of attractive intermolecular interactions. To prevent that, surfactants are used to form a stable dispersion, that leads to foam's regular pore size while it prevents coalescence of bubbles during the foaming process, which forms the porous structure of rigid foams. To that end, B-8404 was employed in this work. It was bought from Evonik, Parsippany, NJ, USA.

2.1.7. Flame-retardants

There were three additives FR investigated in this work:

A. Expandable graphite

Expandable graphite is a balanced material that retains the main characteristics of graphite such as low cost, electrical conductibility, abundance, and enhanced FR properties. The synthesis of this material consists of mixing graphite flakes with concentrated sulfuric acid along with strong oxidizing agents such as hydrogen peroxide [45, 46]. This procedure creates a structure that consists of a graphite layer intercalated with sulfate anions. The structure of EG is displayed in **Figure 2.2** [47]. It was purchased from Sigma-Aldrich, St. Louis, MO, USA.

B. Aluminum trihydroxide

Aluminum trihydroxide is one of the most used FR in the industry due to its inexpensive cost and environmentally friendly features, even though it often requires high loading to

be effective as FR. It was purchased from Sigma-Aldrich, St. Louis, MO, USA. The chemical structure of ATH is given in **Figure 2.3.**

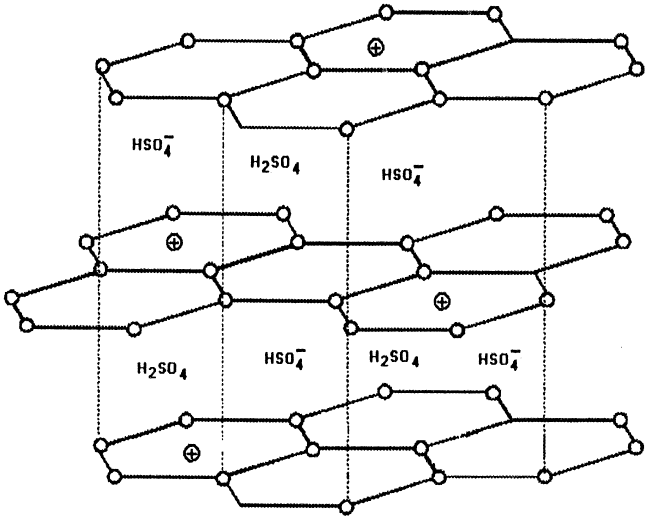

Figure 2.2. Chemical structure of expandable graphite [47].

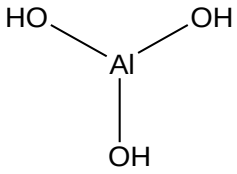

Figure 2.3. Chemical structure of aluminum trihydroxide.

C. Aluminum hypophosphite

Aluminum hypophosphite (AHP) is an inorganic salt that combines the FR properties of Al and P, providing an interesting synergy effect, while it is also an eco-friendly material and relatively low cost if compared with other P-based FR. The reagents used for its synthesis were aluminum chloride hexahydrate ($AlCl_3.6H_2O$) and sodium hypophosphite dihydrate ($NaPO_2H_2 \cdot 2H_2O$) all purchased from Sigma-Aldrich, St. Louis, MO, USA. AHP was

synthesized through the following procedure: In a 250 mL three-necked flask, 50.88 g (0.48 mol) of $NaH_2PO_2.2H_2O$ was dissolved in 30 mL of distilled water and stirred for 15 min at 50 °C. After complete dissolution, the temperature was raised to 85 °C and maintained for 25 min. A solution containing 38.54 g (0.16 mol) of $AlCl_3.6H_2O$ was prepared and added dropwise. The reaction mixture eventually became hazy producing a white precipitate. The temperature of the reaction mixture was maintained at 85 °C for 1h. The white product was filtered at room temperature and washed with distilled water. After that, it was dried in the oven at 100 °C [48]. The expected chemical structure of AHP is shown in **Figure 2.4.**

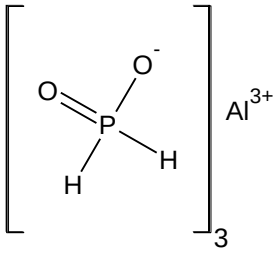

Figure 2.4. Chemical structure of aluminum hypophosphite.

2.2 Synthesis of carvone-based polyol

For the synthesis of carvone-based polyol (C-ME-Polyol), 100 g of carvone was reacted with 150 g of 2-mercaptoethanol in the presence of 2-hydroxy-2-methyl propiophenone (3 wt.%) as a photoinitiator in a 250 mL flask. The system was exposed to UV light (365 nm) under continuous stirring for 8 h. The photoinitiator catalyzes the homolytic scission of the S-H bond into a thyil (-$S^{\bullet}$) and hydrogen ($H^{\bullet}$) radicals. The $S^{\bullet}$ reacts with the double bonds through radical addition forming a new C-S bond. Through that, a primary hydroxyl

group is chemically introduced into the carvone molecule due to the presence of this group in 2-mercaptoethanol's structure. **Figure 2.5** shows the thiol-ene reaction for the synthesis of polyol.

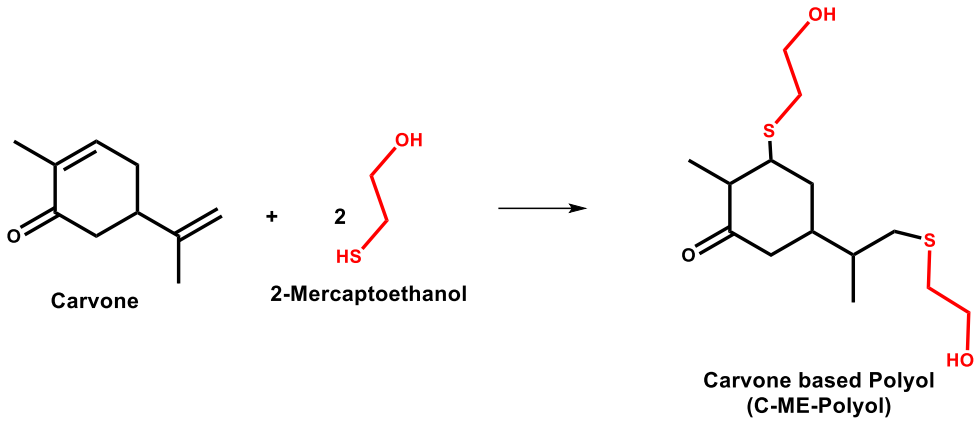

Figure 2.5. The chemical reaction for the synthesis of carvone-based polyol [22].

2.3. Characterization of polyols

The characterization methods adopted in this thesis were based on the American Society for Testing and Materials (ASTM) and International Organization for Standardization (ISO) and applied in the starting materials as well as products.

2.3.1. Gel permeation chromatography (GPC)

Gel permeation chromatography was performed on the polyol and starting materials using a Waters system from Milford, Massachusetts. The system consists of a column with the dimensions of 300 × 7.8 mm with different pores from 50 and 102 to 104 Å. The standard eluent used was tetrahydrofuran injecting 20 µL for 50 min per sample at 30 °C.

2.3.2. Viscosity measurement

The viscosity of carvone, polyol, and Jeffol 522 was measured using a TA Instruments rheometer from New Castle, Delaware at room temperature by increasing the shear stress from the range of 0.1 to 100 Pa. A cone with a 2° angle and 25 mm diameter was used.

2.3.3. Fourier transform infrared spectroscopy (FT-IR)

FT-IR spectra were obtained using a PerkinElmer Spectrum two from Waltham, Maryland.

2.3.4. Iodine value

By using the Hanus method, the iodine number for carvone was determined.

2.3.5. Hydroxyl number determination

The hydroxyl number of the polyol was obtained according to ASTM E1899-16 Method by reacting the polyol with *p*-toluenesulfonyl isocyanate (TSI) followed by potentiometric titration (888 Titrando, Tiamo Software system by Metrohm, AG, Switzerland).

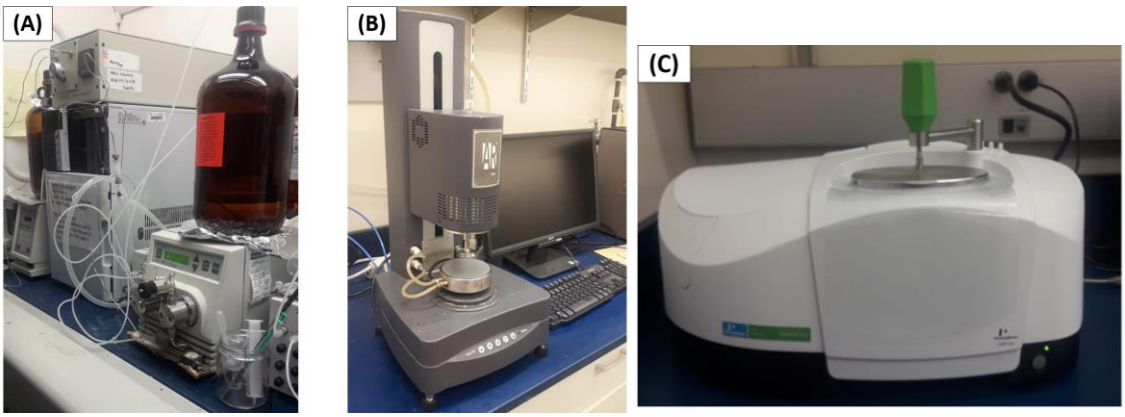

Figure 2.6. (A) Gel permeation chromatography instrument by Waters system software. (B) Rheometer model AR 2000 dynamic stress. (C) Fourier transformed Infra-red equipment by PerkinElmer Spectrum.

2.4. Preparation of flame-retardant rigid polyurethane foams

The rigid FR PUFs were prepared through the one-shot method, which consisted of mixing all the ingredients, except isocyanate in one plastic cup. After that, isocyanate was added and quickly stirred to make the polyurethane foam. In a detailed description: First, in a 500 mL plastic cup, Polyol, Jeffol 520, and FRs were added and stirred at 3,000 rpm to guarantee a homogenous system, because the solid particles of FR must disperse into the polyol for an even distribution throughout the foam. Then all the other ingredients except isocyanate were added. Hence, water, surfactants, and catalysts were added and stirred for around 30 s. After that, MDI, the isocyanate, was quickly charged into the plastic cup and the system was again stirred to make the rigid polyurethane foams. There were three sets of FR foams each one with increasing amounts of each FR. The Foams EG, ATH, and

AHP contained their respective flame retardant. **Table 2.1**, **2.2,** and **2.3** describe the formulation for the foams containing EG, ATH, and AHP, respectively.

Table 2.1. Formulation for polyurethane foams containing EG, with the weight reported in grams.

Components	**Jeffol**	**C-0**	**EG 0.5**	**EG 1.5**	**EG 3**	**EG 5**	**EG 8**	**EG 10**
Polyol	0	10	10	10	10	10	10	10
Jeffol 520	20	10	10	10	10	10	10	10
A-1	0.14	0.14	0.14	0.14	0.14	0.14	0.14	0.14
Water	0.8	0.8	0.8	0.8	0.8	0.8	0.8	0.8
T-12	0.04	0.04	0.04	0.04	0.04	0.04	0.04	0.04
B8404	0.4	0.4	0.4	0.4	0.4	0.4	0.4	0.4
MDI	37.14	33.39	33.39	33.39	33.39	33.39	33.39	33.39
EG	0	0	0.5	1.5	3	5	8	10
% EG	0	0	0.91	2.67	5.19	8.37	12.75	15.44

Table 2.2. Formulation for polyurethane foams containing ATH, with the weight reported in grams.

Components	**ATH-1**	**ATH-2**	**ATH-3**	**ATH-4**	**ATH-5**	**ATH-6**
Polyol	10	10	10	10	10	10
Jeffol 520	10	10	10	10	10	10
A-1	0.14	0.14	0.14	0.14	0.14	0.14
Water	0.8	0.8	0.8	0.8	0.8	0.8
T-12	0.04	0.04	0.04	0.04	0.04	0.04
B8404	0.4	0.4	0.4	0.4	0.4	0.4
MDI	33.39	33.39	33.39	33.39	33.39	33.39
ATH	0.5	1.5	3	5	8	10
% ATH	0.91	2.67	5.19	8.37	12.75	15.44

Table 2.3. Formulation for polyurethane foams containing AHP, with the weight reported in grams.

Components	AHP-1	AHP-2	AHP-3	AHP-4	AHP-5	AHP-6
Polyol	10	10	10	10	10	10
Jeffol 520	10	10	10	10	10	10
A-1	0.14	0.14	0.14	0.14	0.14	0.14
Water	0.8	0.8	0.8	0.8	0.8	0.8
T-12	0.04	0.04	0.04	0.04	0.04	0.04
B8404	0.4	0.4	0.4	0.4	0.4	0.4
MDI	33.39	33.39	33.39	33.39	33.39	33.39
AHP	0.5	1.5	3	5	8	10
% AHP	0.91	2.67	5.19	8.37	12.75	15.44

2.5. Characterization of the rigid polyurethane foams

To better understand the properties of the polyurethanes several characterizations were performed which are described in the following sessions, some of the instruments are displayed in **Figure 2.7**.

2.5.1. Apparent density

The apparent density of the foams was measured by adopting the ASTMD 1622 related to the density of rigid cellular plastics. The foams were cut into a cylindrical shape with a height and diameter of 30 and 45 mm, respectively. The weight of the cylinders was then measured on a scale with ± 5 mg precision.

2.5.2. Compression test

To determine the foam's compressive strength the samples were cut into cylinders with the dimensions of 30 and 45 mm of height and diameter, respectively. Then, the foams

were compressed to the yield at the break, with a compression rate of 3 cm/min. An Instron instrument from Raileigh, NS, the USA operated by Blue Hill software was used for the measurement, which complied with ISO 844:2016.

2.5.3. Closed-cell content

To measure the closed-cell content for the foams an Humi Pyc Ultra pycnometer and relative humidity (RH) instrument were used.

2.5.4. Thermogravimetric analysis (TGA)

The thermal behavior of the foams was analyzed through TGA using a Q500 Discovery from Trios, New Castle, DE, USA. The analysis was performed separately in air rich and nitrogen atmosphere from 25 to 700 °C, at ramp temperature of 10 °C increase per minute.

2.5.5. Scanning electron microscope

Cubes of 0.5 cm^3 volume were cut and used to obtain images for SEM by using a Phenom Particle X AM Desktop SEM by Thermo Scientific, USA. For enhanced imaging, a Magnetron Sputtering along with a monitor from Kurt J. Lesker Company (Jefferson Hills, PA, USA) was used to perform gold (Au) sputtering on the samples' surface to coat it with a thin layer of Au. The system was flushed several times with Ar gas. Also, a 50 mBar vacuum was applied while the samples were exposed to the plasma bean for 1 minute.

2.5.6. Horizontal burning test

Fire retardancy was determined by adopting the ASTM D 4986-18 standard test, which consisted of applying a direct flame onto the sample with dimensions of 150 × 50 × 12.5

(mm^3) height, length, and thickness respectively, in a horizontal position for 10 s. After removal of the flame, the time taken for the sample to quench the fire by itself along with the weight loss percentage was recorded.

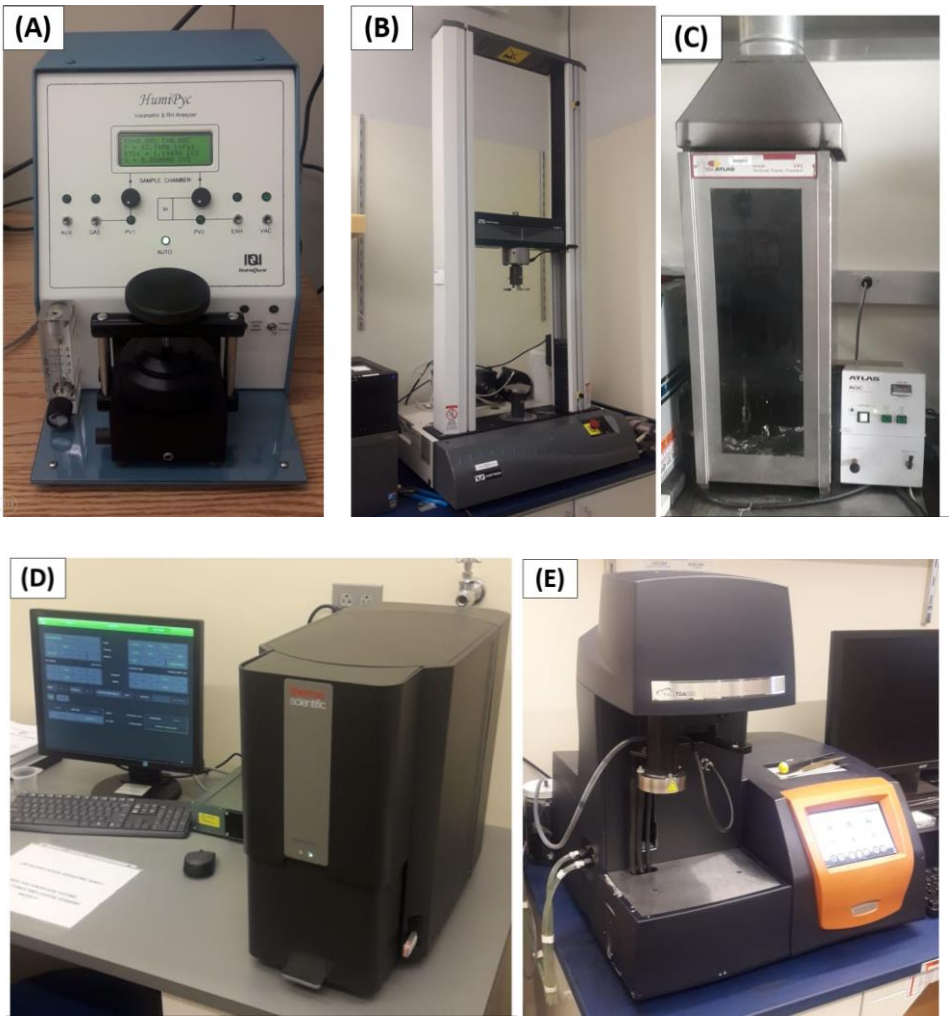

Figure 2.7. Some of the instruments used for foam characterization. (A) Ultra Pycnometer Ultra-foam 1000. (B) Instron instrument operated by Blue Hill software**.** (C) Horizontal burner coupled with timer. (D) SEM from Thermo Scientific. (E) TGA from Q500 Discovery from Trios**.**

CHAPTER III

RESULTS AND DISCUSSIONS

3.1. Polyol data and discussions

3.1.1. Gel permeation chromatography

The GPC chromatogram for carvone, 2-ME, and Polyol is ascribed in **Figure 3.1**. The reduced retention time for polyol (36 min) as compared to carvone (42 min) suggests an increase in the molecular weight of polyol. No extra peaks were observed in GPC curves for unreacted compounds, which confirms that the reaction was completed. The carvone structure consists of two double bonds which are relatively exposed for radical addition of mercaptan group. The increase in molecular weight, observed by the decrease in elution time, showed that the reaction occurred. The peak at 38 min could be linked to the disruption of both double bonds of carvone that reacted with 2-ME to form the polyol. However, thiol-ene reaction forms carbon radicals that can react with each other leading to oligomers, which is related to the peak at 36 min. Similar behavior has been previously reported by other researchers [49, 50].

3.1.2. Viscosity measurement

The reaction proceeding for polyol synthesis can also be correlated to an increase in viscosity of Polyol (2.70 Pa.s) compared to that of carvone (0.0062 Pa.s.). The viscosity of a commercial polyol (Jeffol 522) was 26.59 Pa.s. Jeffol 522 is a sucrose-based polyol with a hydroxyl number of 520 mg KOH/g and a hydroxyl functionality of 5. Although the viscosity value for polyol showed an obvious increase as compared to carvone, it was low in terms of materials processing and mixing and therefore allowed easy processing for PUF [51].

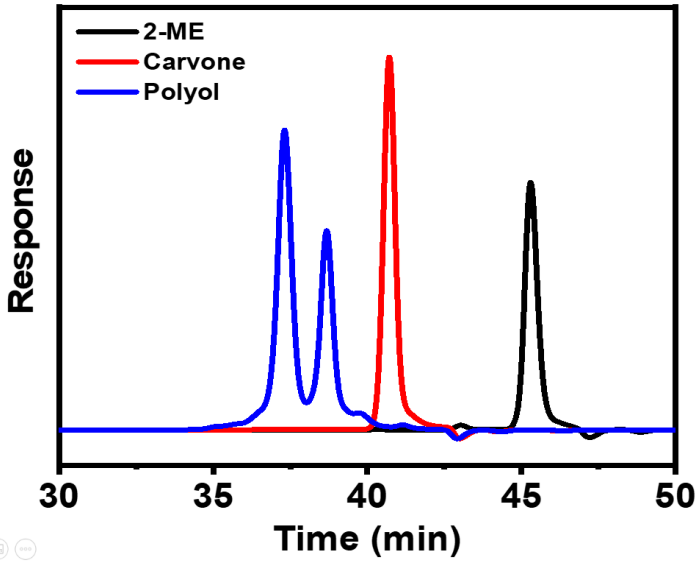

Figure 3.1. GPC for carvone, 2-ME, and carvone-based polyol.

3.1.3. Fourier transform infrared spectroscopy

The structural analysis of synthesized AHP was performed using FTIR spectroscopy. As seen in **Figure 3.2**, the peak near 1100-1200 cm^{-1} is related to P=O [52]. The stretch around 1085-1075 cm^{-1} is related to PH_2 stretch in both $NaPO_2H_2 \cdot 2H_2O$ (NaHP) and AHP spectra [53]. The peak around 500 cm^{-1} is due to Al-O stretch in both $AlCl_3.6H_2O$ and AHP [54, 55]. Other peaks were observed for $AlCl_3.6H_2O$ structure such as Al-OH stretch at 1200 cm^{-1} and two peaks related to OH stretch, one at 1600 and the other at 2500 cm^{-1} [53]. The characteristics peaks of AHP observed in the FTIR spectrum confirm its formation.

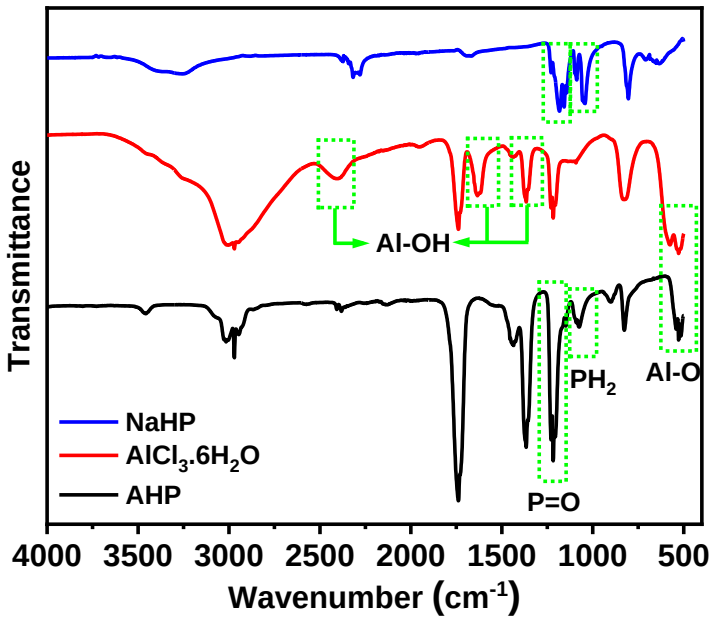

Figure 3.2. FTIR spectra for AHP and its starting reagents.

The proceedings for the thiol-ene reaction between carvone and 2-ME were analyzed using FT-IR spectra shown in **Figure 3.3**. For carvone, there is a stretching vibration for the carbon-carbon double bond around 3008 cm^{-1} and a signal at 895 cm^{-1} related to =C-H bend [49, 56]. While, for 2-ME, the weak vibration band at 2568 cm^{-1} represents the S-H bond, and the large band at 3416 cm^{-1} is assigned to the O-H bond stretch [57]. After the thiol-ene reaction, the S-H stretch, =C-H stretch, and the =C-H bend, at 2568, 3008, and 895 cm^{-1}, respectively, disappeared due to the consumption of carbon-carbon double bonds for the formation of a CH-S bond in the range of 600-700 cm^{-1} with a simultaneous appearance of O-H stretch at 3385 cm^{-1} and C-O stretch at 1094 cm^{-1} for Polyol [13, 20, 26]. Similar behavior was reported by Feng et al.[57] for the synthesis of soybean oil and 2-ME based polyol via thiol-ene reaction.

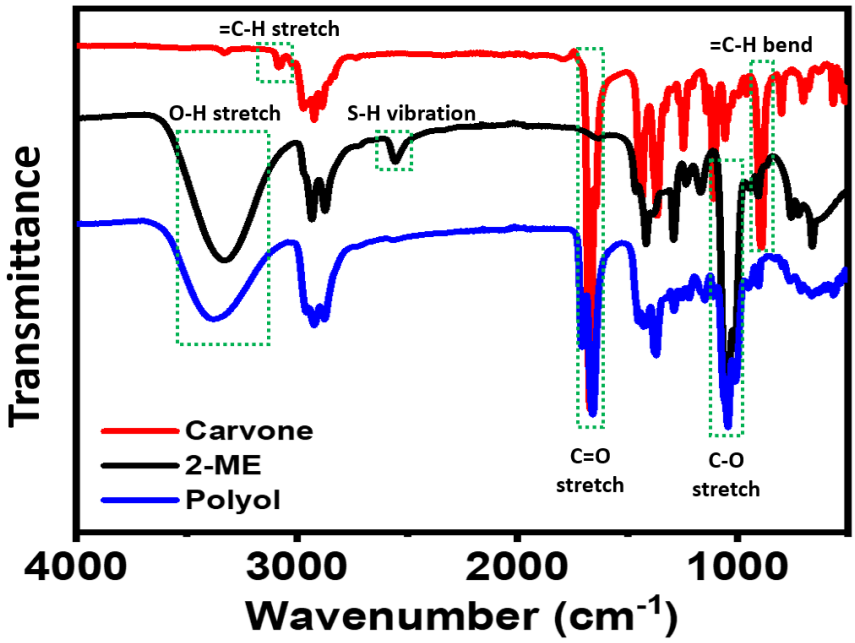

Figure 3.3. FTIR spectra for carvone, 2-ME, and carvone-based polyol.

3.1.4. Hydroxyl number determination

The hydroxyl number for the synthesized polyol was 365 mg KOH/g, while the theoretical value was 367 mg KOH/g, which suggested a high conversion of essential oil into polyol structure. Since the observed hydroxyl number of the synthesized polyol matches well with the theoretical value calculated using a reaction of one mol of carvone with two moles of 2-ME, the possibilities of reaction in only one double bond could be eliminated. It is more likely to form oligomers of the polyol. **Figure 3.4** shows the possible reaction of the formation of minor products. Similar behavior was reported in thiol-ene chemistry by other researchers also [49, 50].

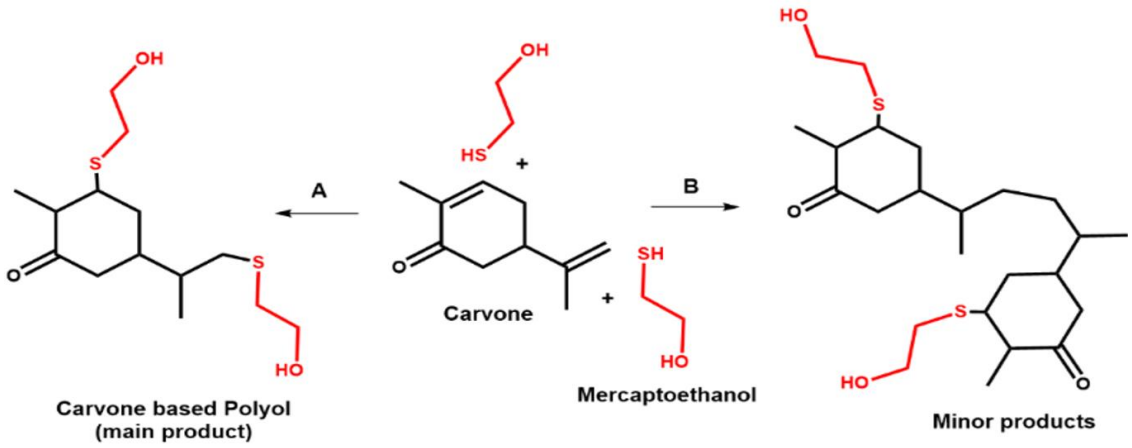

Figure 3.4. The chemical reaction for the synthesis of carvone-based polyol (A) along with expected byproduct (B) [22].

3.2. Properties of carvone-based polyurethane foams

3.2.1. Digital photos of rigid polyurethane foams

Digital pictures of the foams obtained through the formulations demonstrated in **Tables 2.1, 2.2,** and **2.3** are shown in **Figures 3.5, 3.6,** and **3.7**. The appearance of these foams is similar to the industrial-grade and was cut in several shapes to run through the analysis of density, closed-cell content, thermal stability, flammability, and morphology.

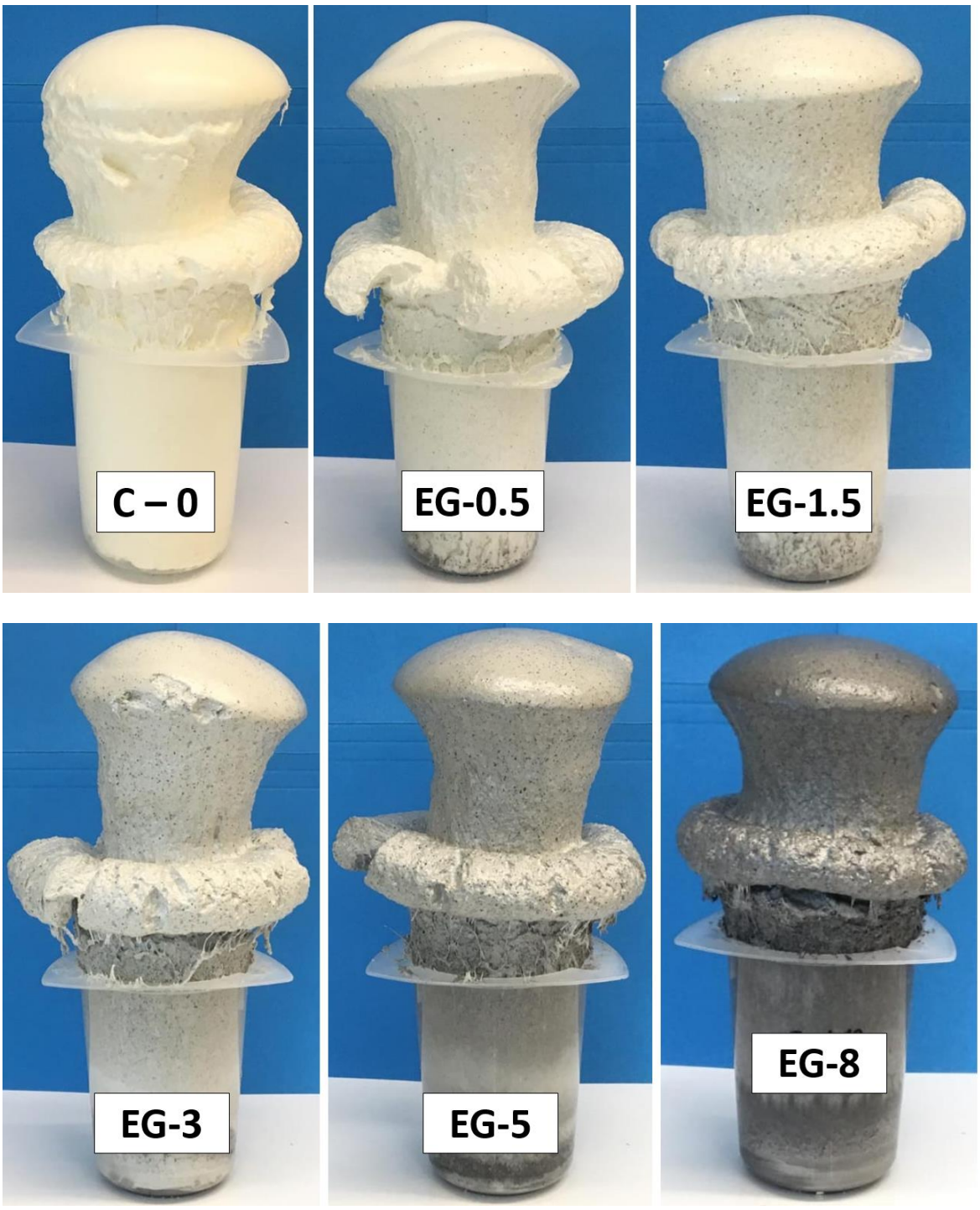

Figure 3.5. Rigid polyurethane foams containing EG.

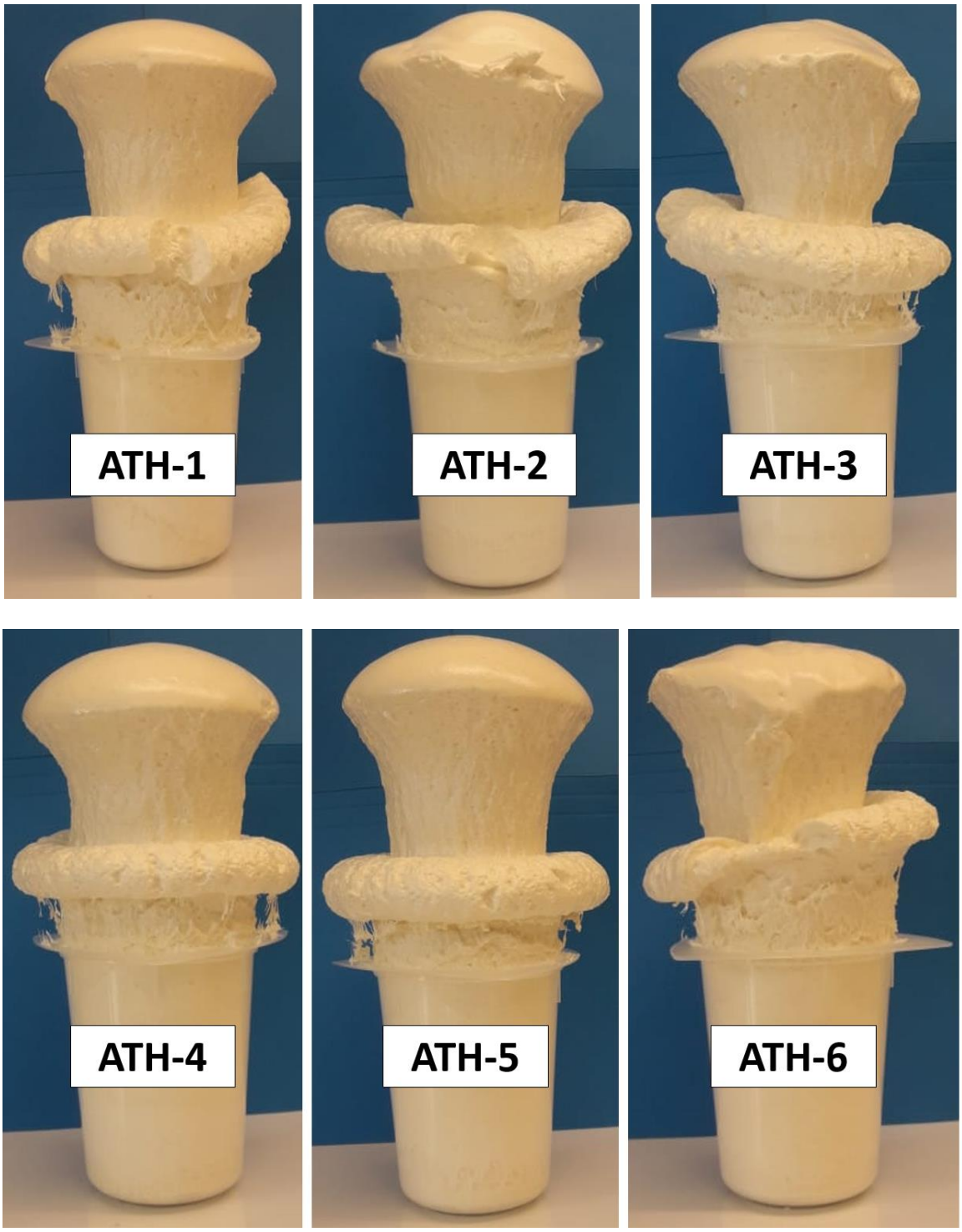

Figure 3.6. Rigid polyurethane foams containing ATH.

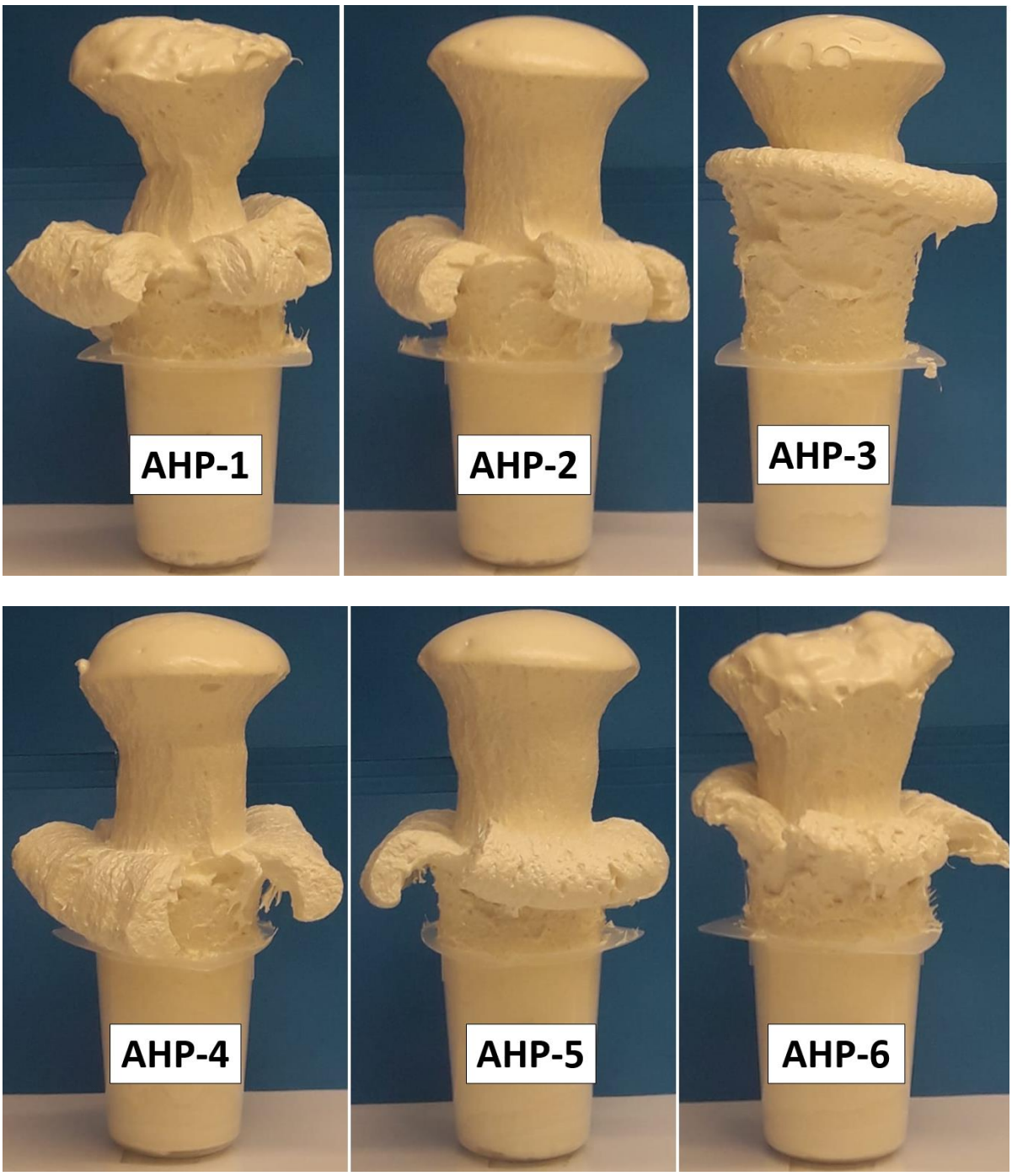

Figure 3.7. Rigid polyurethane foams containing AHP.

3.2.2. FTIR for polyurethane foams

The FTIR spectra for all the foams containing different concentrations of EG, ATH, and AHP can be summarized in **Figures 3.8, 3.9,** and **3.10**. During the synthesis of foams, the isocyanate group from MDI reacts with a hydroxyl group of polyol, resulting in a polyurethane group consisting of -OC(O)NH- bonds. The bands near 1510 cm^{-1} represent hydrogen-bonded urethane groups (-OC(O)NH-) confirming the desired polyurethane reaction [58, 59]. Small peaks were observed for N-H stretch and C=O stretch around 3300 cm^{-1} and 1700 cm^{-1}, respectively, corresponding to polyurea structure resulting from the reaction between water (used as blowing agent) and MDI during the synthesis of PUFs [60].

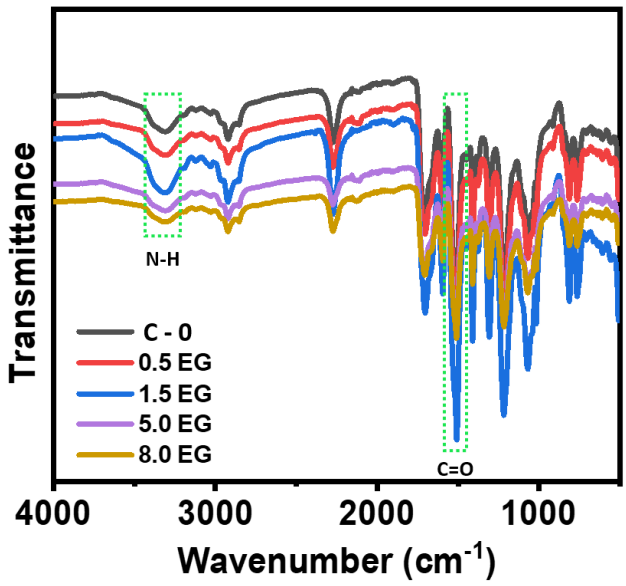

Figure 3.8. FTIR for the rigid polyurethane foams containing EG.

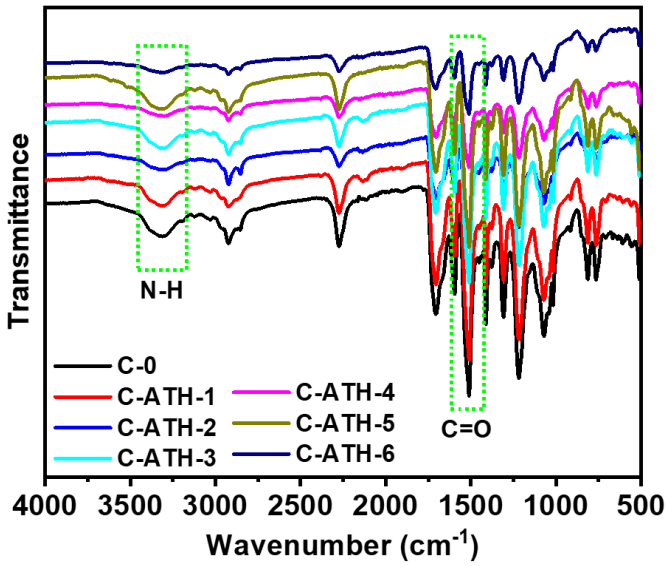

Figure 3.9. FTIR for the rigid polyurethane foams containing ATH.

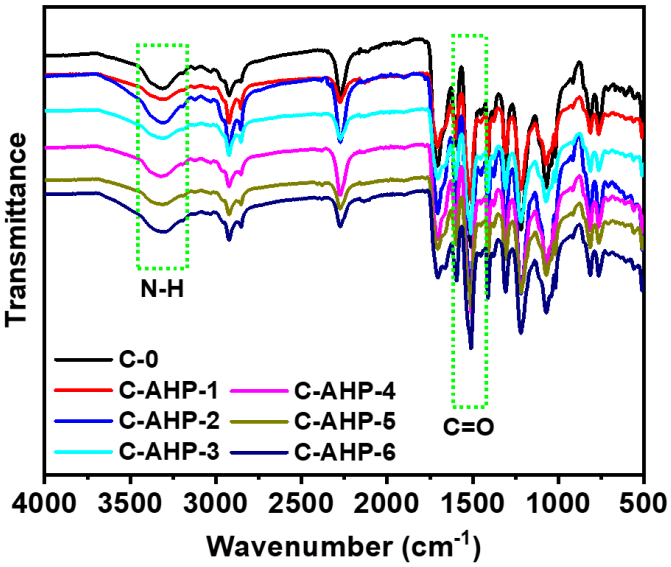

Figure 3.10. FTIR for the rigid polyurethane foams containing increasing concentrations of AHP.

3.2.3. Apparent density

The density is an important physical property that can define the field of application for certain materials. Since rigid polyurethanes are widely used in houses and buildings it is desired that these polymers present low density, meaning that they should add low weight and occupy a larger volume to be more effective and economically viable. The same principle is applied to interior parts and seats for cars. The effect of EG concentration on the apparent density of PUF is summarized in **Figure 3.11**. The foams showed an apparent density in the range of 30-45 kg/m^3. The density of the PUF prepared using commercial polyol (Jeffol 522) was 43 kg/m^3. As the amount of the EG exceeds 8.37 wt%, the density values increased. This could be due to the presence of sulfuric acid in between the graphitic layers that reduce the effect of catalyst and slow down the rise time of the foams [80,81]. This causes an increase in the apparent density of the foams. The addition of a higher amount of catalyst could decrease the rise time, hence increasing the height and maintaining the density of the foams [20]. Regardless of that, all the densities were following industry standards and can be used for rigid foam applications [19]. Hence, no further modifications were made to the concentration of the catalyst. The rise time for the foams EG 0, EG 0.5, EG 1.5, EG 3.0, EG 5.0, EG 8.0, and EG 10.0 was about 14, 14, 12, 12, 11, 9, and 8 seconds, respectively. The rise time of the foam prepared using Jeffol 522 was about 13 seconds.

The density for the ATH and AHP foams is demonstrated in **Figures 3.12** and **3.13**, respectively. The increase in density was more expressive for ATH than AHP samples due

to better intermolecular interaction between filler and foam. The hydroxyl groups in ATH can interact with urethane groups in polyurethane foam via hydrogen bonding and allows proper packing of the structure along with better dispersion as is later shown by SEM images. While in the case of AHP foams, the absence of hydroxyl groups and the presence of flexible (O=P-O-) groups adds a plasticizing effect to the foams slightly reducing the wall thickness of the cells [62].

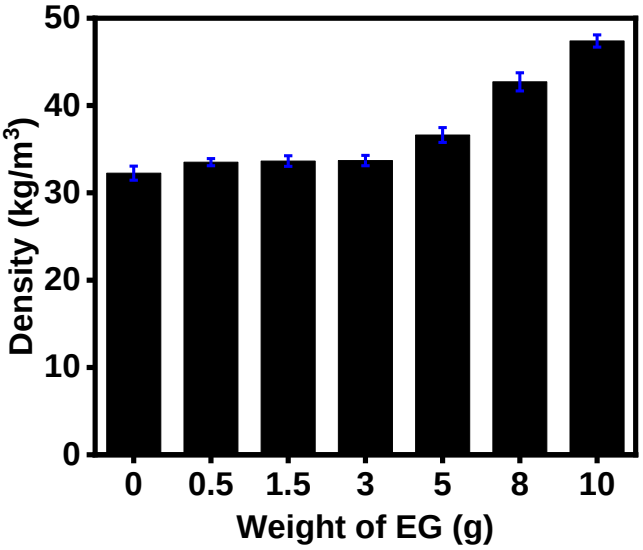

Figure 3.11. Density for polyurethane foam with an increasing amount of EG.

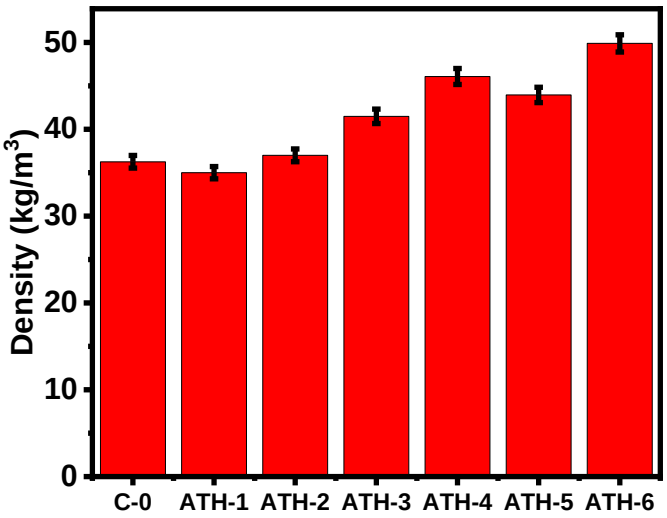

Figure 3.12. Density for polyurethane foam with an increasing amount of ATH.

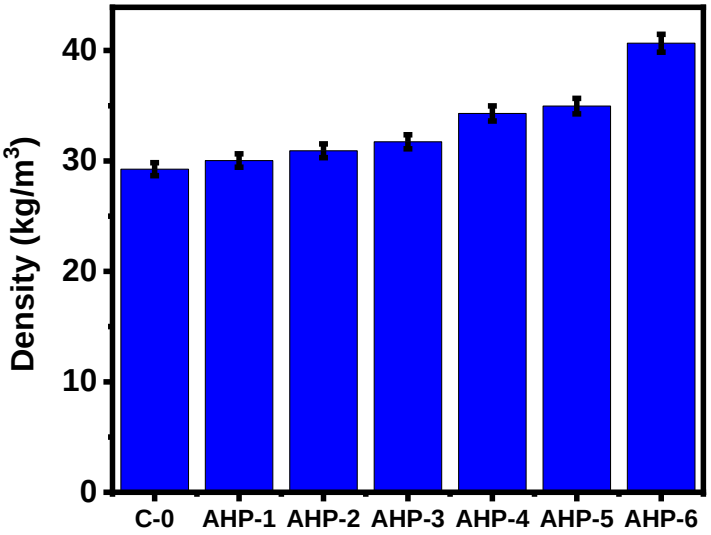

Figure 3.13. Density for polyurethane foam with an increasing amount of AHP.

3.2.4. Closed-cell content

The closed-cell content of the prepared foams was measured using ASTM D2856 method. **Figure 3.14** shows the closed-cell content of all the foams containing EG. It was observed that the values were around 90 to 95%. The prepared foam using Jeffol 522 reached 93%. Furthermore, the effect of increasing ATH and AHP concentration in separate sets on the closed-cell content of PUFs was measured and shown in **Figures 3.15** and **3.16**, respectively. All the FR foams containing AHP and ATH maintained the closed-cell structure >95%, which was higher than the neat sample, suggesting an advantageous property for better thermal insulations [41, 63]. Although the addition of AHP and ATH presented notable effects on the density and compression strength of the foams, no effect on the closed-cell structure was observed. High closed-cell content is usually related to a high thermal insulation property for the foams. This suggests that EG, AHP, and ATH can be used as effective FR additives for rigid PUF.

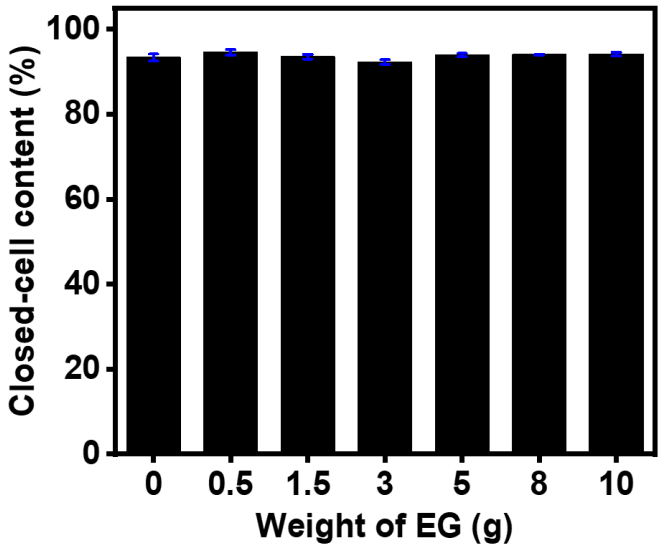

Figure 3.14. Closed-cell content for rigid polyurethane foams with increasing concentration of EG.

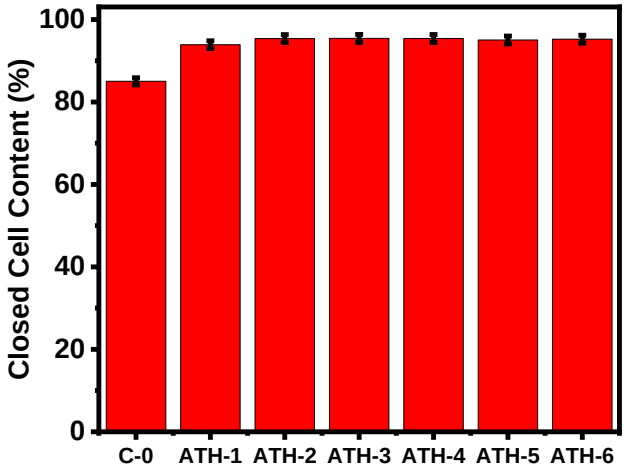

Figure 3.15. Closed-cell content for rigid polyurethane foams with increasing concentration of ATH.

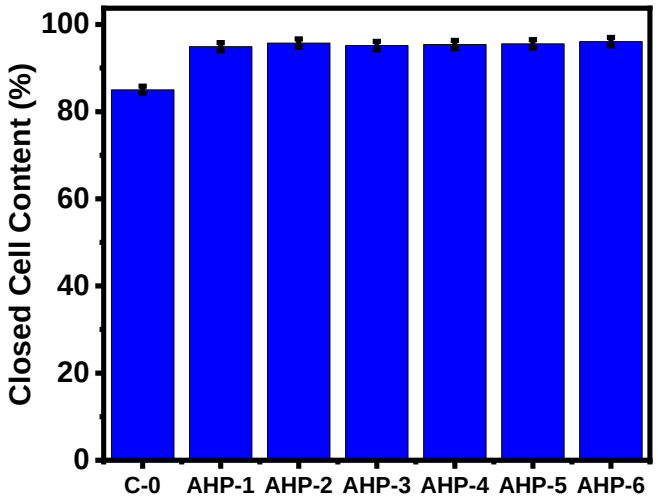

Figure 3.16. Closed-cell content for rigid polyurethane foams with increasing concentration of AHP.

3.2.5. Microstructural and morphology of the polyurethane foams

The Scanning Electron Microscopy images for all the synthesized PUF with uniform cellular structures containing EG can be summarized in **Figure 3.17**. Increasing the concentration from 0 (C-0) to 15.44 wt% (EG-10) decreased the average cell size from 160 to 120 microns. These results are following the density values. As the amount of EG exceeds 5 g in the foam, the acid content within the reaction mixture of PUF increases which slows down the rise time of the foam and raises the apparent density of the foams. However, unlike previous reports for PUF containing EG, we observed a highly closed-cell structure >95% for our EG containing polyurethane foams, which could be due to the compatibility of EG with carvone-based polyol structure [64, 65]. A high and nearly

constant value for closed-cell content with low variance in density can present rigid polyurethane foams with good thermal insulation properties [18, 66].

The morphology and cellular structure of rigid PUFs are important characteristics to understand their physical and mechanical properties. The SEM micrographs in **Figure 3.18** and **Figure 3.19** correspond to foams containing ATH and AHP, respectively. For ATH foams, the size of pores decreased from 150 to around 80 µm with increased loading of ATH within the foams. A decrease in pore size while maintaining the cell wall thickness, increases the amount of solid region within the foam and therefore increases the apparent density. The cell wall thickness for all the ATH containing foams was maintained around 5 to 8 µm. While in the case of AHP the size of pores decreased from 150 to 50 µm as the amount of AHP increased. Here, with an increasing concentration of AHP from 0.96 to 12.92% the cell wall thickness was slightly reduced from 5 to 3 µm, respectively. This behavior could result in a slight difference in the physical and mechanical properties of AHP foams as compared to ATH foams. In both cases, the cellular structure was preserved without much disruption. The decrease in cellular size resulted in an increase in apparent density with the addition of ATH and AHP. As shown in **Figures 3.12** and **3.13**, the addition of ATH and AHP showed a systematic increase in the density of the foams. Although the increase in density was significant, all the foams still maintained the average density range between 30-50 kg/m^3, an acceptable range for rigid PUFs.

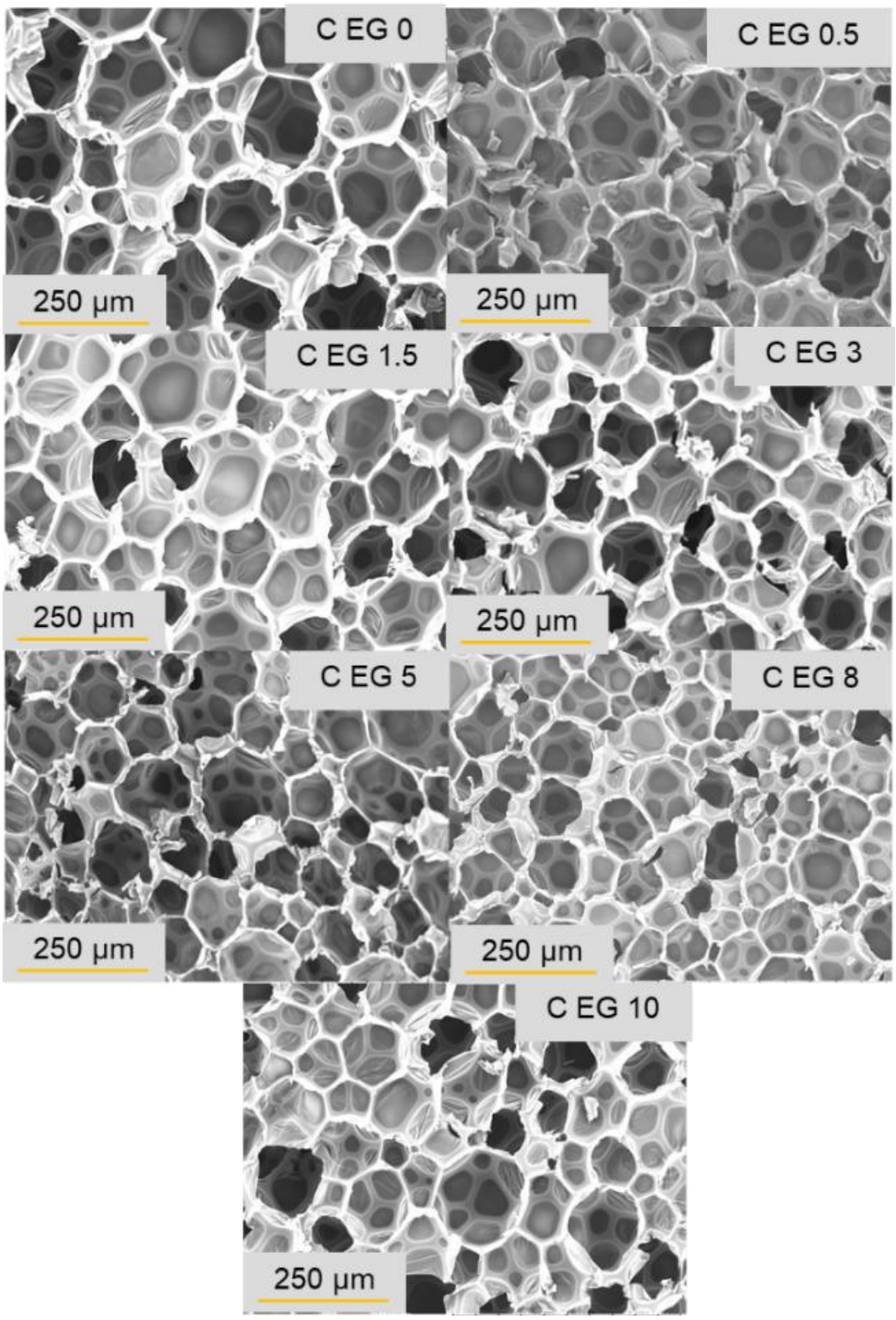

Figure 3.17. Micrographs for the rigid polyurethane foams containing EG.

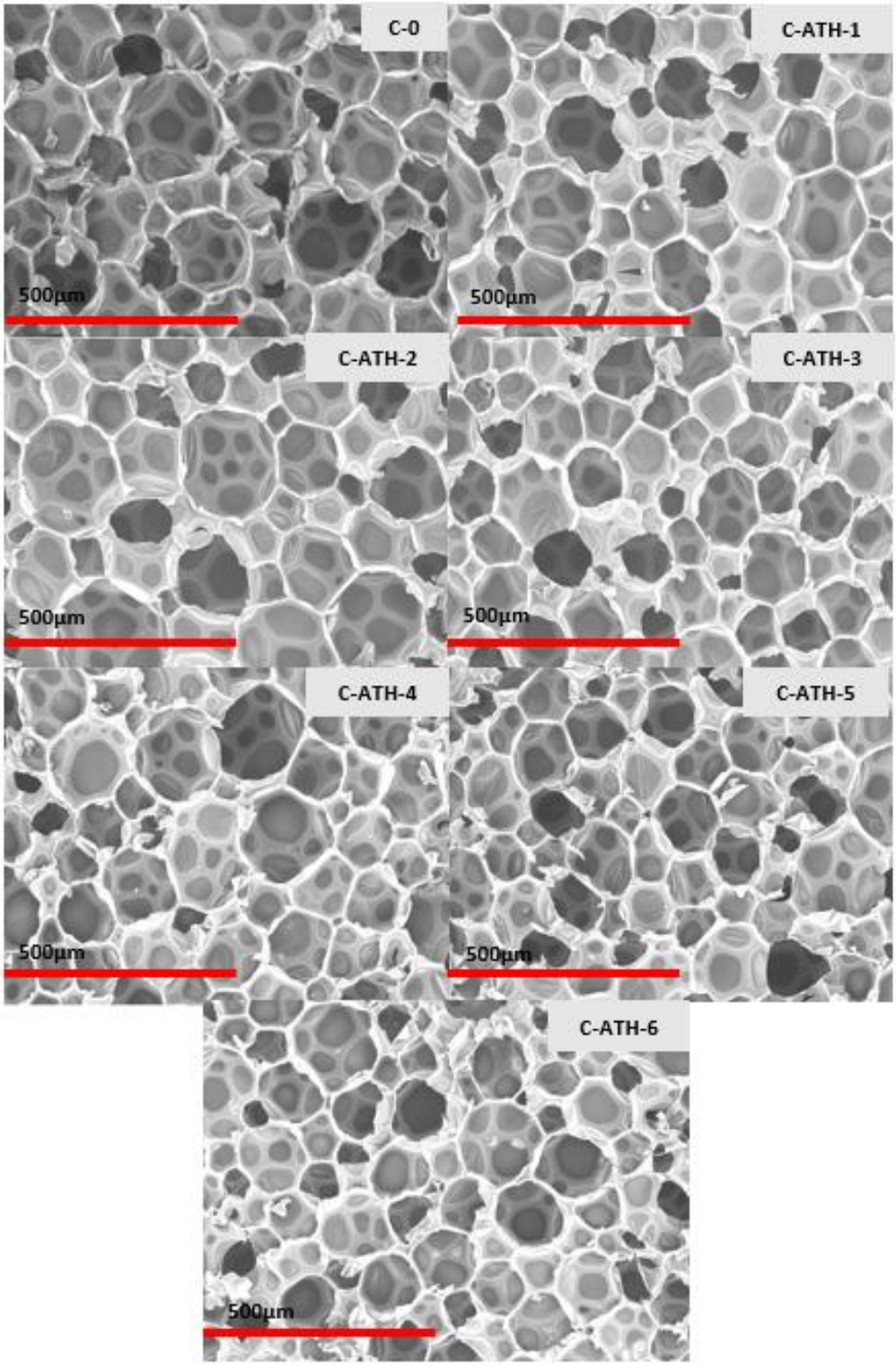

Figure 3.18. Micrographs for the rigid polyurethane foams containing ATH.

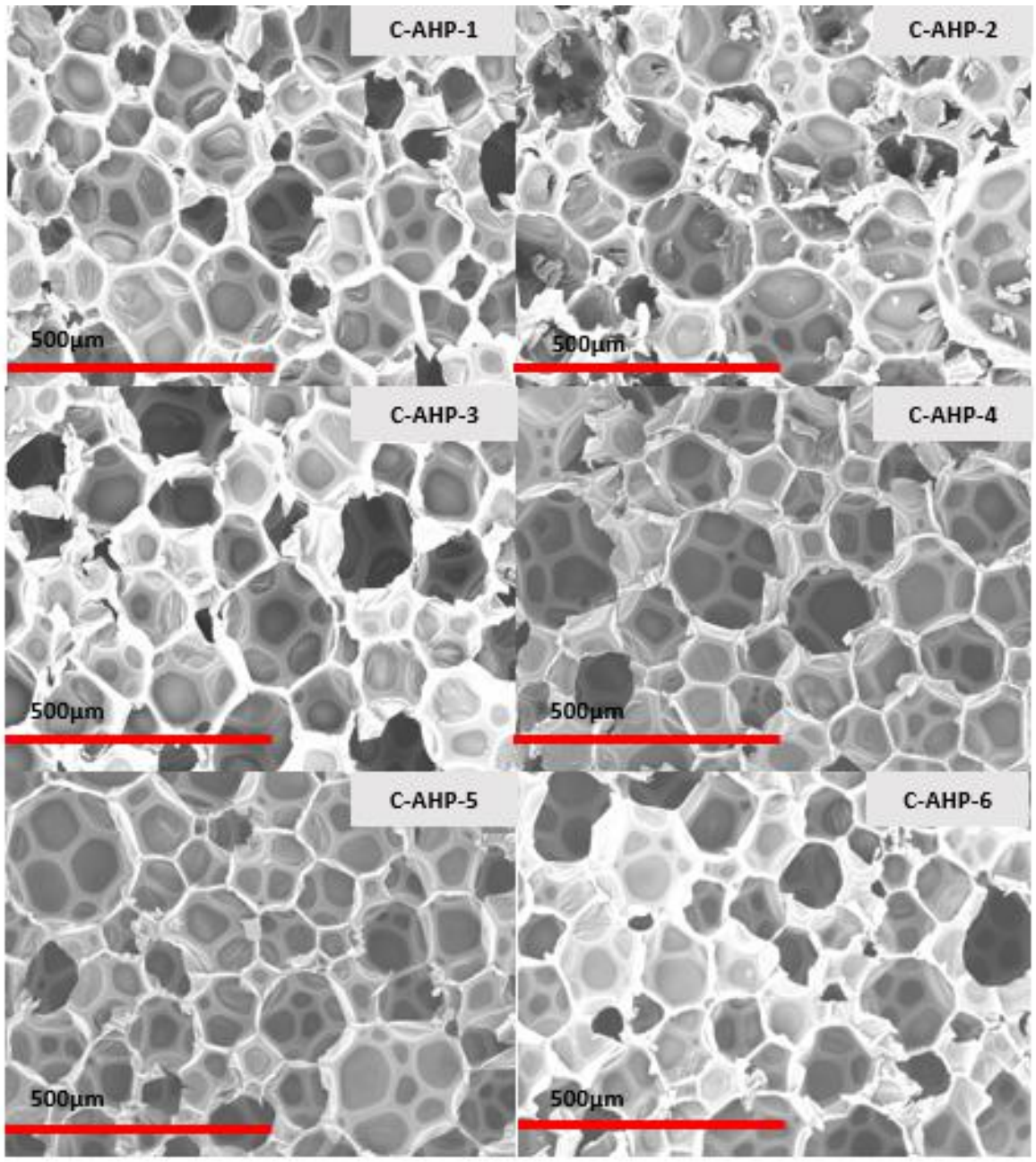

Figure 3.19. Micrographs for the rigid polyurethane foams containing AHP.

3.2.6. Compression Test

A compression test was performed to analyze the effect of an increasing amount of EG on the mechanical properties of PUF (**Figure 3.20**). EG is being reported as a cost-effective FR with the drawbacks of harder processing and a decrease in mechanical strength [67, 68]. The ultimate compressive strength value was found to be 210 kPa and 209 kPa for neat PUF prepared using synthesized biopolyol and Jeffol 522, respectively. As we increase the content of EG, the compression strength of PUF slightly decreased. The 10 EG foam showed a yield at the break of 175 kPa. Although EG acts as an effective FR when used in the form of flakes, its higher concentration in the PUF may cause defects in the macrosegments of the foam, hence deteriorating some of its mechanical properties causing the compressive strength to vary [47, 67, 69, 70]. Even though there was a decrease in mechanical properties with increasing concentration of EG, all the EG-containing polyurethane foams showed higher compression strength than foams originated from castor, cardanol, and corn oils that were 150, 130, and 75 kPa respectively [20, 71].

The stress-strain curves for the compressive strength of the ATH and AHP foams are shown in **Figures 3.21** and **3.22**. It was noticed that with increasing amounts of ATH from 0.96 to 16.92 wt. %, the tensile strength required to deform the rigid PUF and induce 10% strain, increased from 210 to 290 kPa, respectively (**Figure 3.21**). This could be correlated to an increased cellular density of the foams while maintaining the thickness of the cells. However, due to the plasticizing effect presented by flexible (O=P-O-) structure in AHP,

the decrease in cell wall thickness adversely affects the compression strength of AHP containing foams (**Figure 3.22**). Even though there was a considerable decrease in compressive strength of the AHP foams, the obtained values were still in an acceptable range for commercially applicable PUF [72].

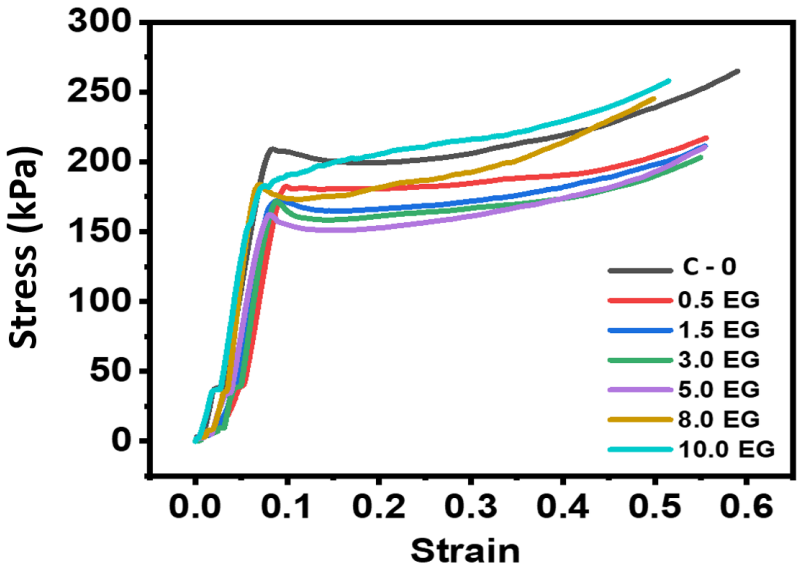

Figure 3.20. Compressive strength for EG containing polyurethane foams.

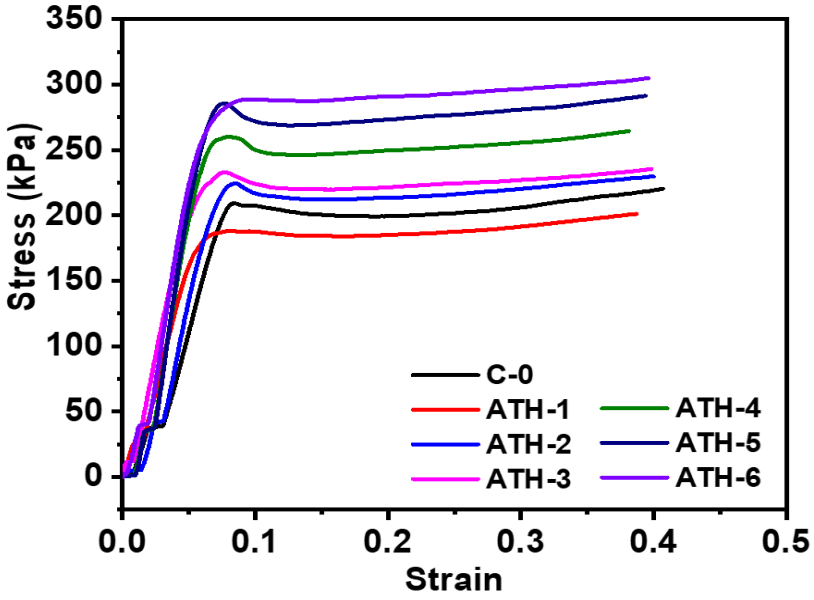

Figure 3.21. Compressive strength for ATH containing polyurethane foams.

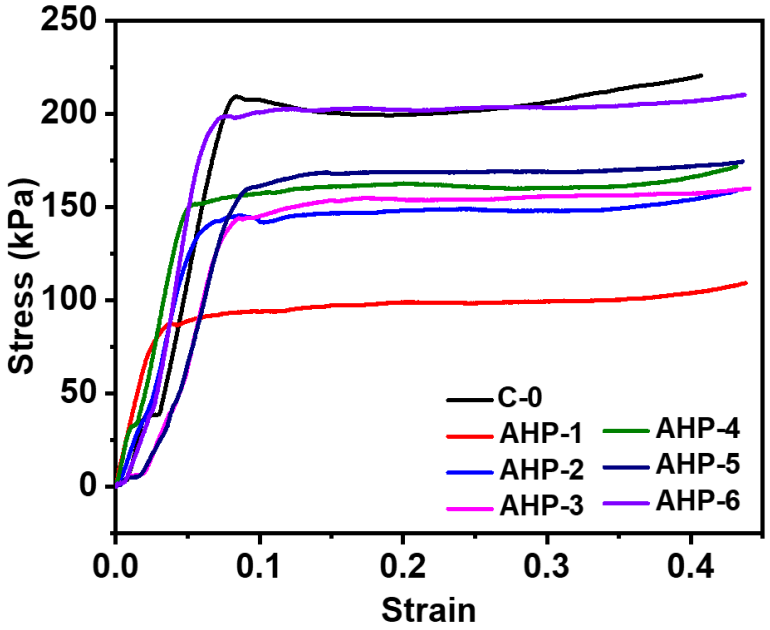

Figure 3.22. Compressive strength for AHP containing polyurethane foams.

3.2.7. Thermogravimetric analysis

The thermal analysis of EG containing PUF was performed by thermogravimetric analysis, as described in **Figure 3.23** and derivative thermogravimetric analysis (DTGA) in **Figure 3.24** in both nitrogen and air atmosphere. The weight loss curve in TGA and DTGA showed a two-step thermal decomposition behavior. At 250 °C, the hydrocarbon chains in the PUF start to decompose and EG starts its irreversible expansion, forming a protective char layer on the foam's surface [47]. The first maximum decomposition occurs at 285 °C (**Figure 3.24**). It can be noted that with an increasing amount of EG, there was a systematic decrease in the weight loss of the foams. This means that protective char formation increases with EG concentration and stabilizes the surface of the foam. The EG pyrolysis comprises SO_2, CO_2, and water that gets entrapped while escaping near the edges of the graphitic structure, leading to the irreversible expansion of EG [47]. The expansion then creates a graphitic char layer on the surface of the foam that prevents the heat transfer through the solid phase and stops the fire [47, 67, 69]. This type of phenomenon is observed by the expansion of foam's surface after the test, which may sometimes form blisters of charred graphite. A second degradation peak near 550 °C corresponds to the disintegration of polyurethane structure along with char resulting in weight loss for all the foams [97,101]. As compared to neat polyurethane foams, EG containing foams showed relatively lower weight loss suggesting increased char stability with EG concentration. The thermal behavior of the prepared foams with increasing amounts of EG under air atmosphere is shown in **Figure 3.25** along with the DTGA

expressed in **Figure 3.26**. The foams showed similar behavior under nitrogen and air atmosphere, however, the maximum decomposition temperature for the foams was observed to shift towards lower a temperature (270 ^{o}C) in the air. Also, at higher temperatures, the foams under air reached maximum decomposition around 600 ^{o}C. It is important to highlight the thermal behavior for the 10 EG sample under air atmosphere (**Figure 3.25**), which differed from the other samples. It showed a higher weight loss for the first decomposition, meaning that EG was expanding and combusting due to the presence of oxygen. This condition led to the formation of more char that acted as a thermal stable shield that prevented further degradation of the polyurethane underneath. This effect led to a shift in the second thermal decomposition to higher temperature seen in both **Figures 3.25** and **3.26**, suggesting an increase in thermal stability for 10 EG foam among the other samples. Also, the sudden decrease of weight loss towards 700 °C was due to the EG expansion that caused fragments charred sample to fall off from the sample holder, leading to fluctuation in the weight values. Some of the important thermal characteristics of the foams in nitrogen and air atmosphere are given in **Table 3.1**.

The thermal characteristics of all the foams containing ATH were analyzed using TGA and DTGA in nitrogen and air atmosphere, shown in **Figures 3.27, 3.28, 3.29,** and **3.30**. The TGA and DTGA for the AHP containing foams under nitrogen and air atmosphere are described in **Figures 3.31, 3.32, 3.33,** and **3.34**, respectively. Also, the TGA for pure ATH and AHP in both nitrogen and air atmosphere is described in **Figure 3.35,** and **3.36**,

respectively. As observed in **Figures 3.27** and **3.28**, the TGA and DTGA peaks showed that the decomposition of ATH ($Al(OH)_3$) occurs at 260 °C resulting in the release of water and formation of alumina (Al_2O_3) char. All the foams containing ATH showed higher weight loss near 260-300 ^oC corresponding to the decomposition of ATH and formation of char from the polyurethane matrix, which prevents further weight loss during the second degradation stage near 550 ^oC. To understand this behavior in detail, we performed FTIR analysis for ATH and ATH-6 foam, before and after TGA analysis. As shown in **Figure 3.37**, a peak near 3500 cm^{-1} for ATH before TGA analysis indicates the presence of O-H groups along with two peaks around 1080 and 510 cm^{-1} relating to the Al-O stretch [74]. After the TGA analysis, the ATH converted into Al_2O_3 resulting in a disappearance of the O-H stretch band. This behavior was similar in the ATH-6 sample and therefore, increased the char in the ATH-6 sample. The thermal degradation for the foams containing ATH in the air atmosphere was similar to that of nitrogen. The compiled information for the thermal analysis of ATH containing foams is summarized in **Table 3.2**.

Unlike ATH, AHP containing foams showed higher weight loss during the first phase of decomposition near 280-300 ^oC. The increase in weight loss corresponds to a higher decomposition temperature of AHP near 310 ^oC observed from TGA and DTGA curves in **Figure 3.31** and **3.32**, respectively. According to previous reports, AHP presents two thermal transitions around 310 and 450 °C related to the pyrolysis reactions represented in **Scheme 3.1** [75, 76]. To elucidate the thermal decomposition behavior for AHP, we performed the FTIR analysis of AHP and AHP-6 foam before and after the TGA analysis. As

shown in **Figure 3.38**, the decomposition of AHP results in the formation of $Al_4(P_2O_7)_3$ and is supported by the presence of P-O-P stretch near 1120 cm^{-1}, which is also present in the char of the AHP-6 foam after TGA analysis [75, 77]. This char formation increased the thermal stability of the foams. The compiled information for the thermal analysis of AHP containing foams is summarized in **Table 3.3**.

To understand the difference in oxygen environment during the TGA analysis, we performed TGA in N_2 and air for ATH (**Figure 3.35**). No noticeable change was observed in weight-loss curves for ATH during TGA analysis in the air compared to the N_2 atmosphere. However, the reaction mechanism differs in the case of AHP samples in **Figure 3.36**. The decomposition of AHP occurs near 310 °C resulting in slight fluctuations in TGA curves performed under the N_2 atmosphere. While, the O_2 in the air reacts with AHP to form phosphoric acid which causes noticeable absorption of the surrounding O_2 during the decomposition process of AHP and results in negative weight loss after 310 ^oC [78, 79]. The resulting phosphoric acid is known to allow accelerated char formation in foams leading to increased char weight during the TGA analysis [75, 80, 81].

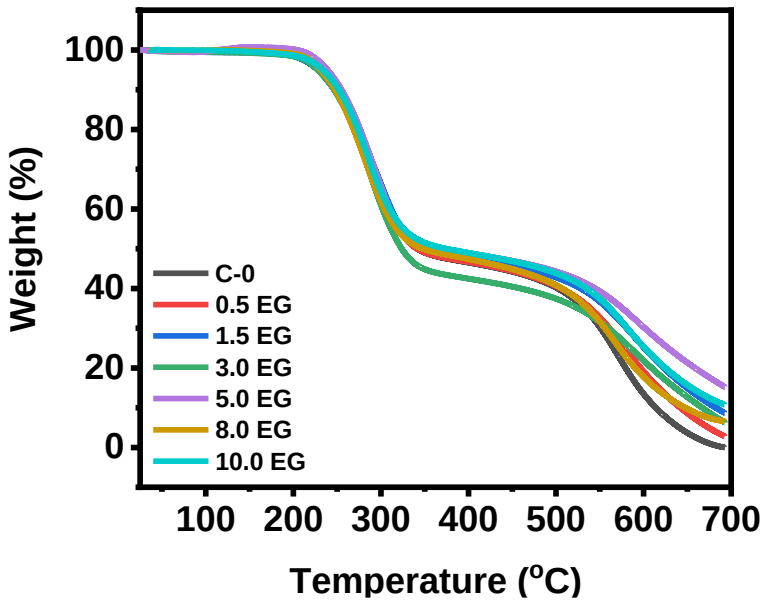

Figure 3.23. TGA for the foam containing EG in nitrogen atmosphere.

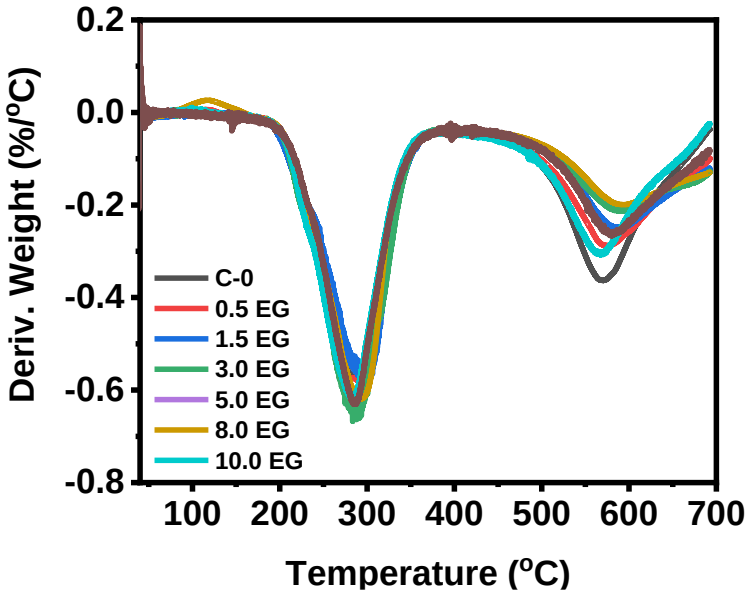

Figure 3.24. DTGA for the foam containing EG in nitrogen atmosphere.

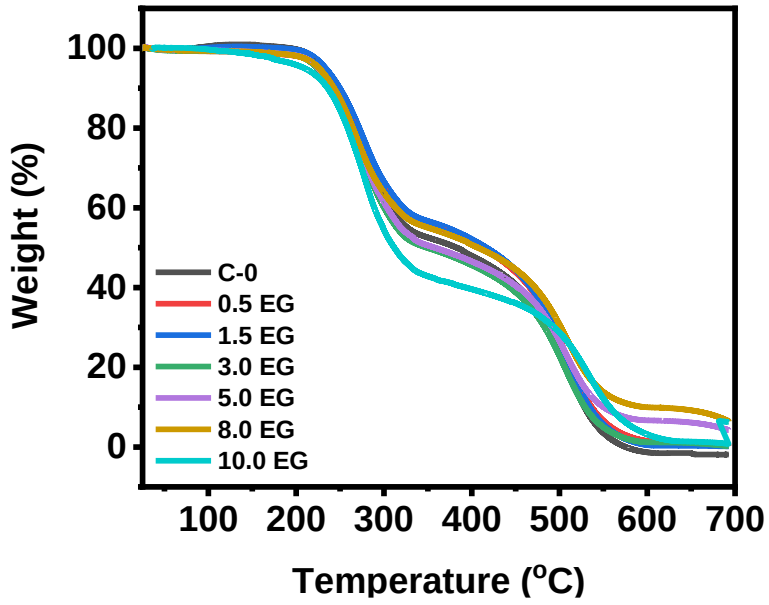

Figure 3.25. TGA for the foam containing EG in air atmosphere.

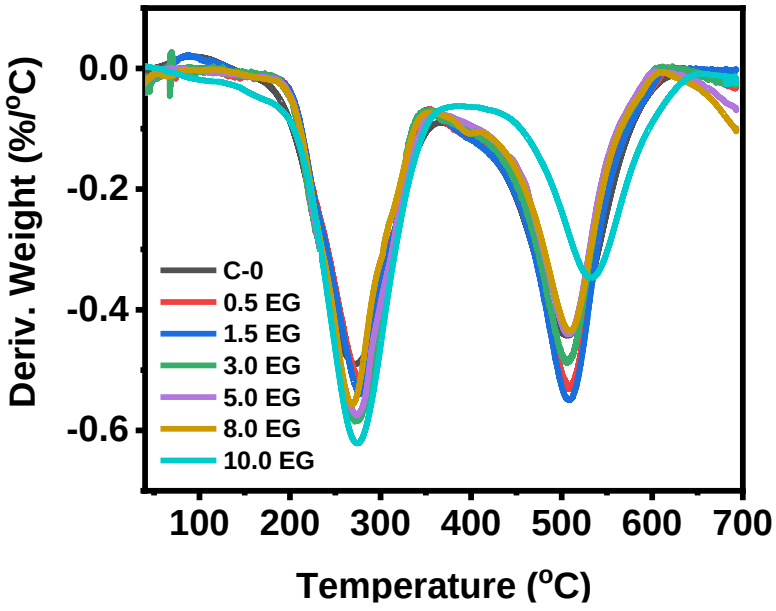

Figure 3.26. DTGA for the foam containing EG in the air atmosphere.

Table 3.1. Thermal properties of the polyurethane foams containing EG.

	N_2	N_2	N_2	Air	Air	Air
Foam	$T_{d5\%}$	$T_{d50\%}$	**Wt. %** $_{700}$	$T_{d5\%}$	$T_{d50\%}$	**Wt. %** $_{700}$
C-0	231.2	336.8	0.007	231.6	382.7	0.005
0.5 EG	233	313.8	2.81	226.9	411.4	0.338
1.5 EG	228	325.8	5.69	233.5	416.7	0.160
3.0 EG	227.8	381.6	6.27	224	349	0.217
5.0 EG	229.6	372.4	6.35	225.7	357.9	4.24
8.0 EG	231.4	370.2	6.61	225.9	407	6.47
10.0 EG	233.5	374.9	10.78	221	369.7	6.28

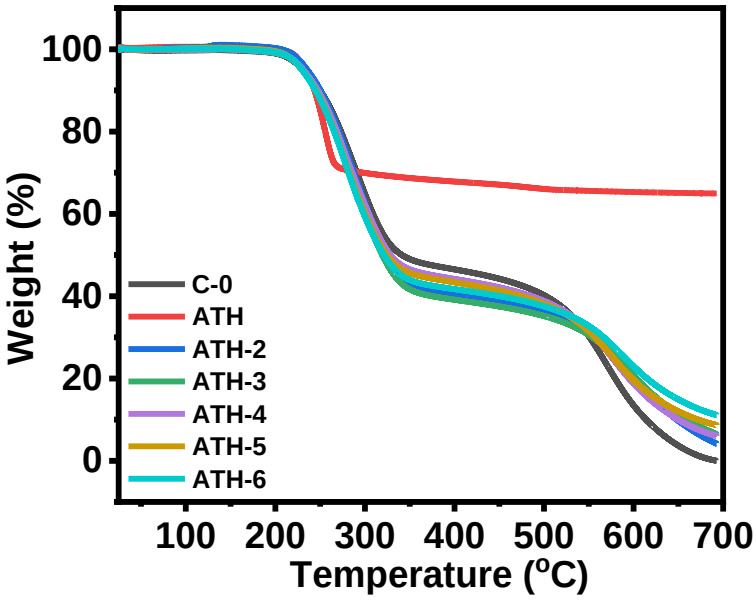

Figure 3.27. TGA for the polyurethanes containing ATH under nitrogen.

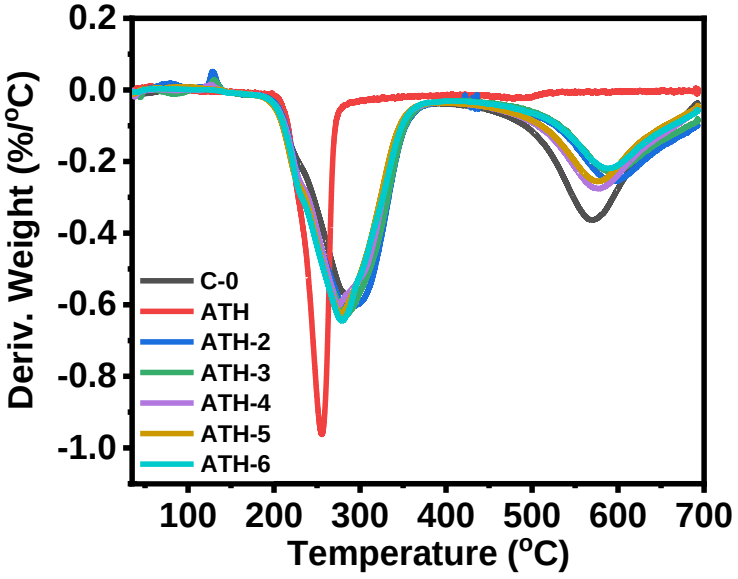

Figure 3.28. DTGA for the polyurethanes containing ATH under nitrogen.

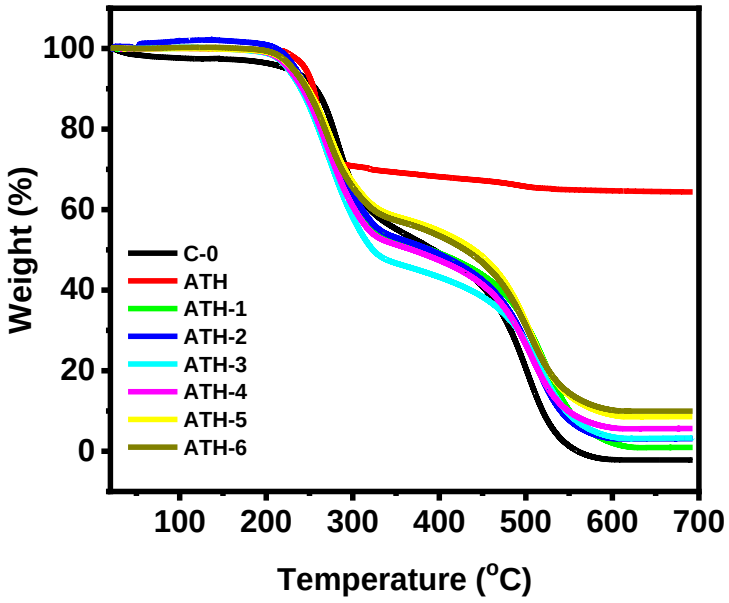

Figure 3.29. TGA for the polyurethanes containing ATH under air.

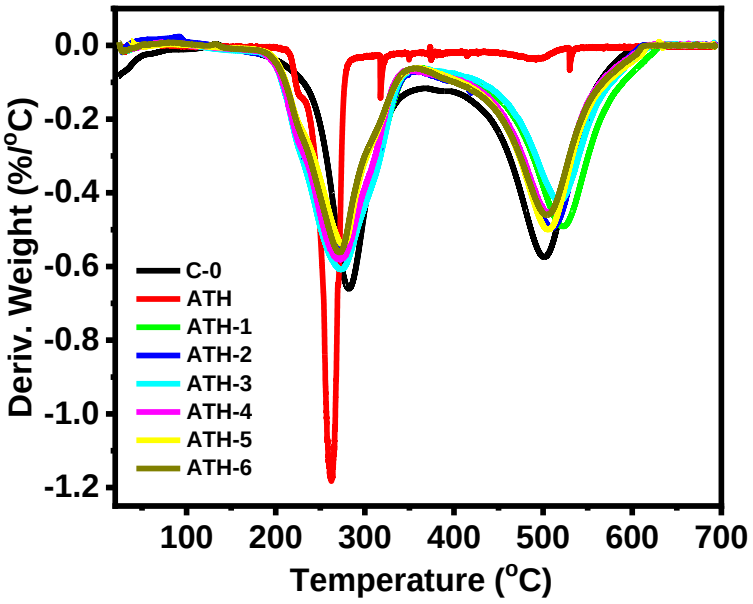

Figure 3.30. DTGA for the polyurethanes containing ATH under air.

Table 3.2. Thermal properties of the polyurethane foams containing ATH.

	N_2	N_2	N_2	Air	Air	Air
Foam	$T_{d5\%}$	$T_{d50\%}$	**Wt. %** $_{700}$	$T_{d5\%}$	$T_{d50\%}$	**Wt. %** $_{700}$
C-0	231.2	336.8	0.007	231.6	382.7	0.005
ATH-1	227.1	305.6	3.39	229.1	389.8	0.96
ATH-2	235	323.7	4.14	234	388.7	3.1
ATH-3	229.7	319.4	6.45	225	323.4	3.28
ATH-4	230.9	328.5	6.07	226.4	368.4	5.62
ATH-5	229.5	324.4	8.68	230.9	440	8.57
ATH-6	229.6	321.3	11.11	230.8	430	9.94

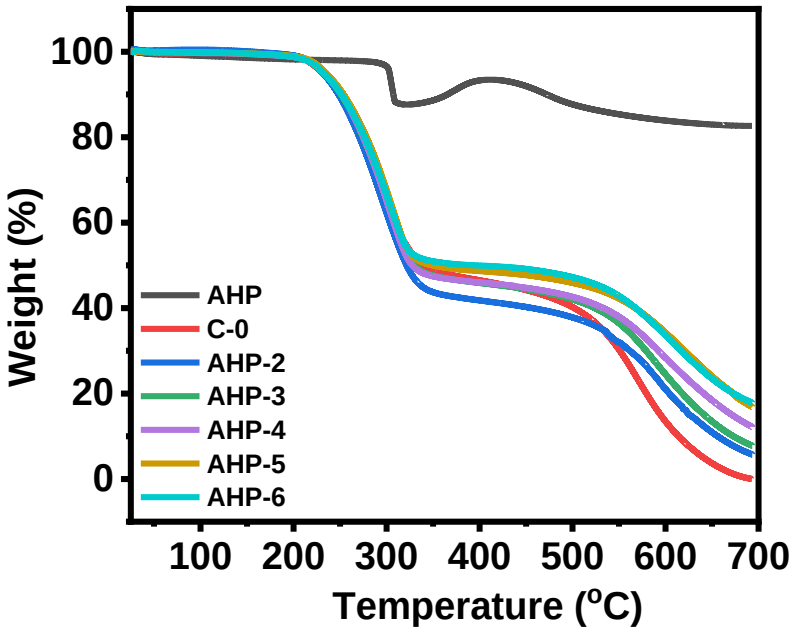

Figure 3.31. TGA for the polyurethanes containing AHP under nitrogen.

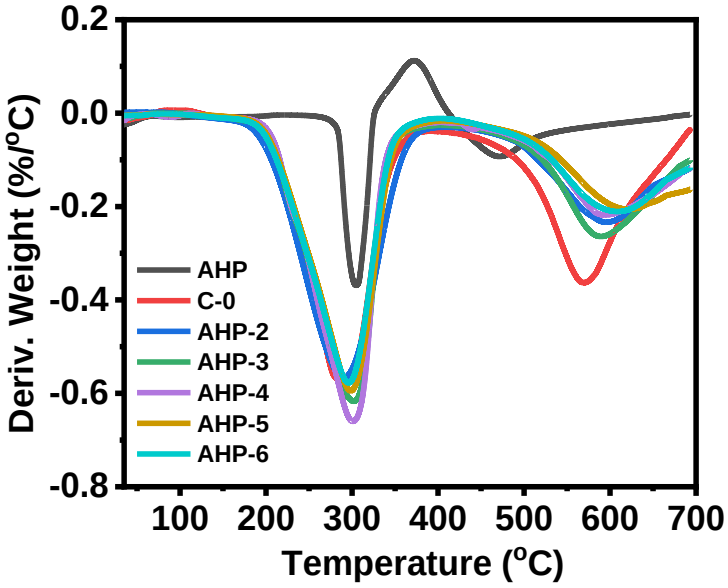

Figure 3.32. DTGA for the polyurethanes containing AHP under nitrogen.

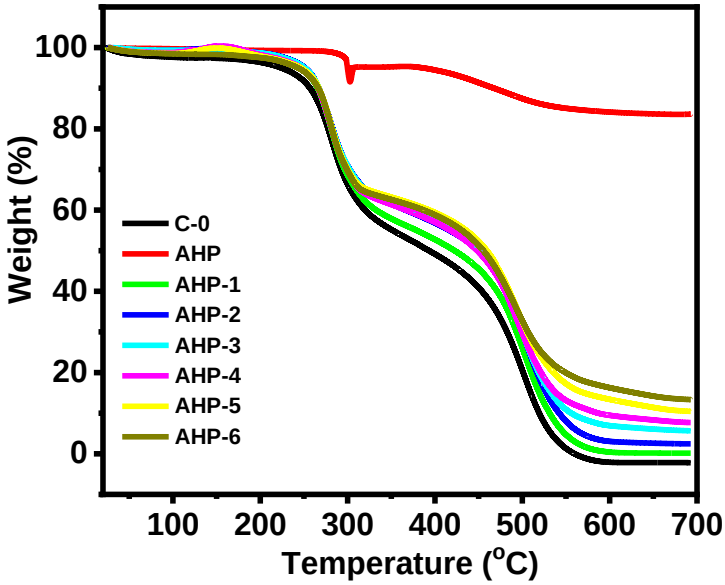

Figure 3.33. TGA for the polyurethanes containing AHP under air.

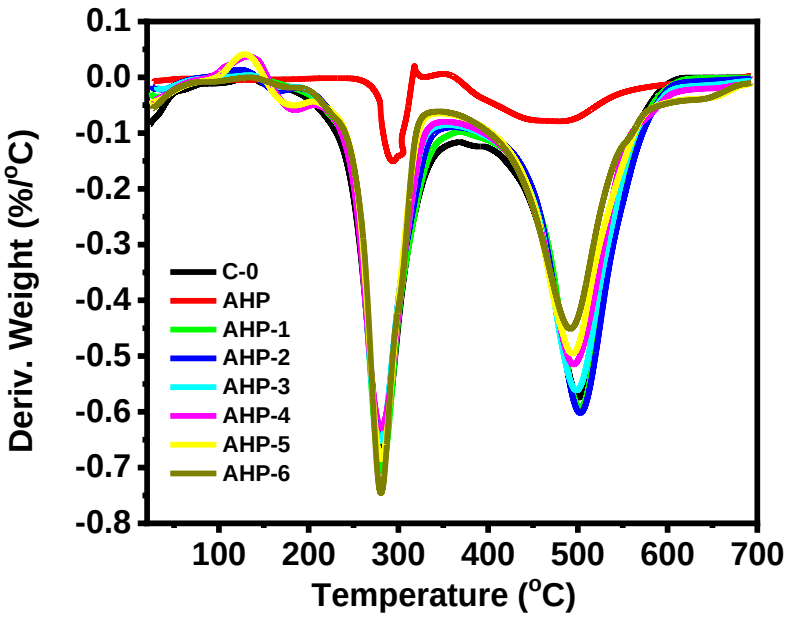

Figure 3.34. DTGA for the polyurethanes containing AHP under air.

Table 3.3. Thermal properties of the polyurethane foams containing AHP.

	N_2	N_2	N_2	Air	Air	Air
Foam	$T_{d5\%}$	$T_{d50\%}$	**Wt. %** $_{700}$	$T_{d5\%}$	$T_{d50\%}$	**Wt. %** $_{700}$
C-0	231.2	336.8	0.007	231.6	382.7	0.005
AHP-1	230.8	317.2	7.25	245.4	422.5	0.147
AHP-2	231.6	321.5	5.73	251.4	449.8	2.44
AHP-3	232.4	330	7.79	250.5	451.2	5.66
AHP-4	233.1	327.7	12.18	246.6	448.5	7.68
AHP-5	234.8	349.4	16.87	246.3	459.4	10.44
AHP-6	232.8	395.5	17.82	243.1	455.3	13.3

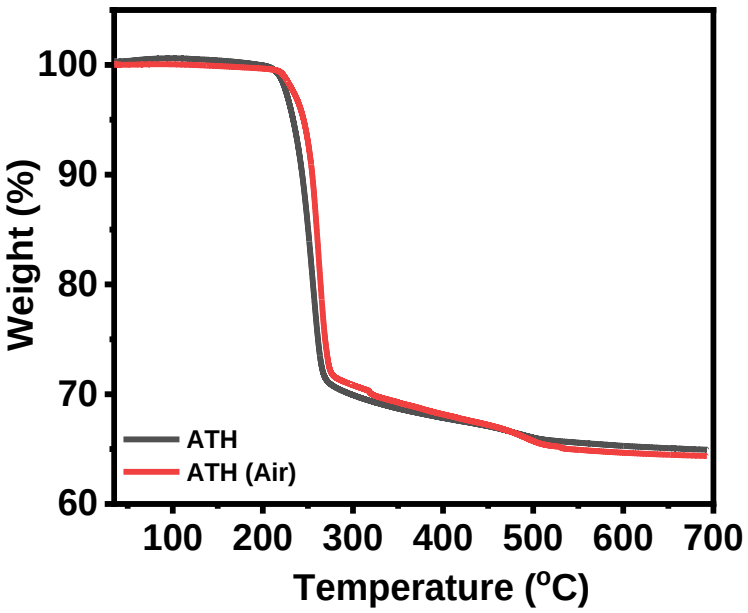

Figure 3.35. TGA for pure ATH under nitrogen and air.

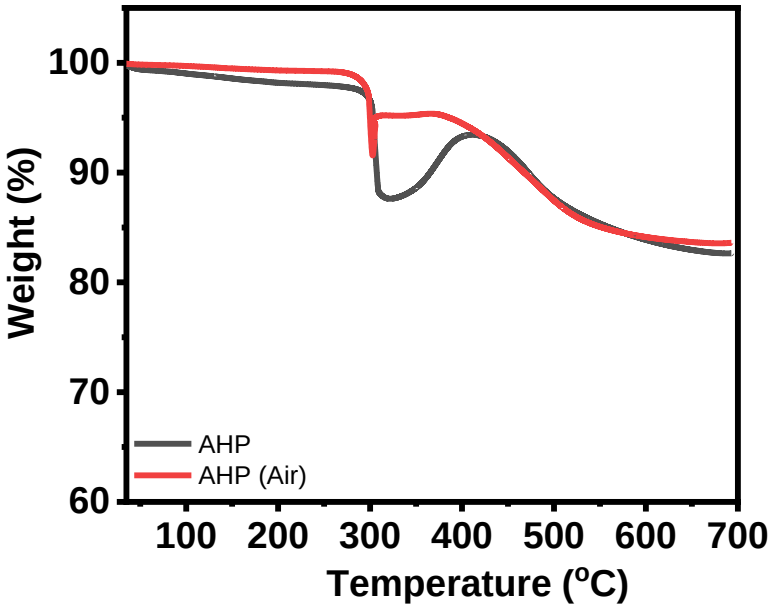

Figure 3.36. TGA for pure AHP under nitrogen and air.

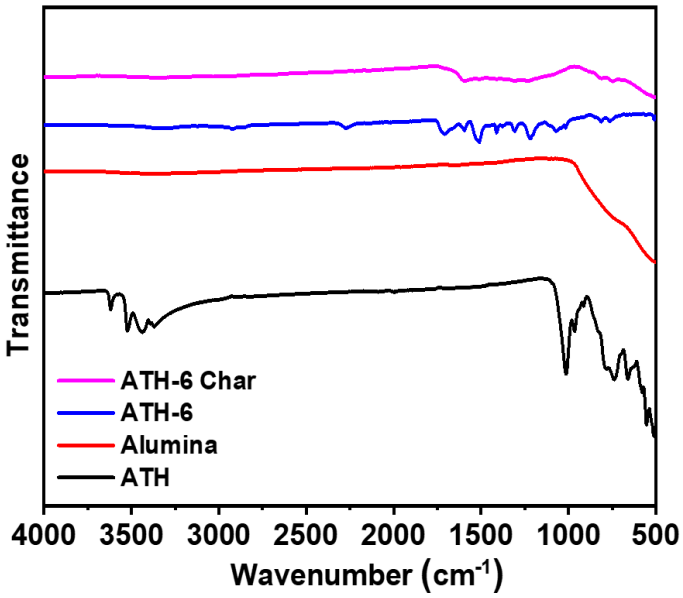

Figure 3.37. FTIR for the foam containing ATH and pure ATH before and after burning.

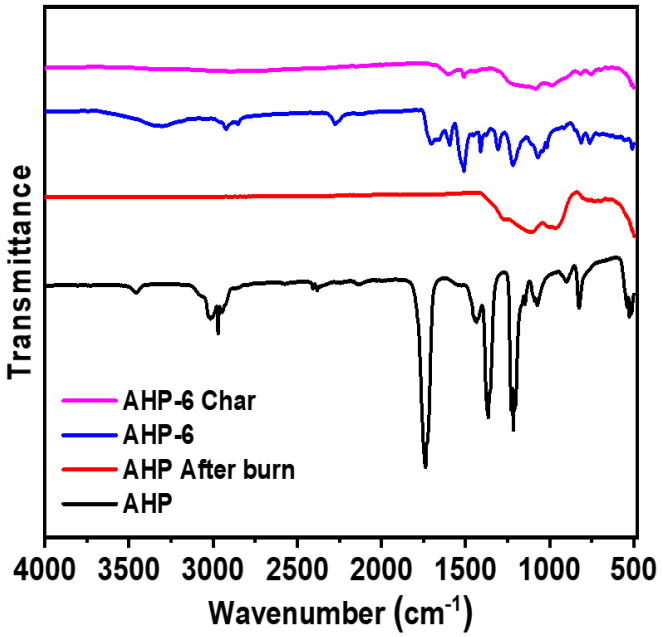

Figure 3.38. FTIR for the foam containing AHP and pure AHP before and after burning.

$$2\ Al(H_2PO_2)_3 \xrightarrow{\Delta} Al_2(HPO_4)_3 + 3\ PH_3$$

$$2\ Al_2(HPO_4)_3 \xrightarrow{\Delta} Al_4(P_2O_7)_3 + 3\ H_2O$$

$$3\ PH_3 + 2\ O_2 \xrightarrow{\Delta} 3\ H_3PO_4$$

$$PH_3 + 4\ H_2O \xrightarrow{\Delta} H_3PO_4 + 4\ H_2$$

$$n\ H_3PO_4 \xrightarrow{\Delta} \left[-P(=O)(OH)-O- \right]_n + n\ H_2O$$

Scheme 3.1. Thermal decomposition reaction sequence for AHP.

3.2.8. Horizontal burning test

The flame-retardant properties for all the polyurethane foams were analyzed using a horizontal burning test. In this study, the foams were held in the horizontal position and subjected to a flame for 10 seconds. The flame time and weight loss after the self-extinction were recorded. The burning time and weight loss for the EG containing foams are expressed in **Figures 3.39** and **3.40**. The neat polyurethane showed the longest flame time of 98 seconds and the highest weight loss of 46%. The best result for the EG containing foams set was achieved for the foam containing 12.75 wt.% of EG (8 EG), which presented the lowest flame time of 11 s and weight loss of 3.55%. A systematic reduction in the burnt area of samples with increasing EG content can be summarized in **Figure 3.41**. However, with a further increase in EG concentration (>12.75 wt.%), there were no major considerable changes observed in flame retardant properties. The foam prepared using only Jeffol 522 displayed a burning time of 95 seconds with a weight loss of 44%. The observed flame time was comparable to previously reported polyurethane foams. For example, Ranaweera et al.[40] prepared limonene-based FR polyurethane foams using DMMP as a flame retardant. The self-extinguish time for the best limonene-based flame-retardant PUF was reported to be 19 seconds. Similarly, Ramanujam et. al.[20] reported a functionalized corn-based flame-retardant polyurethane foams using DMMP and presented remarkable fire-retardant properties by reducing the weight loss from 38 wt.% from the neat polyurethane to 5.5 wt.% by addition of 1.94 wt.% of P. Unlike EG, DMMP can release toxic fumes containing PH_3 and it is almost three times more expensive than

EG, which significantly increases the cost during the large-scale production. In contrast, EG also acts as a filler and can be used to reduce the overall cost of polyurethane foams. The resulting self-extinguishing time, weight loss, and optical images of the burnt samples for ATH are presented in **Figures 3.42, 3.43,** and **3.44**, respectively. For the AHP containing foams the burning time, weight loss, and digital pictures for the burnt samples are demonstrated in Figures **3.45, 3.46,** and **3.47**, respectively. As shown in **Figures 3.42** and **3.43**, the foams containing ATH with increasing concentration showed a systematic reduction in burning time and consequently weight loss during the flammability test. However, there was slight unevenness in self-extinguishing time with an increasing concentration of ATH. This could be due to the solid phase reaction of ATH as demonstrated by our TGA analysis. The burning pattern for ATH foams can be observed in the photocopies given in **Figure 3.44**. For ATH to act as a flame retardant, it needs to first decompose and form a protective char layer on the surface to prevent further combustion beneath the polymeric matrix. Due to this, all the foams surfaces were burnt with uneven flame times but lower respective weight loss. **Figure 3.48** shows the visual aspect of ATH-6 and AHP-6 samples after the burning test showing that AHP char on the surface prevents the combustion to propagate underneath the surface of the PU matrix, resulting in a lower weight loss if compared to ATH.

To further improve the flame retardancy, both solid and gas phase combustion reactions need to be inhibited. As presented by our TGA and FTIR analysis, the flame retardancy in AHP foams in the air can be achieved due to the decomposition of AHP by absorbing the

surrounding oxygen to form phosphoric acid that promoted the formation of an insulating char [18, 20, 44, 51, 82, 83]. This mechanism results in preventing gaseous phase as well as solid-phase combustion reactions resulting in a significantly lower self-extinguishing time and weight loss of the AHP containing foams (**Figure 3.45** and **3.46**). At a very low concentration of AHP (5.54 wt.%), the resulting self-extinguishing time and weight losses were 10 s and 4.39% of burning time and weight loss, respectively. Similar behavior can be seen in the digital pictures in **Figure 3.47** as the burning area drastically decreased with the increasing amount of AHP. Hence, increasing AHP concentration in foams enhances the flame retardancy and reduces its burnt area. Our results confirmed that the synergistic flame retardancy mechanism via solid and gas-phase reactions can prove efficient to improve overall flame retardancy in PUFs.

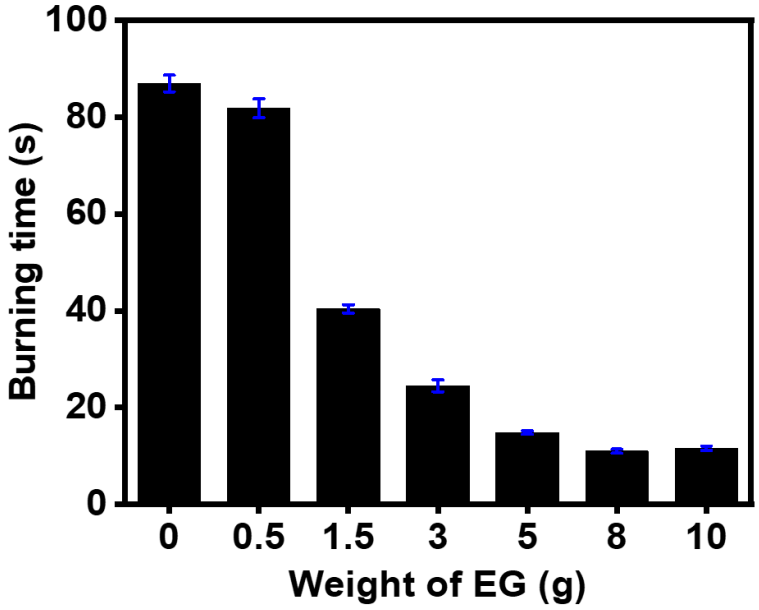

Figure 3.39. Burning time for the polyurethane foams containing EG.

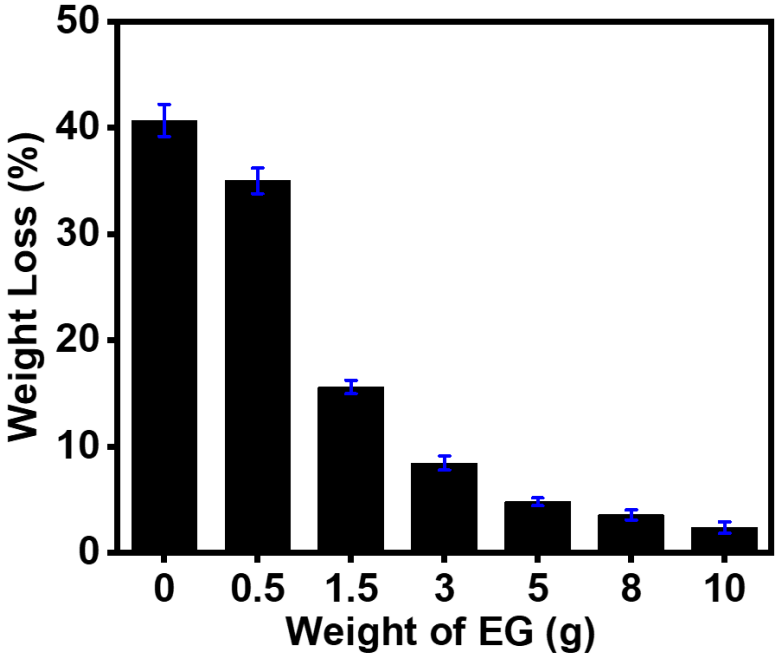

Figure 3.40. Weight loss % for polyurethane foams containing EG.

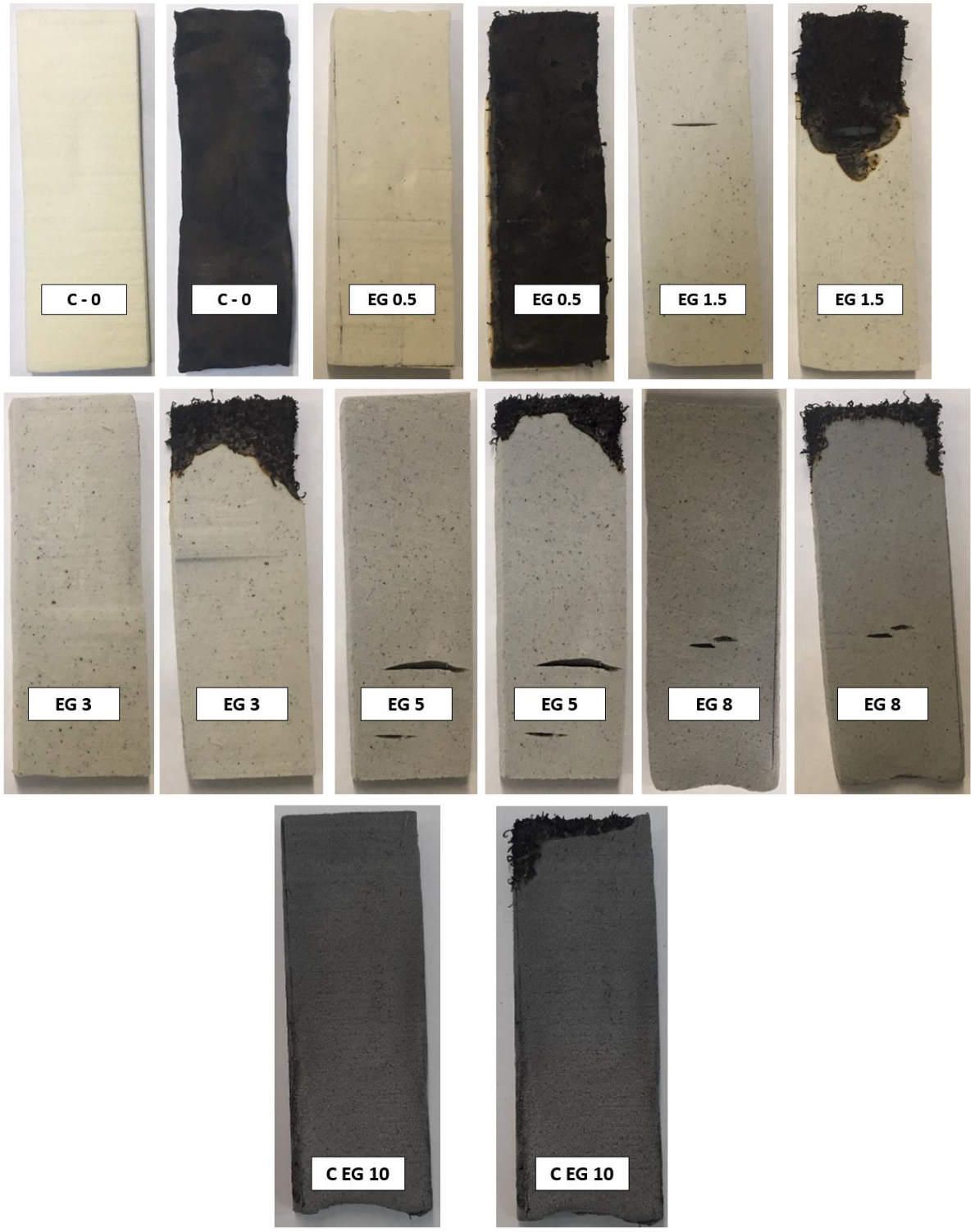

Figure 3.41. Digital images for the flame retardant rigid polyurethane foams containing EG before and after the burning test.

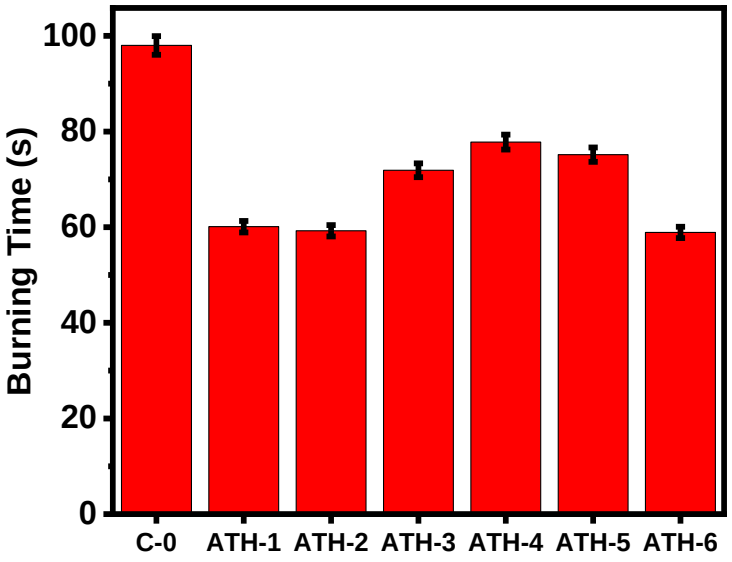

Figure 3.42. Burning time for the polyurethane foams containing ATH.

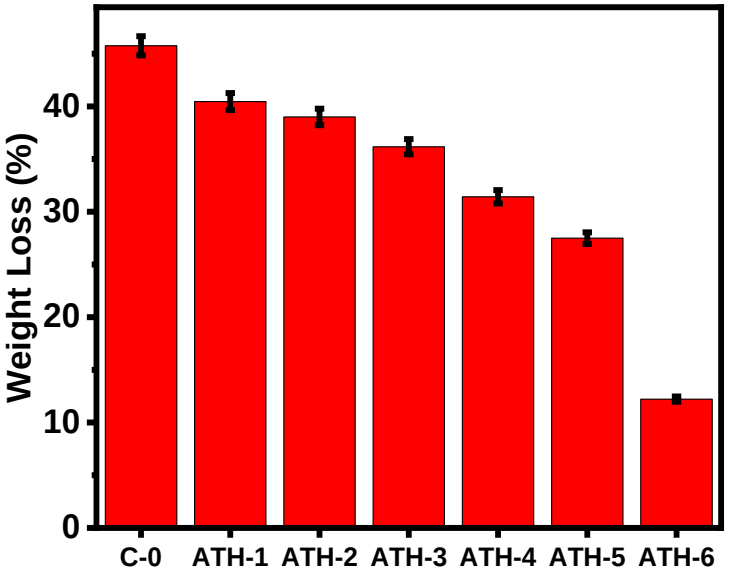

Figure 3.43. Weight loss % for polyurethane foams containing ATH.

Figure 3.44. Digital images for the flame retardant rigid polyurethane foams containing ATH before and after the burning test.

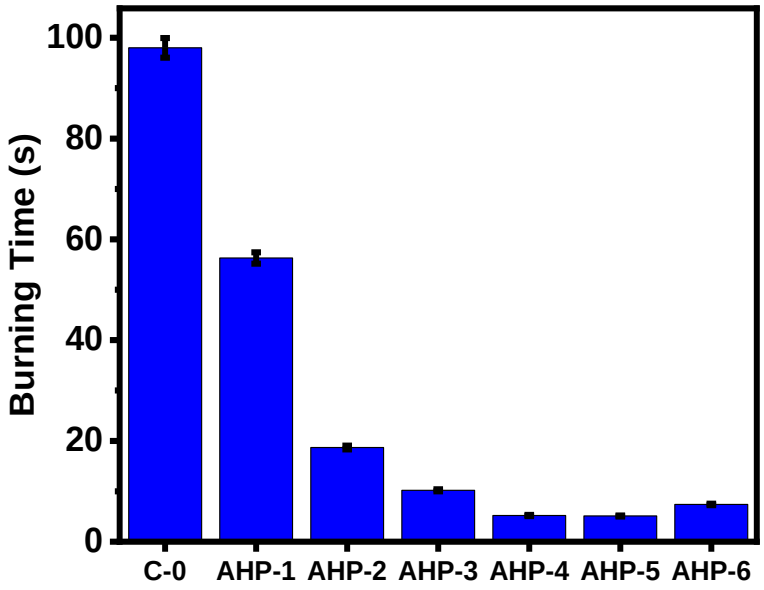

Figure 3.45. Burning time for the polyurethane foams containing AHP.

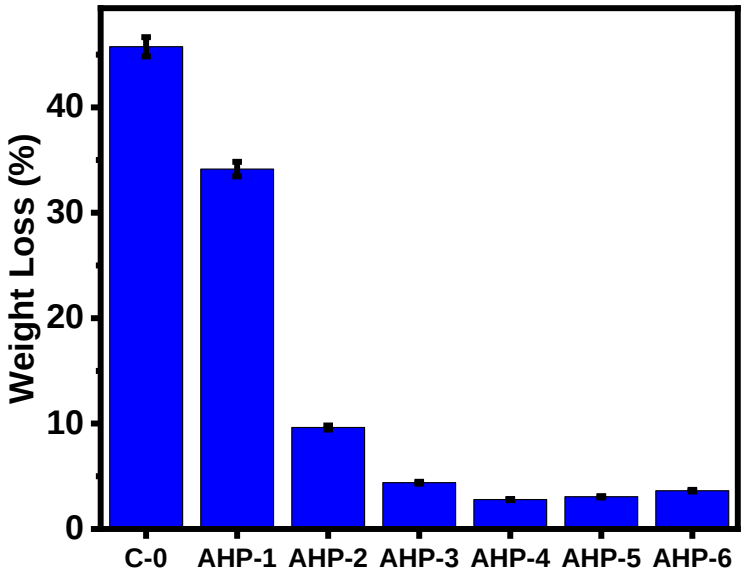

Figure 3.46. Weight loss % for polyurethane foams containing AHP.

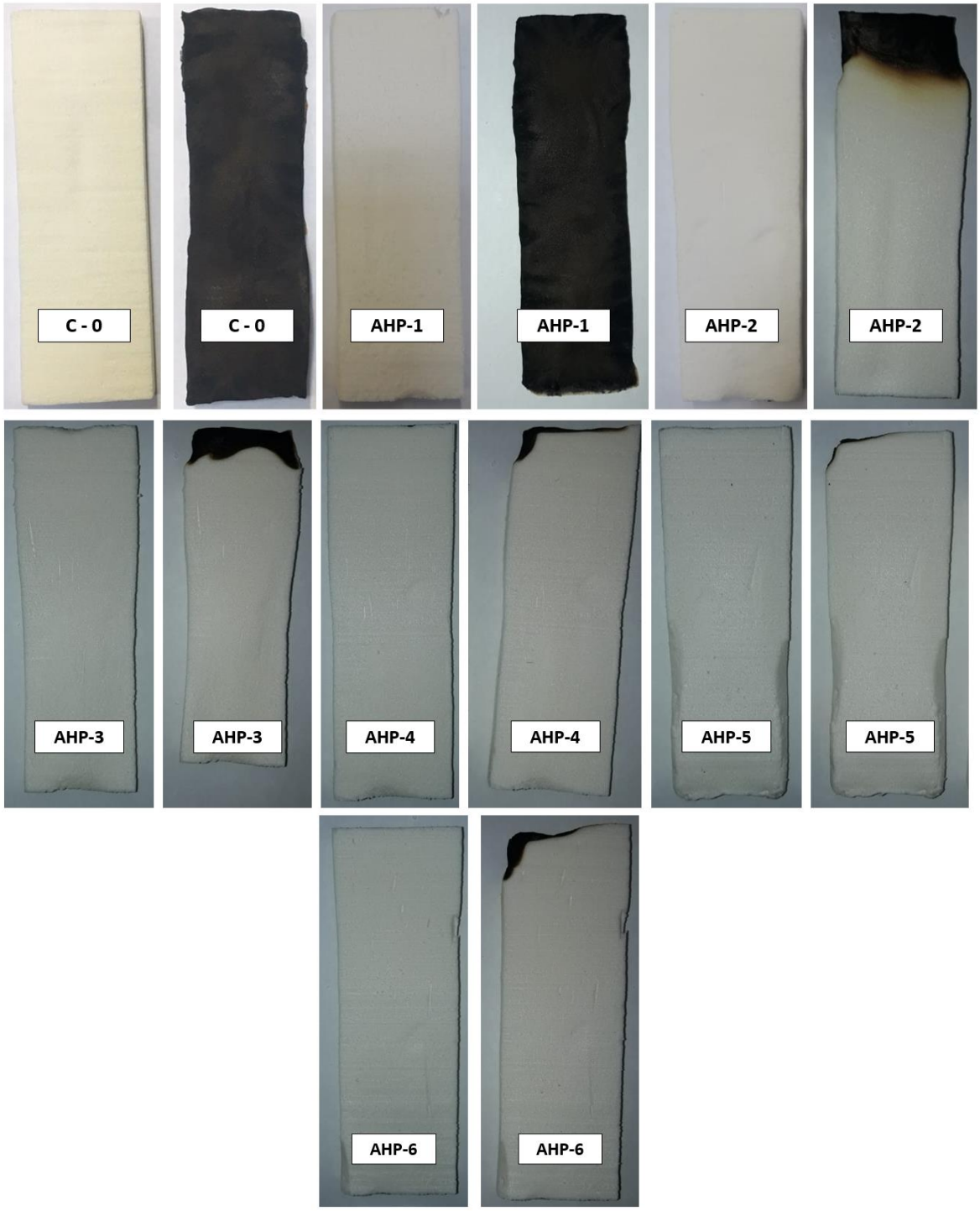

Figure 3.47. Digital images for the flame retardant rigid polyurethane foams containing AHP before and after the burning test.

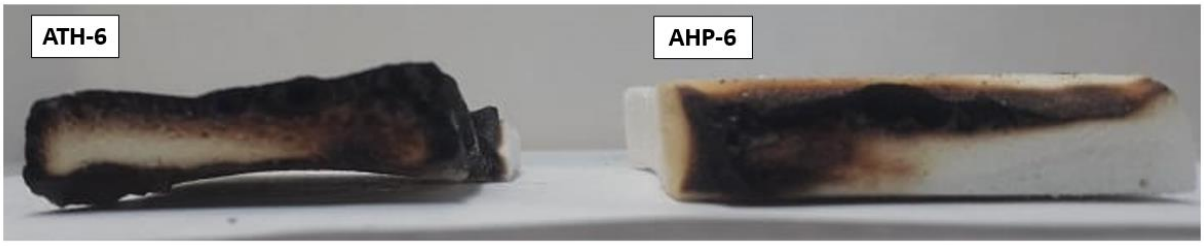

Figure 3.48. Visual aspect of the burnt samples.

CHAPTER IV

CONCLUSION

A bio-based PUF was successfully synthesized using a bio-oil named carvone and converted into a polyol using a facile and single-step thiol-ene reaction. The synthesized polyol was used as a sustainable alternative to petroleum-based polyol to make polyurethane foams. To enhance the flame retardancy of the rigid PUF, EG, ATH, and AHP were added separately in different concentrations during the foaming step. An overall increase in the evaluated properties was observed, aside from compressive strength for EG and AHP containing foams. The foams had an acceptable range of density for industrial applications, its closed-cell content was higher than 93% along with a general improvement in thermal properties and flame retardancy. Despite the fluctuation of mechanical properties, the rigid foams still reached satisfactory values when compared with others found in the literature. Finally, the flame retardancy was drastically improved which dropped the burning time of the neat foam from around 98 to the fastest of 5.2 s. Hence, this thesis describes an effective and facile way to synthesize biobased rigid PUF with eco-friendly flame-retardant components. These factors suggest that this material can be easily utilized in large-scale processing in near future.

CONSIDERATIONS FOR THE FUTURE

- Test other bio renewable materials such as phellandrene, terpinene, and ocimene, which are chemically similar to carvone. Then convert these compounds into polyols to make polyurethanes.
- Prepare polyurethane foams using the non-isocyanate route and evaluate potential FR candidates in these formulations.
- Use other FR such as graphene, magnesium hydroxide, and dimethyl methyl phosphonate to understand their flammability mechanism as well as their influence on the polyurethane's properties.
- Prepare polyurethanes on a pilot scale to validate their potential for commercial application.
- Propose the synthesis of new reactive FR polyols through approaches such as Mannich reaction to chemically attach nitrogen or phosphorus-based FR into the polyol's structure.

REFERENCES

1. Ionescu M (2006) Chemistry and Technology of Polyols for Polyurethanes. Rapra Technology, UK
2. Gama N V, Ferreira A, Barros-Timmons A (2018) Polyurethane Foams: Past, Present, and Future. Materials (Basel) 11. https://doi.org/10.3390/ma11101841
3. Akindoyo JO, Beg MDH, Ghazali S, Islam MR, Jeyaratnam N, Yuvaraj AR (2016) Polyurethane types, synthesis and applications-a review. RSC Adv 6:114453–114482. https://doi.org/10.1039/c6ra14525f
4. Hăloiu A, Iosif D (2013) Bio-source composite materials used in the automotive industry. In Sci. Bulletim Automot. Ser. Mech. Technol. Univ. Pitesti. https://automotive.upit.ro/index_files/2014/2014_8_.pdf
5. Somarathna HMCC, Raman SN, Mohotti D, Mutalib AA, Badri KH (2018) The use of polyurethane for structural and infrastructural engineering applications: A state-of-the-art review. Constr Build Mater 190:995–1014. https://doi.org/https://doi.org/10.1016/j.conbuildmat.2018.09.166
6. Nordon A, Meunier C, Carr RH, Gemperline PJ, Littlejohn D (2002) Determination of the ethylene oxide content of polyether polyols by low-field 1H nuclear magnetic resonance spectrometry. Anal Chim Acta 472:133–140. https://doi.org/https://doi.org/10.1016/S0003-2670(02)00939-X
7. Dasgupta Q, Chatterjee K, Madras G (2014) Combinatorial Approach to Develop Tailored Biodegradable Poly(xylitol dicarboxylate) Polyesters. Biomacromolecules

15:4302–4313. https://doi.org/10.1021/bm5013025

8. Lee A, Deng Y (2015) Green polyurethane from lignin and soybean oil through non-isocyanate reactions. Eur Polym J 63:67–73. https://doi.org/10.1016/j.eurpolymj.2014.11.023

9. Zhao R, Torley P, Halley PJ (2008) Emerging biodegradable materials: starch-and protein-based bio-nanocomposites. J Mater Sci 43:3058–3071. https://doi.org/https://doi.org/10.1007/s10853-007-2434-8

10. Kale G, Kijchavengkul T, Auras R, Rubino M, Selke SE, Singh SP (2007) Compostability of bioplastic packaging materials: an overview. Macromol Biosci 7:255–277. https://doi.org/https://doi.org/10.1002/mabi.200600168

11. Chidambarampadmavathy K, Karthikeyan OP, Heimann K (2017) Sustainable bio-plastic production through landfill methane recycling. Renew Sustain Energy Rev 71:555–562. https://doi.org/https://doi.org/10.1016/j.rser.2016.12.083

12. Llevot A, Dannecker PK, von Czapiewski M, Over LC, Söyler Z, Meier MAR (2016) Renewability is not Enough: Recent Advances in the Sustainable Synthesis of Biomass-Derived Monomers and Polymers. Chem - A Eur J 22:11510–11521. https://doi.org/10.1002/chem.201602068

13. Kolb HC, Finn MG, Sharpless KB (2001) Click Chemistry: Diverse Chemical Function from a Few Good Reactions. Angew Chemie - Int Ed 40:2004–2021. https://doi.org/10.1002/1521-3773(20010601)40:11<2004::AID-ANIE2004>3.0.CO;2-5

14. Belgacem MN, Gandini A (2008) Monomers, Polymers, and Composites from Renewable Resources, 1st ed. Elsevier Ltd, Amsterdam

15. Mu Y, Wan X, Han Z, Peng Y, Zhong S (2012) Rigid polyurethane foams based on activated soybean meal. J Appl Polym Sci 124:4331–4338. https://doi.org/10.1002/app.35612

16. Petrovic ZS, Cvetković I, Hong D, Wan X, Zhang W (2008) Polyester Polyols and Polyurethanes from Ricinoleic Acid. J Appl Polym Sci 108:1184–1190. https://doi.org/10.1002/app.27783

17. Dworakowska S, Bogdal D, Prociak A (2012) Microwave-assisted synthesis of polyols from rapeseed oil and properties of flexible polyurethane foams. Polymers (Basel) 4:1462–1477. https://doi.org/10.3390/polym4031462

18. Zhang C, Bhoyate S, Ionescu M, Kahol PK, Gupta RK (2018) Highly flame retardant and bio-based rigid polyurethane foams derived from orange peel oil. Polym Eng Sci 58:2078–2087. https://doi.org/10.1002/pen.24819

19. Elbers N, Ranaweera CK, Ionescu M, Wan X, Kahol PK, Gupta RK (2017) Synthesis of Novel Biobased Polyol via Thiol-Ene Chemistry for Rigid Polyurethane Foams. J Renew Mater 5:74–83. https://doi.org/10.7569/jrm.2017.634137

20. Ramanujam S, Zequine C, Bhoyate S, Neria B, Kahol P, Gupta R (2019) Novel Biobased Polyol Using Corn Oil for Highly Flame-Retardant Polyurethane Foams. C 5:13. https://doi.org/10.3390/c5010013

21. Javni I, Zhang W, Petrović ZS (2003) Effect of different isocyanates on the

properties of soy-based polyurethanes. J Appl Polym Sci 88:2912–2916. https://doi.org/doi:10.1002/app.11966

22. M. de Souza F, Choi J, Bhoyate S, Kahol PK, Gupta RK (2020) Expendable Graphite as an Efficient Flame-Retardant for Novel Partial Bio-Based Rigid Polyurethane Foams. C — J Carbon Res 6:27. https://doi.org/10.3390/c6020027

23. Challoner KR, McCarron MM (1990) Castor bean intoxication. Ann Emerg Med 19:1177–1183. https://doi.org/https://doi.org/10.1016/S0196-0644(05)81525-2

24. de Miliano J-W, Woolnough A, Reeves A, Shepherd D (2010) Ecologically significant invasive species, a monitoring framework for natural resource management groups in Western Australia. https://researchlibrary.agric.wa.gov.au/cgi/viewcontent.cgi?referer=https://scholar.google.com/&httpsredir=1&article=1164&context=bulletins

25. Babb DA (2011) Polyurethanes from renewable resources. In: Babb DA (ed) Synthetic biodegradable polymers. Springer, Verlag Berlin, Verlag, pp 315–360

26. Wilbon PA, Chu F, Tang C (2013) Progress in renewable polymers from natural terpenes, terpenoids, and rosin. Macromol Rapid Commun 34:8–37 . https://doi.org/10.1002/marc.201200513

27. Clark JH (1999) Green Chemistry: Challenges and Opportunities. Green Chem 1:1–8. https://doi.org/10.1039/A807961G

28. Ruzicka L (1953) The isoprene rule and the biogenesis of terpenic compounds. Experientia 9:357–367. https://doi.org/https://doi.org/10.1007/BF02167631

29. De Carvalho CCCR, Da Fonseca MMR (2006) Carvone: Why and how should one bother to produce this terpene. Food Chem 95:413–422. https://doi.org/10.1016/j.foodchem.2005.01.003

30. Ameh S (2014) Diversity, Utility, Analytical Methods and Use Implications of Aroma-active Compounds from Select Angiosperm Families. European J Med Plants 4:1046–1086. https://doi.org/10.9734/ejmp/2014/10779

31. Garin DL (1976) Steam distillation of essential oils - Carvone from caraway. J Chem Educ 53:105. https://doi.org/10.1021/ed053p105

32. Silvestre AJD, Gandini A (2008) Terpenes: major sources, properties, and applications. In: Monomers, polymers, and composites from renewable resources. Elsevier, pp 17–38

33. Beatson RP (2011) Chemicals from extractives. ACS Symp Ser 1067:279–297. https://doi.org/10.1021/bk-2011-1067.ch011

34. Furukawa Y (1998) Inventing polymer science: Staudinger, Carothers, and the emergence of macromolecular chemistry. University of Pennsylvania Press

35. Obrecht W, Lambert J, Happ M, Oppenheimer-Stix C, Dunn J, Krüger R (2011) Rubber, 4. Emulsion Rubbers. In: Ullmann's Encyclopedia of Industrial Chemistry. Wiley Online Library, Verlag

36. Hauenstein O, Reiter M, Agarwal S, Rieger B, Greiner A (2016) Bio-based polycarbonate from limonene oxide and CO2 with high molecular weight, excellent thermal resistance, hardness, and transparency. Green Chem 18:760–

770. https://doi.org/10.1039/c5gc01694k

37. Park HJ, Ryu CY, Crivello J V. (2013) Photoinitiated cationic polymerization of limonene 1,2-oxide and α-pinene oxide. J Polym Sci Part A Polym Chem 51:109–117. https://doi.org/10.1002/pola.26280

38. Bähr M, Bitto A, Mülhaupt R (2012) Cyclic limonene dicarbonate as a new monomer for non-isocyanate oligo- and polyurethanes (NIPU) based upon terpenes. Green Chem 14:1447–1454 . https://doi.org/10.1039/c2gc35099h

39. Gupta RK, Ionescu M, Wan X, Radojcic D, Petrovic ZS (2015) Synthesis of a Novel Limonene Based Mannich Polyol for Rigid Polyurethane Foams. J Polym Environ 23:261–268. https://doi.org/10.1007/s10924-015-0717-8

40. Ranaweera CK, Ionescu M, Bilic N, Wan X, Kahol PK, Gupta RK (2017) Biobased Polyols Using Thiol-Ene Chemistry for Rigid Polyurethane Foams with Enhanced Flame-Retardant Properties. J Renew Mater 5:1. https://doi.org/https://doi.org/10.7569/JRM.2017.634105

41. Gupta RK, Ionescu M, Radojcic D, Wan X, Petrovic ZS (2014) Novel Renewable Polyols Based on Limonene for Rigid Polyurethane Foams. J Polym Environ 22:304. https://doi.org/https://doi.org/10.1007/s10924-014-0641-3

42. Laoutid F, Bonnaud L, Alexandre M, Lopez-Cuesta JM, Dubois P (2009) New prospects in flame retardant polymer materials: From fundamentals to nanocomposites. Mater Sci Eng R Reports 63:100–125. https://doi.org/10.1016/j.mser.2008.09.002

43. Troitzsch J (1987) Flame Retardants. Kunststoffe - Ger Plast 77:90–91 . https://doi.org/https://doi.org/10.1002/masy.19930740115

44. Bhoyate S, Ionescu M, Radojcic D, Kahol PK, Chen J, Mishra SR, Gupta RK (2018) Highly flame-retardant bio-based polyurethanes using novel reactive polyols. J Appl Polym Sci 135. https://doi.org/10.1002/app.46027

45. Hummers WS, Offeman RE (1958) Preparation of Graphitic Oxide. J Am Chem Soc 80:1339. https://doi.org/10.1021/ja01539a017

46. Wang X, Kalali EN, Wan J-T, Wang D-Y (2017) Carbon-family materials for flame retardant polymeric materials. Prog Polym Sci 69:22–46. https://doi.org/https://doi.org/10.1016/j.progpolymsci.2017.02.001

47. Camino G, Duquesne S, Delobel R, Eling B, Lindsay C, Roels T (2001) Mechanism of Expandable Graphite Fire Retardant Action in Polyurethanes. ACS Symp Ser 797:90–109. https://doi.org/10.1021/bk-2001-0797.ch008

48. Zhao B, Hu Z, Chen L, Liu Y, Liu Y, Wang Y-Z (2011) A phosphorus-containing inorganic compound as an effective flame retardant for glass-fiber-reinforced polyamide 6. J Appl Polym Sci 119:2379–2385. https://doi.org/https://doi.org/10.1002/app.32860

49. Desroches M, Caillol S, Lapinte V, Auvergne R m., Boutevin B (2011) Synthesis of Biobased Polyols by Thiol–Ene Coupling from Vegetable Oils. Macromolecules 44:2489 . https://doi.org/https://doi.org/10.1021/ma102884w

50. Hoyle CE, Lee TY, Roper T (2004) Thiol-enes: Chemistry of the past with promise

for the future. J Polym Sci, Part A Polym Chem 42:5301. https://doi.org/https://doi.org/10.1002/pola.20366

51. Bhoyate S, Ionescu M, Kahol PK, Chen J, Mishra SR, Gupta RK (2018) Highly flame-retardant polyurethane foam based on reactive phosphorus polyol and limonene-based polyol. J Appl Polym Sci 135:16–19. https://doi.org/10.1002/app.46224

52. Noisong P, Danvirutai C (2010) A new synthetic route, characterization and vibrational studies of manganese hypophosphite monohydrate at ambient temperature. Spectrochim Acta - Part A Mol Biomol Spectrosc 77:890–894. https://doi.org/10.1016/j.saa.2010.08.028

53. Wilpiszewska K, Spychaj T, Paździoch W (2016) Carboxymethyl starch/montmorillonite composite microparticles: Properties and controlled release of isoproturon. Carbohydr Polym 136:101–106. https://doi.org/10.1016/j.carbpol.2015.09.021

54. Tang G, Wang X, Zhang R, Yang W, Hu Y, Song L, Gong X (2013) Facile synthesis of lanthanum hypophosphite and its application in glass-fiber reinforced polyamide 6 as a novel flame retardant. Compos Part A Appl Sci Manuf 54:1–9. https://doi.org/https://doi.org/10.1016/j.compositesa.2013.07.001

55. González Gómez M, Belderbos S, Yáñez S, piñeiro Y, Cleeren F, Bormans G, Deroose C, Gsell W, Himmelreich U, Rivas J (2019) Development of Superparamagnetic Nanoparticles Coated with Polyacrylic Acid and Aluminum Hydroxide as an Efficient Contrast Agent for Multimodal Imaging. Nanomaterials

9:1626. https://doi.org/10.3390/nano9111626

56. Feng Y, Liang H, Yang Z, Yuan T, Luo Y, Li P, Yang Z, Zhang C (2017) A Solvent-Free and Scalable Method To Prepare Soybean-Oil-Based Polyols by Thiol–Ene Photo-Click Reaction and Biobased Polyurethanes Therefrom. ACS Sustain Chem & Eng 5:7365–7373. https://doi.org/10.1021/acssuschemeng.7b01672

57. Feng Y, Liang H, Yang Z, Yuan T, Luo Y, Li P, Yang Z, Zhang C (2017) A Solvent-Free and Scalable Method To Prepare Soybean-Oil-Based Polyols by Thiol–Ene Photo-Click Reaction and Biobased Polyurethanes Therefrom. ACS Sustain Chem Eng 5:7365–7373. https://doi.org/10.1021/acssuschemeng.7b01672

58. Adnan S, Tuan Ismail TNM, Mohd Noor N, Nek Mat Din NSM, Hanzah N, Shoot Kian Y, Abu Hassan H (2016) Development of Flexible Polyurethane Nanostructured Biocomposite Foams Derived from Palm Olein-Based Polyol. Adv Mater Sci Eng 2016. https://doi.org/10.1155/2016/4316424

59. Chen T-K, Tien Y-I, Wei K-H (2000) Synthesis and characterization of novel segmented polyurethane/clay nanocomposites. Polymer (Guildf) 41:1345–1353. https://doi.org/https://doi.org/10.1016/S0032-3861(99)00280-3

60. Czupryński B, Paciorek-Sadowska J, Liszkowska J (2006) Modifications of the rigid polyurethane - Polyisocyanurate foams. J Appl Polym Sci 100:2020–2029. https://doi.org/10.1002/app.22604

61. Liu Y, He J, Yang R (2015) Effects of Dimethyl Methylphosphonate, Aluminum Hydroxide, Ammonium Polyphosphate, and Expandable Graphite on the Flame

Retardancy and Thermal Properties of Polyisocyanurate–Polyurethane Foams. Ind & Eng Chem Res 54:5876–5884. https://doi.org/10.1021/acs.iecr.5b01019

62. Formicola C, de Fenzo A, Zarrelli M, Frach A, Giordano M, Camino G (2009) Synergistic effects of zinc borate and aluminum trihydroxide on flammability behavior of aerospace epoxy system. Express Polym Lett 3:376–384. https://doi.org/10.3144/expresspolymlett.2009.47

63. Feng F, Qian L (2014) The flame retardant behaviors and synergistic effect of expandable graphite and dimethyl methylphosphonate in rigid polyurethane foams. Polym Compos 35:301–309. https://doi.org/10.1002/pc.22662

64. Wang WJ, He K, Dong QX, Fan Y, Zhu N, Xia YB, Li HF, Wang J, Yuan Z, Wang EP, Wang X, Ma HW (2013) Influence of Aluminum Hydroxide and Expandable Graphite on the Flammability of Polyisocyanurate-Polyurethane Foams. Appl Mech Mater 368:741. https://doi.org/10.4028/www.scientific.net/AMM.368-370.741

65. Gharehbaghi a., Bashirzadeh R, Ahmadi Z (2011) Polyurethane flexible foam fire-resisting by melamine and expandable graphite: Industrial approach. J Cell Plast 47:549. https://doi.org/10.1177/0021955X11414789

66. Hejna A, Kirpluks M, Kosmela P, Cabulis U, Haponiuk J, Piszczyk Ł (2017) The influence of crude glycerol and castor oil-based polyol on the structure and performance of rigid polyurethane-polyisocyanurate foams. Ind Crops Prod 95:113–125. https://doi.org/10.1016/J.INDCROP.2016.10.023

67. Liu Y, He J, Yang R (2015) Effects of Dimethyl Methylphosphonate, Aluminum Hydroxide, Ammonium Polyphosphate, and Expandable Graphite on the Flame Retardancy and Thermal Properties of Polyisocyanurate-Polyurethane Foams. Ind Eng Chem Res 54:5876–5884. https://doi.org/10.1021/acs.iecr.5b01019

68. Hu X-M, Wang D-M (2013) Enhanced fire behavior of rigid polyurethane foam by intumescent flame retardants. J Appl Polym Sci 129:238–246. https://doi.org/doi:10.1002/app.38722

69. Wang Y, Wang F, Dong Q, Xie M, Liu P, Ding Y, Zhang S, Yang M, Zheng G (2017) Core-shell expandable graphite @ aluminum hydroxide as a flame-retardant for rigid polyurethane foams. Polym Degrad Stab 146:267–276. https://doi.org/10.1016/j.polymdegradstab.2017.10.017

70. Shi L, Li Z-M, Xie B-H, Wang J-H, Tian C-R, Yang M-B (2006) Flame retardancy of different-sized expandable graphite particles for high-density rigid polyurethane foams. Polym Int 55:862–871. https://doi.org/10.1002/pi.2021

71. Liu C, Wang C, Hu Y, Zhang F, Shang Q, Lei W, Zhou Y, Cai Z (2018) Castor oil-based polyfunctional acrylate monomers: Synthesis and utilization in UV-curable materials. Prog Org Coatings 121:236–246. https://doi.org/https://doi.org/10.1016/j.porgcoat.2018.04.020

72. Sérgio Augusto Mello Da S, André Luis C, Raquel G, Francisco Antonio Rocco L (2013) Strength Properties of Medium Density Fiberboards (MDF) Manufactured with Pinus Elliottii Wood and Polyurethane Resin Derived from Castor Oil. Int J

Compos Mater 3:7–14. https://doi.org/10.5923/j.cmaterials.20130301.02

73. Ye L, Meng X-Y, Liu X-M, Tang J-H, Li Z-M (2009) Flame-retardant and mechanical properties of high-density rigid polyurethane foams filled with Deca brominated diphenyl ethane and expandable graphite. J Appl Polym Sci 111:2372–2380. https://doi.org/10.1002/app.29242

74. González-Gómez MA, Belderbos S, Yañez-Vilar S, Piñeiro Y, Cleeren F, Bormans G, Deroose CM, Gsell W, Himmelreich U, Rivas J (2019) Development of superparamagnetic nanoparticles coated with polyacrylic acid and aluminum hydroxide as an efficient contrast agent for multimodal imaging. Nanomaterials 9:1–20. https://doi.org/10.3390/nano9111626

75. Yuan B, Bao C, Guo Y, Song L, Liew KM, Hu Y (2012) Preparation and characterization of flame-retardant aluminum hypophosphite/poly(vinyl alcohol) composite. Ind Eng Chem Res 51:14065–14075. https://doi.org/10.1021/ie301650f

76. Yan YW, Huang JQ, Guan YH, Shang K, Jian RK, Wang YZ (2014) Flame retardance and thermal degradation mechanism of polystyrene modified with aluminum hypophosphite. Polym Degrad Stab 99:35–42. https://doi.org/10.1016/j.polymdegradstab.2013.12.014

77. Qian X, Song L, Hu Y, Yuen RKK, Chen L, Guo Y, Hong N, Jiang S (2011) Combustion and thermal degradation mechanism of a novel intumescent flame retardant for epoxy acrylate containing phosphorus and nitrogen. Ind Eng Chem Res 50:1881–

1892. https://doi.org/https://doi.org/10.1021/ie102196k

78. Zhang H, Lu J, Yang H, Lang J, Yang H (2019) Comparative study on the flame-retardant properties and mechanical properties of PA66 with different dicyclohexyl hypophosphite acid metal salts. Polymers (Basel) 11. https://doi.org/10.3390/polym11121956

79. Cheng X, Wu J, Yao C, Yang G (2019) Aluminum hypophosphite and aluminum phenylphosphinate: A comprehensive comparison of chemical interaction during pyrolysis in flame-retarded glass-fiber-reinforced polyamide 6. J Fire Sci 37:193–212. https://doi.org/10.1177/0734904119836208

80. Wu S, Deng D, Zhou L, Zhang P, Tang G (2019) Flame retardancy and thermal degradation of rigid polyurethane foams composites based on aluminum hypophosphite. Mater Res Express 6:105365. https://doi.org/10.1088/2053-1591/ab41b2

81. Yuan Y, Ma C, Shi Y, Song L, Hu Y, Hu W (2018) Highly-efficient reinforcement and flame retardancy of rigid polyurethane foam with phosphorus-containing additive and nitrogen-containing compound. Mater Chem Phys 211:42–53. https://doi.org/https://doi.org/10.1016/j.matchemphys.2018.02.007

82. Bhoyate S, Ionescu M, Kahol PK, Gupta RK (2019) Castor-oil derived nonhalogenated reactive flame-retardant-based polyurethane foams with significant reduced heat release rate. J Appl Polym Sci 136:47276. https://doi.org/10.1002/app.47276

83. Bhoyate S, Ionescu M, Kahol PK, Gupta RK (2018) Sustainable flame-retardant polyurethanes using renewable resources. Ind Crops Prod 123:480–488. https://doi.org/10.1016/j.indcrop.2018.07.025